Tuberculosis Transcriptomics: Host Protection and Immune Evasion Mechanisms

Mumin OZTURK

Thesis submitted to the University of Cape Town in fulfillment of the

degree Doctor of Philosophy

Cytokines and Disease Group,
International Centre for Genetic Engineering and Biotechnology (ICGEB), Cape Town Component and Institute of Infectious Diseases and Molecular Medicine (IDM), Division of Immunology, Faculty of Health Sciences, University of Cape Town,
Cape Town, South Africa.

University of Cape Town

The copyright of this thesis vests in the author. No quotation from it or information derived from it is to be published without full acknowledgement of the source. The thesis is to be used for private study or non-commercial research purposes only.

Published by the University of Cape Town (UCT) in terms of the non-exclusive license granted to UCT by the author.

University of Cape Town

TABLE OF CONTENTS

ACKNOWLEDGEMENTS

I would like to thank my supervisors Prof. Frank Brombacher and Dr Reto Guler for giving me the chance of participating in an intriguing and fruitful study. They have been exceptional mentors, providing intellectual support at every step. I am grateful to Dr Reto Guler for his insightful advices, encouragement of independent thinking and finding time for discussions. I also want to thank Dr. Suraj Parihar, who taught me literally the basics of experimental immunology and microbiology.

I want to thank as well my friends and colleagues in Brombacher group for their support. Thank you for the laughs, the frustration and the successes. Science is not easy, but it doesn't matter when you're working on it alongside friends rather than colleagues.

Furthermore, I am indebted to my supportive partner Kerry for her endurance over 4 years.

Last but not least, I would like to express my gratitude to my mother and father, who have always supported me throughout my scientific career.

ABSTRACT

Mycobacterium tuberculosis (Mtb) is the leading cause of death from an infectious disease. The success of the pathogen lies in its ability to subvert hostile intracellular macrophage environment. We performed genome-wide transcriptional deep sequencing on total RNA in murine bone marrow-derived macrophages (BMDM) infected with hypervirulent Beijing strain (HN878) in an extensive time kinetic manner using single molecule sequencer and cap analysis gene expression (CAGE) technique. CAGE analysis revealed nearly 36000 unique RNA transcripts with approximately 16000 are not unannotated to a specific gene. This thesis addressed global changes in RNA expression levels in macrophages infected with Mtb in a time kinetic manner to pinpoint novel host protection and immune evasion genes and elucidate the role of these genes *in vitro* macrophage assays and *in vivo* knockout mouse studies.

The data in this thesis showed that basic leucine zipper transcription factor 2 (Batf2) was an important factor that regulates inflammatory responses in Mtb infection. Deletion of Batf2 led to the survival of mice with reduced lung inflammation and histopathology due to reduced recruitment of inflammatory macrophages. We also showed that Batf2 was highly expressed in peripheral blood from adolescents who progressed from infection to tuberculosis disease and a predictive human biomarker for tuberculosis disease. In contrast to Batf2, we showed that Protein Kinase C-delta (PKC-δ) deficient mice are highly susceptible to tuberculosis and human lung proteomics dataset revealed that PKC-δ was highly upregulated in the necrotic and cavitory regions of human granulomas in multi-drug resistant subjects. PKC-δ deficient mice had a significant reduction in alveolar macrophages and dendritic cells, reduced accumulation of lipid bodies and serum fatty acids. *In vitro* experiments showed that PKCδ was required for optimal killing effector functions which were independent of phagosome maturation and autophagy in primary murine macrophages. Our studies suggested that these novel genes play a role in the immune response to Mtb and should be studied more thoroughly to evaluate their potential in possible TB interventions.

List of Publications

In addition to the work presented in this thesis, the author has made significant contributions in following publications.

1) IRNdb: the database of immunologically relevant non-coding RNAs. Elena Denisenko, Daniel Ho, Ousman Tamgue, **Mumin Ozturk,** Harukazu Suzuki, Frank Brombacher, Reto Guler, Sebastian Schmeier. *Database* 2016, baw138
2) Redefining the transcriptional regulatory dynamics of classically and alternatively activated macrophages by deepCAGE transcriptomics. Sugata Roy, Sebastian Schmeier, Erik Arner, Tanvir Alam, Suraj P Parihar, **Mumin Ozturk**, Ousman Tamgue, Hideya Kawaji, Michiel JL de Hoon, Masayoshi Itoh, Timo Lassmann, Piero Carninci, Yoshihide Hayashizaki, Alistair RR Forrest, Vladimir B Bajic, Reto Guler, Frank Brombacher, Harukazu Suzuki, Fantom Consortium. *Nucleic acids research* 2015, 43-14: 6969-6982
3) Batf2/Irf1 induces inflammatory responses in classically activated macrophages, lipopolysaccharides, and mycobacterial infection. Sugata Roy, Reto Guler, Suraj P Parihar, Sebastian Schmeier, Bogumil Kaczkowski, Hajime Nishimura, Jay W Shin, Yutaka Negishi, **Mumin Ozturk**, Ramona Hurdayal, Atsutaka Kubosaki, Yasumasa Kimura, Michiel JL de Hoon, Yoshihide Hayashizaki, Frank Brombacher, Harukazu Suzuki. *The Journal of Immunology* 2015,194-12: 6035-6044
4) IL-4Rα-Dependent Alternative Activation of Macrophages Is Not Decisive for Mycobacterium tuberculosis Pathology and Bacterial Burden in Mice. Reto Guler, Suraj P Parihar, Suzana Savvi, Erin Logan, Anita Schwegmann, Sugata Roy, Natalie E Nieuwenhuizen, **Mumin Ozturk,** Sebastian Schmeier, Harukazu Suzuki, Frank Brombacher. *PloS one* 2015, 310: e012107

List of Abbreviations

ARG1 Arginase 1

ATG5 Autophagy protein 5

ATP Adenosine triphosphate

BC Before Christ

BCG Bacillus Calmette Guérin

CCL Chemokine (C-C motif) ligand

CD Cluster of Differentiation

C/EBP CCAAT-enhancer-binding proteins

cGAS cGMP- AMP Synthase

CLIP class II-associated Ii peptide

CIITA MHC II transcriptional transactivator

CXCR C-X-C chemokine receptor

DAP Diaminopimelic acid

DC-SIGN Dendritic Cell-Specific Intercellular adhesion molecule-3-Grabbing Non-integrin

DNA Deoxyribonucleic Acid

ESX Early secretory antigenic target (ESAT6) protein family secretion

G-CSF Granulocyte colony stimulating factor

GTP Guanosine 5′-triphosphate

HIV Human Immunodeficiency Virus

HLA-DR Human Leukocyte Antigen – antigen D Related

IDO Indoleamine-pyrrole 2,3-dioxygenase

IFNγ Interferon γ

IL- Interleukin

iNKT invariant Natural Killer T cells

iNOS inducible nitric oxide synthase

IRF3 Interferon regulatory factor 3

IRG Interferon Response Genes

LTBI Latent Tuberculosis Infection

LYSM Lysozyme M

MARCO Macrophage Receptor with Collagenous Structure

MBL Mannose-binding lectin

MCL Macrophage C-type lectin

MCP-1 Monocyte chemoattractant protein-1

MHC Major Histocompatibility complex

MMP Matrix Metalloproteinase

MTB Mycobacterium tuberculosis

MYD88 Myeloid differentiation primary response gene 88

NDK Nucleoside diphosphate kinase

NFκB Nuclear factor κB

NOD Nucleotide-binding oligomerization domain-containing protein

NOX2 Nicotinamide adenine dinucleotide phosphate (NADPH) oxidase

PAS Para-aminosalicylic acid

PCR Polymerase Chain Reaction

PGE_2 Prostaglandin E_2

pH Potential of Hydrogen

PhD Doctor of Philosophy

PHOX phagocyte oxidase

PI_3P Phosphatidylinositol 3-phosphate

PMN Polymorphonuclear leukocytes

PPAR Peroxisome proliferator-activated receptor

PtpA Protein tyrosine phosphatase A

RAC1 Ras-related C3 botulinum toxin substrate 1

ROS Reactive Oxygen Species

SapM Secreted acid phosphatase M

SP-A Surfactant protein A

STING Stimulator of Interferon Genes

TB Tuberculosis

Th1 T helper 1

TLR Toll like receptor

TNF Tumor necrosis factor

TRAF6 TNF receptor associated factor 6

VPS33B vesicular protein sorting 33B

CHAPTER I

LITERATURE REVIEW

1. HISTORY of TUBERCULOSIS

Tuberculosis has been haunting the humankind for centuries. The etiologic agent mycobacteria were hypothesized to be existing since the Jurassic geological period nearly 150 000 years [1]. The initial analysis of mycobacterial DNA in human remains using various genotyping methods introduced the hypothesis that *Mycobacterium tuberculosis* (Mtb) emerged through zoonotic transmission of ancient *Mycobacterium bovis* during domestication of cows [2]. With the advent of whole genome sequencing and comparative genomic analyses, it was revealed that *M.bovis* is actually nested within a tree of human adapted lineage of *Mycobacterium africanum* which is restricted to Western Africa. In a recent analysis, the deepest origins of Mtb are traced back to ancestral species that are predominantly environmental and human pathogenesis arose by the occurrence of several transitions [3].

The earliest evidence of Mtb has been found in the bones of extinct bison from Wyoming, USA dating back to 17000 years ago by PCR sequencing and detection of mycobacterial lipids [4, 5]. The earliest human tuberculosis evidence was found in an infant and woman buried together in an Eastern Mediterranean village with evidence of agriculture and animal domestication dating back to 9000 years ago [6]. In ancient Greece, Hippocrates (460-376 BC) named the disease as "phthisis" which translates to wasting. He described phthisis as mostly fatal, with constant sweats but not diffused all around the body, attacked mainly young adults, occurred mostly in summer and autumn rather than acute respiratory infections of winter seasons, and recommended a special diet based on wine, bread and milk [7].

"White plague" surged to nearly 1000 deaths per 100 000 population across Europe and reported responsible for up to 25% of deaths in the 19th century. It was deemed as poor people's ailment; however, tuberculosis affected all layers of society while poverty was definitely exerting substantial effects [8]. A German physician Hermann Brehmer changed the course of tuberculosis treatment by housing the victims of tuberculosis in healthy havens, sanatoriums. He initially believed the disproportionate ratio of heart and lung sizes of his patients is the main reason and the constant low air pressure at high altitude would lead to enlargement of heart sizes. In 1854, the first facility for treatment of tuberculosis was constructed in Görbersdorf, Silesia on Sudeten Mountains with the help of his friend Alexander von Humboldt and it was called *Heilenstalt*

translated as a healing place. Such facilities were prevalent for the treatment of the disease over the next century and called sanitarium which comes from Latin *sanare* to heal [9].

French physician Jean Antoine Villemin proved the first time that tuberculosis was contagious by transferring tuberculous material from bovine and humans to rabbits and established an etiological link [10]. The prodigious event in tuberculosis history was the discovery of the cause of tuberculosis by the German physician Robert Koch on 1882 [11]. Robert Koch and Paul Ehrlich modified alcohol-methylene blue staining and the technique was finalized by Franz Ziehl and Friedrich Neelsen [12]. Using new staining method, Koch described that the culprit bacteria are rod-shaped looking similar to leprosy bacilli and present in a group within the lesions. Besides that, Koch was also successful to isolate Mtb and culture them from infected guinea pigs, bovine, and humans. Koch proved his postulates that;

i) The infectious agent of tuberculosis was observed in tuberculous lesions but not in other lesions or in healthy tissues.
ii) Mtb was isolated from a diseased organism and cultured *in vitro* outside the infected organism.
iii) After growing *in* vitro, the cultured Mtb caused disease when reintroduced into a healthy animal, causing tuberculous lesions.
iv) The infectious agent was then reisolated from the inoculated, diseased host and identified as being identical to the original agent.

Koch also observed that non-inoculated guinea pigs that were housed in the same room with infected guinea pigs showed signs of tuberculosis which proved the airborne route of transmission for Mtb. A few years after Koch identified Mtb, he reported on an inexplicable substance that can alleviate tuberculosis. He revealed that the substance was purified from Mtb supernatant grown in vitro that is currently known as tuberculin. Despite his unsuccessful attempts to prove tuberculin ameliorates the disease, it became a key component of tuberculosis diagnostics that is still used widespread nowadays. Robert Koch was granted the Nobel Prize in Physiology or Medicine in 1905 for his investigations and discoveries in tuberculosis field.

Although Koch was unsuccessful with his hypothesis about tuberculin, French physician Charles Mantoux described the use of cannulated syringe and needle to inject tuberculin intracutaneously which would lead to a reaction in individuals that are latently infected, not manifesting tuberculosis symptoms. Mantoux test, aka tuberculin skin test, was first described in

1908 led to an understanding of much of physiopathology of tuberculosis infection and is still widely used with well standardized purified protein derivative injections.

Perhaps French physician Albert Calmette and veterinarian Camille Guérin had more substantial effects among early 20th-century tuberculosis researchers in terms of public health. They used the organism known as *Mycobacterium bovis* (M.bovis) which was isolated from tuberculous cow to develop a vaccine. However; they were stymied by the presence of clumps in their liquid culture and they added ox bile to prevent clumping which resulted in a consequential decrease in virulence in M.bovis infected guinea pigs [13]. With their laborious effort, the bacteria were subcultured more than 200 times between 1908 and 1921. The first human Bacillus Calmette Guérin (BCG) vaccine recipient was a 3-day old infant whose mother died of tuberculosis just after birth and grandmother had smear-positive tuberculosis. After three doses of oral administration of BCG vaccine, the infant did not show any signs of tuberculosis at 6 months in spite of constant exposure from the grandmother. Over the following 7 years, 100 000 children were vaccinated in Europe and the vaccine was used United States, Canada, and all the countries in South America [14].

As the housing and nutrition standards started to improve in early 20th century, the death toll started to drop before the onset of treatment with antituberculosis drugs. Edward Livingston Trudeau was one of the noteworthy scientists in the history of the fight against tuberculosis in the late 19th and early 20th century. After contracting the disease, he established Saranac Laboratory for Study of Tuberculosis later renamed Trudeau Institute as the first research organization to study tuberculosis in the United States. He performed many experiments with tubercular rabbits to study the efficacy of different treatment options. He pointed out the significance of chemotherapy for tuberculosis in an article published after his death from tuberculosis. “My faith in the possibilities of chemotherapy for tuberculosis is based simply on what Ehrlich has demonstrated as possible in syphilis --namely, that a chemical compound could be discovered which killed the germ without injuring the cell… Such an agent, when properly used, would prove of great value in the treatment of this disease.” [15]. As a side note, Paul Ehrlich whom Trudeau mentioned in his excerpt, is 1908 Nobel Prize laureate in Physiology and Medicine for his contributions in the field of immunity and his laboratory discovered first antibacterial, Salvarsan for the treatment of syphilis in 1909. Salvarsan was the first sensational victory of a systemic chemotherapy against a microorganism.

Year	Historical Step
1854	Hermann Brehmer established the first anti-tuberculosis sanatorium in Görbersdorf, Poland.
1869	Jean Antoine Villemin proved tuberculosis is contagious by injecting tuberculous matter from human cadavers to rabbits.
1882	Robert Koch reported that the disease was caused by an infectious agent.
1894	Edward Livingston Trudeau established the first center to study tuberculosis in Saranac Lake, New York.
1906	Albert Calmette and Camille Guerin developed attenuated Mycobacterium bovis strain as BCG vaccine.
1944	Albert Schatz and Selman Waksman discovered streptomycin
1946	Jorgen Lehmann discovered para-aminosalicylic acid (PAS)
1951	Three independent groups in Squibb Institute New Jersey, Hoffmann-La Roche and Bayer reported anti-tuberculosis drug, isoniazid.
1952	Sir John Crofton revolutionizes TB chemotherapy by introducing streptomycin + para-aminosalicylic acid+ isoniazid combination therapy
1956	Commencement of Madras study
1961	Ethambutol was discovered
1966	Rifampicin was introduced to TB drug pipeline

Table 1.1: Historical landmarks in tuberculosis research and treatment

The governing theory during sanatorium era was that if the rest was beneficial for tuberculosis patients, rest of tuberculous lungs might be beneficial, too. Thus, novel therapeutic interventions like artificial pneumothorax aiming pulmonary collapse were introduced. The physicians forced nitrogen or air into the pleural cavity resulting in collapsing of the lung, cavity closure and sputum conversion to negative. Although pneumothorax method was not rigorously checked for efficacy, the first study from Denmark illustrated that 191 sputum-positive patients that received artificial pneumothorax intervention between 1925 and 1931 resulted in 107 successful cases [16]. The other collapse therapies which were used for treatment of cavitary pulmonary tuberculosis were artificial pneumoperitoneum (increasing intraperitoneal pressure by administering air and elevating diaphragm), thoracoplasty (surgical removal of several rib bones), plombage (creating

cavity underneath the rib cage and filling with inert material like olive oil or Lucite ball), phrenic nerve crush (cutting off the nerve to diaphragm that is paralyzed, remains in relaxed and elevated state) and pulmonary resection which is presently still effective for drug-resistant cases.

With the onset of antituberculosis chemotherapy, lung collapse therapies and sanatoriums were starting to become expendable. Most of the sanatoriums were closed by 1960s; furthermore, patients receiving treatment promptly became non-infectious showing efficacy of ambulatory treatment. The Madras study which was designed to compare the treatment of patients with 12 months at home or in sanatorium showed no difference between hospital care and home treatment in either treatment outcomes or infection of household contacts [17].

American chest physician Corwin Hinshaw and his collaborator veterinarian William Feldman are the pioneers of the chemotherapy against this global scourge. They developed a guinea pig model of tuberculosis that enabled them to check the efficacy of candidate compounds meticulously. The first candidate was developed in 1940, dapsone-derived compound promine, was successful in guinea pigs, had promising results in first human trials; however, the drug did not convince National Tuberculosis Association to be introduced as a first anti-TB drug. Nonetheless, the drug was shown to favorably cure leprosy and became the treatment of choice [18]. The history of tuberculosis treatment was changed by the discovery of streptomycin, first bactericidal chemical effective against *Mycobacterium tuberculosis* to be later used in humans. Russian biochemist Selman Waksman and his Ph.D. student American microbiologist Albert Schatz discovered streptomycin in Rutgers University, New Jersey [19]. Waksman later sent a limited amount of streptomycin to Hinshaw and Fendman to check in Mtb infected guinea pigs. Their first result conclusively reported that streptomycin would arrest and at times eradicate tuberculous lesions in guinea pigs [20]. British Medical Research Council reported the first controlled trial of streptomycin on TB patients by randomly assigning them streptomycin plus bed-rest or bed-rest only groups. After 6 months of treatment; 51 of 55 (93%) streptomycin-treated patients versus 38 of 52 (73%) control group patients survived [21]. After 5 years, another Medical Research Council trial did not find any significant differences between streptomycin-treated and control arms by virtue of the acquired streptomycin resistance of the bacilli [22].

Swedish physician and chemist Jörgen Lehmann was a skilled scientist to work on metabolism on tubercle bacillus. With the hint of previous work done on salicylates, he discovered that salicylates increased the oxygen consumption of pathogenic strains in culture but not non-

pathogenic BCG strain [23]. In an accompanying article, he tried nearly 50 derivatives of salicylates to find competitive inhibitors with the idea that these inhibitors might have bacteriostatic effects. He discovered para-aminosalicylic as a potent anti mycobacterial agent in culture, in rats and in two TB patients [24]. Although PAS was discovered earlier than streptomycin, the acceptance by Swedish authorities slowed its introduction of treatment for tuberculosis.

Three independent groups, scientists from Bayer Chemical in Germany, Hoffman-La Roche, and Squibb in the United States, discovered efficacious, safe and inexpensive wonder drug isoniazid extraordinarily at the same time in 1951. Time-consuming and tortuous patent war was luckily avoided since it was noticed that two Czech Ph.D. students synthesized the drug without knowing its profound potential in TB treatment 40 years earlier [25]. After the introduction of isoniazid into TB drug pipeline, many trials were conducted to optimize the triple therapy which consisted of oral isoniazid with PAS for 18 to 24 months and intramuscular streptomycin injection for the first 6 months. This regimen was called "Edinburgh Method" which was pioneered by Sir John Crofton and his team at Edinburgh University and it formed the basis of today's TB drug regimens.

The manifestation of side effects, the emergence of drug resistance and the increasing burden of tuberculosis incidents motivated TB drug development. In 1961, a synthetic compound ethambutol was found to be comparable with isoniazid when given orally and comparable with streptomycin when given parenterally in mice. It was effective on isoniazid and streptomycin resistant mycobacteria [26]. Initially, ethambutol was administered in retreatment cases and was found to be well-tolerated compared to PAS. Clinical trials showed that low doses of ethambutol were as effective as standard PAS dosage in sputum conversion which provided less bulky, better tolerated and less expensive alternative to physicians [27].

Rifamycins were first synthesized naturally from bacterium *Amycolatopsis rifamycinica* which was isolated from soil samples in southern France in 1957 [28]. Rifampicin is the synthetic orally active form of rifamycin SV. Rifampicin was first introduced in clinical trials in 1966 and in the next decade, it became the essential component of TB regimens. Treatment with rifampicin plus isoniazid supplemented by ethambutol for first two months decreased therapy duration to 9 months with decreased relapse rates in 1976 clinical trial completed in Britain [29].

In late 1940s nicotinic acid was found to markedly suppress the spread of tuberculosis on experimentally infected Swiss mice [30]. Later pyrazinamide (nicotinic acid analog) was discovered to be bacteriostatic only in acidic pH. Initial clinical trials showed that pyrazinamide was equally as effective as PAS in combination treatments with isoniazid; however, hepatotoxicity was a significant side effect of pyrazinamide treatment. Hence, it was not recommended for use in the initial phase of TB treatment [31]. Singapore Tuberculosis Service and British Medical Research Council trial result announced in 1979 showed that two months intensive phase of streptomycin, isoniazid, rifampicin, and pyrazinamide followed by 4-month isoniazid and rifampicin continuation phase was very effective in TB treatment [32]. Additional antimycobacterials; cycloserine [33], ethionamide [34], kanamycin [35], capreomycin [36] developed during late 1950s played important role in drug-resistant cases.

2. TUBERCULOSIS: CURRENT SITUATION and INSIGHTS

Despite the discovery of first anti-tuberculosis drugs more than 70 years ago, tuberculosis still accounts for 1.5 million deaths each year. In 2014, there were estimated 9.6 million new cases of active tuberculosis worldwide (5.4 million men, 3.2 million women, and 1 million children). Among 9.6 million people fallen sick with TB, estimated 1.2 million people were co-infected with HIV. TB killed 1.5 million people including 390 000 deaths among HIV-infected patients showing a slight decrease from peak numbers in the mid-2000s [37]. It is predicted that there were 480 000 multi-drug resistant tuberculosis cases defined as resistance to at least rifampicin and isoniazid, the two most efficacious anti-TB drugs. More than 40% of these cases were reported in India, China, Russia, Ukraine, and the Philippines. A total of 105 countries has reported extensively drug-resistant cases defined as multidrug resistance plus resistance to at least one fluoroquinolone and any of three second-line injectables, kanamycin, amikacin and capreomycin. Nearly 9.7% of multi-drug resistance cases were extensive drug-resistant with Belarus (29%) and Lithuania (25%) being highest. Sub-Saharan African countries have the highest estimated TB incidence rates, driven mainly by HIV epidemic. The absolute number of TB cases is highest in Asian countries, China, India, and Indonesia having the greatest epidemiological burden of the disease globally. In Western highly developed countries, the considerable amount of cases occur in foreign-born residents and immigrants from TB endemic countries [38].

Active pulmonary tuberculosis patients are the source of Mtb. Nearly 90% of individuals infected with Mtb, they contain the pathogen as asymptomatic latent infection and they have 10%

chance of developing active disease in their lifetime. Some individuals may eliminate acute Mtb infection according to recent studies [39]. There are 2 billion people latently infected with Mtb on the estimate and are at risk of TB reactivation. Interestingly; latently infected individuals much lower risk of progressive tuberculosis on repeated exposure than uninfected individuals [40]. In contrast, individuals treated successfully for TB are associated with increased risk of developing TB from reinfection than new cases of TB [41].

3. TUBERCULOSIS IMMUNOPATHOLOGY

The immunopathological hallmark of Mtb infection is the granuloma. To simply define granuloma, it is organized collection of mononuclear phagocytes, neutrophils, and lymphocytes (Figure 1.1). Granuloma formation initiates when inhaled bacilli interact and are phagocytosed by alveolar macrophages which are sentinel cells of the lung. Activated macrophages release cytokines and chemokines to attract neutrophils instantly. Monocytes from blood circulation are also recruited to the site of infection and differentiate into macrophages. The professional antigen presenting dendritic cells also arrive at the site of infection to phagocytose bacterial antigens, live bacteria or dying cells by efferocytosis which later to be transferred to the lymphatic system and draining lymph nodes. Since each type of cells' killing effector functions varies, the survival of Mtb differs in these cell types as the fate of the infected cell. All things considered, the initial response of these innate cell types is insufficient for the control of Mtb replication which occurs exponentially until the adaptive immune response call into action. The onset of adaptive response fully potentiates effector functions of infected macrophages which can control the bacterial replication. CD4+ Th1 lymphocytes have been thought to be a principal component of adaptive immunity to TB. However, B lymphocytes, CD8+ T lymphocytes, Th17 lymphocytes, regulatory T lymphocytes and other non-canonical T cells (iNKT cells, group I CD1- restricted T cells, mucosal associated invariant T cells and γδ T cells) appear to have a more appreciated role in TB immunity. The actual role of these cells and definite percentage of these cell populations required for resolution versus immunopathology is still needed to be studied elusively [42].

Many different cell types act in concert or adversely to each other in granulomas which affect the fate of the pathogen within and host immunopathology. Initial studies of an autopsy on human TB patients categorized the granulomas into several distinct subtypes. The canonical TB granuloma is made up of organized macrophages, neutrophils enclosed by fibroblasts, epithelioid macrophages, multinucleated giant cells and a ring of lymphocytes in outside layer. The center of

granuloma may contain caseum which is a coagulated necrotic tissue material with its crumbly, cheese like white appearance on gross examination. If the mycobacterial replication is controlled by the host, the formation of caseum stops, the calcification, and fibrosis of the granuloma takes place over time. The necrotic, soft caseum is generally overladen with high numbers of bacteria. Enlargement of caseum, transformation into a liquefactive form of caseum, the breakdown of surrounding tissue, cavitation, deterioration into airways, dissemination of the bacilli and facilitating transmission into new hosts correlate with the progress of tuberculosis [43].

Foamy macrophages are specialized macrophage subsets that also appear in tuberculosis granulomas. Since their intrinsic abundance of lipid droplets, foamy macrophages serve as a nutrient source for Mtb. It is also known that phagolysosome maturation is delayed and the innate response is dampened due to polarizing towards alternatively activated phenotype in foamy macrophages which provides a safe haven for persistent bacilli phenotype [44]. Electron microscopy showed that Mtb-containing phagosomes move towards lipid bodies in foamy macrophages and lipid bodies can also contain bacilli. The formation of foamy macrophages can be driven by oxygenated mycolic acids and trehalose dimycolate from the bacilli [45].

Multinucleated giant cells are another population that can be found in TB granulomas. Multinucleated cells are formed by macrophage fusion and lipomannan derived from mycobacterial cell wall triggers multinucleation of macrophages [46]. It is proposed that these cells have reduced the ability to phagocytose mycobacteria, restriction on cell-to-cell spread of the bacilli and role in latency. Macrophages can also undergo distinct transformation into epithelioid cells which have firmly interlocked cell membranes to link neighboring cells. These cells are thought to make granuloma as effective containing structures. The role of epithelioid macrophages in Mtb fate and lesion outcome still needs to be studied.

There are a few host factors discovered to play role in granuloma formation. CXCR3 signaling on polymorphonuclear neutrophils (PMN) notably through MIG (CXCL9) partly controls early granuloma formation in low-dose aerosol infected C57BL/6 mice. CXCR3 $^{-/-}$ mice and PMN depleted mice had delayed and impaired granuloma formation without an impact on bacterial loads and survival. The role of CXCR3 signaling in granuloma formation is transient or complemented by other signaling mechanisms in later stages of infection; since CXCR3$^{-/-}$ mice are observed to have normal granulomatous responses in chronic TB [47]. Tissue residing non-hematopoietic

epithelial cells are also shown to act in early granuloma formation by augmenting matrix metalloproteinase (MMP-9) secretion in combination with infected macrophages in transparent

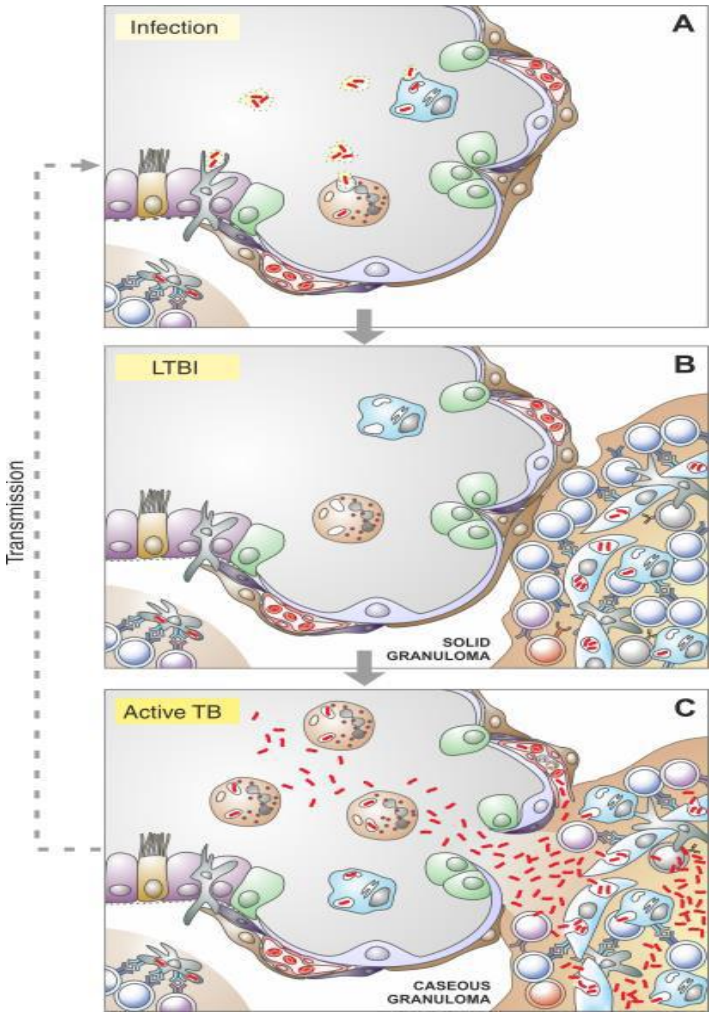

Figure 1.1: **Different stages of tuberculosis immunology and pathology.** (A) After Mtb (red rod) makes its way to alveoli, it is engulfed by an armada of sentinel alveolar macrophages (blue) and neutrophils (orange) in alveolar space and dendritic cells in epithelial lining. Dendritic cells are professional antigen presenting cells which migrate into draining lymph node to initiate adaptive immune responses. (B) During latent tuberculosis infection (LTBI), highly structured solid granulomas are formed that Mtb is contained in mononuclear phagocytes in the central and lymphocytes on the periphery. (C) In the course of active TB, granulomas disorganized and central necrosis occurs which leads to the formation of caseous granuloma. Subsequently, Mtb can easily replicate in caseum, spread to other organs through the bloodstream and spread to the environment through rupture into alveolar space [48].

zebrafish larvae. It is hypothesized that by inducing monocyte migration into infection site through MMP-9 secretion from epithelial cells and infected macrophages, the permissive growth niche for mycobacteria is formed which leads to granuloma maturation and bacterial survival [49]. Data from MMP-$9^{-/-}$ mice also confirm that it is required for early recruitment of macrophages through MCP-1 (CCL2) signaling, tissue remodeling and eventual maturation of granulomas [50]. Tumor necrosis factor alpha (TNF) plays a critical role in the formation and stability of granulomas in murine studies contributing to uncontrolled bacterial growth [51]. Macaque studies revealed that TNF is more important in intra-granulomatous events like macrophage activation and chemokine production rather than formation or maintenance of granulomas [52]. The diverse macrophage response effects of TNF are in coordination with interferon-γ (IFNγ) including controlling autophagy and release of antimicrobial peptides (i.e. cathelicidin and β-defensin 4) to curtail Mtb replication. The other key role of TNF is deciding the cell death fate of infected macrophages in granulomas. In initial stages of granuloma formation, mycobacterial ESX-1 secretion system mediated apoptosis is in favor of mycobacterial dissemination through recruitment and infection of monocytes. However; attenuated Mtb strains (H37Ra, BCG and attenuated live Mtb vaccine MTBVAC) are unable to promote colonization of newly recruited cells into granulomas [53]. In later stages of solid granulomas or during latent infection, there is clinical evidence that the role of TNF is skewed through the host advantage that anti-TNF neutralization therapies in latently infected rheumatoid arthritis patients result in TB reactivation [54]. Excessive levels of TNF can increase susceptibility to Mtb infection through reactive oxygen species (ROS) mediated programmed necrosis or necroptosis which illustrates that TNF is the crucial mediator of inflammation and bacterial clearance in tuberculosis immunopathology [55].

It is regarded that latently infected individuals harbor fibrotic granulomas conventionally; whereas TB patients develop necrotic and liquefied granulomas. Non-human primate models of tuberculosis unraveled that these temporal changes might be more subtle and nonlinear. Recent research on cynomolgus macaques demonstrated a spectrum of granulomas in latent infection with necrotic types and non-necrotizing, fibrocalcified granulomas in macaques with clinically active TB [56]. Furthermore, individual granulomas behave differently within the same host. It is suggested that bacterial numbers in each granuloma can differ significantly within a single macaque. Animals with active disease and latent infection have similar killing effector potential in individual lesions, but there is a predominance of lesions of extensive pathology with limited

killing functions in macaques with active disease [57]. There are still many unknowns about the factors that drive the fate of each granuloma and there is governing view that the outcome of Mtb infection is decided on local granuloma level rather than systemic level. It appears that local balance of T cells producing IL-10 in combination with T cells producing IL-2, TNF or IL-17 is associated with sterility and limit tissue pathology in macaques [58]. It should also be equally considered that diverse bacterial populations can exist in different granulomas which add extra complexity to elucidate heterogeneity in TB lesions.

Plasticity and flexibility are the key features of macrophages. Mtb infection alters the transcriptional and functional landscape and polarizes them towards classical phenotype. Classically activated macrophages activate their antimicrobial effector functions and facilitate Th1 response by releasing pro-inflammatory cytokines like TNF, IL-12, and IL-1. As it generally occurs in the immune system, classical activation is counterbalanced by alternative activation of macrophages which are poorly associated with antimicrobial functions. However; alternatively activated macrophages are primal for wound healing and resolution [59]. Human alveolar macrophages in the steady state do not clearly fit into classically or alternatively activated macrophage phenotype. They are essential for hoovering and phagocytosing the inhaled bacteria which later leads to initiation of the strong inflammatory response, but also they are required for dampening of inflammatory signals and resolution of lung inflammation [60].

Mtb retains many pathogen-associated molecular patterns that can activate Toll-like receptor, C-type lectin receptor, and NOD-like receptor signaling which in turn skew the macrophages in the classically activated state. Furthermore; it is evident TB granulomas includes both classically and alternatively activated macrophages that $Arg1^{high}$ anti-inflammatory macrophages on outer layers and $iNOS^{+}Arg1^{low}$ pro-inflammatory macrophages are situated towards the center where the bacilli burden is high [61]. It is also hypothesized that the ratio of classically activated to alternatively activated macrophages can be predictive of bacterial burden within each granuloma. Researchers tested this hypothesis by implementing a computational model to measure granuloma polarization ratio by averaging macrophage polarization scores over entire granuloma [62]. Although classical macrophage activation skewing Mtb components are relatively well studied; there has not been any virulence factor or signaling mechanisms of Mtb that polarizes macrophages into an alternative state defined yet. It is also possible that host derives alternatively activated macrophages to dampen excessive immunopathology. This phenomenon is partly shown *in vitro*

macrophage BCG infection model in which IL-6, IL-10, and G-CSF can signal in an autocrine/paracrine manner to induce Arg1 in macrophages [63].

4. MTB AND MACROPHAGE INTERPLAY

As it is known at the systemic level, there needs to be balanced response in macrophage level that reduced and enhanced inflammatory responses can both favor Mtb replication. The diminished response can result in limited activation and antimicrobial functions which can lead to increased intracellular bacilli burden. The exaggerated response can stimulate recruitment of Mtb-permissive mononuclear phagocytes, excessive cell necrosis and extracellular replication of the bacilli. The clearance of bacteria or the permissiveness to bacterial replication is determined by immune recognition signals, response to innate and adaptive immune mediators (cytokines and chemokine), cell-autonomous effector mechanisms including oxidative and nitrosative stress, acid exposure and lysosomal killing, immune and non-immune GTPases, ubiquitination and autophagic clearance, antimicrobial peptides, competition for iron, zinc, manganese, magnesium and copper cations, competition for carbon and amino acid metabolism and IDO which is a rate-limiting enzyme in tryptophan metabolism (Figure 1.2) [64].

Macrophages recognize Mtb by their pathogen-associated molecular patterns or in other words; microbe-associated molecular patterns that occur on the plasma membrane, intracellular vesicle, and cytosol. Cell membrane pattern recognition receptors include Mannose Receptor, Mincle, Dectin-1, Dectin-2, Macrophage C-type Lectin (MCL), DC-SIGN, Scavenger Receptor A, MARCO which also bind Mtb to initiate the phagocytosis. Toll-like receptor family receptors that recognize Mtb consist of TLR1/TLR2 heterodimer, TLR2/TLR6 heterodimer, TLR4 and TLR9 (Figure 1.3). In the cytosol, Nucleotide-binding oligomerizing domain-1 (NOD1) recognized diaminopimelic acid (DAP) from peptidoglycan fragments, NOD2 recognizes muramyl dipeptide and galectin-3 sense β-galactosides. In a recent study, Stimulator of Interferon Genes (STING) was discovered to be a receptor for cGMP-AMP which is generated by cGMP- AMP Synthase (cGAS) from microbial DNA and transported into cytosol, in turn induces type I signaling [65]. Humoral immunity components can also recognize Mtb, cover the bacterial surface, by that opsonize the bacilli and bind their receptor in order to promote indirect recognition of Mtb. Surfactant protein A (SP-A), SP-D, mannose-binding lectin (MBL) and complement system components; C1q, C3, C3b facilitate opsonization of Mtb. If the individual encountered Mtb

antigen before through either infection or vaccination, the invading pathogen can also be opsonized by specific antibodies which in turn bind $F_c\gamma$ receptors. Receptor signaling initiates receptor-mediated phagocytosis, secretion of pro-inflammatory cytokines and chemokines and functioning anti-microbial effectors.

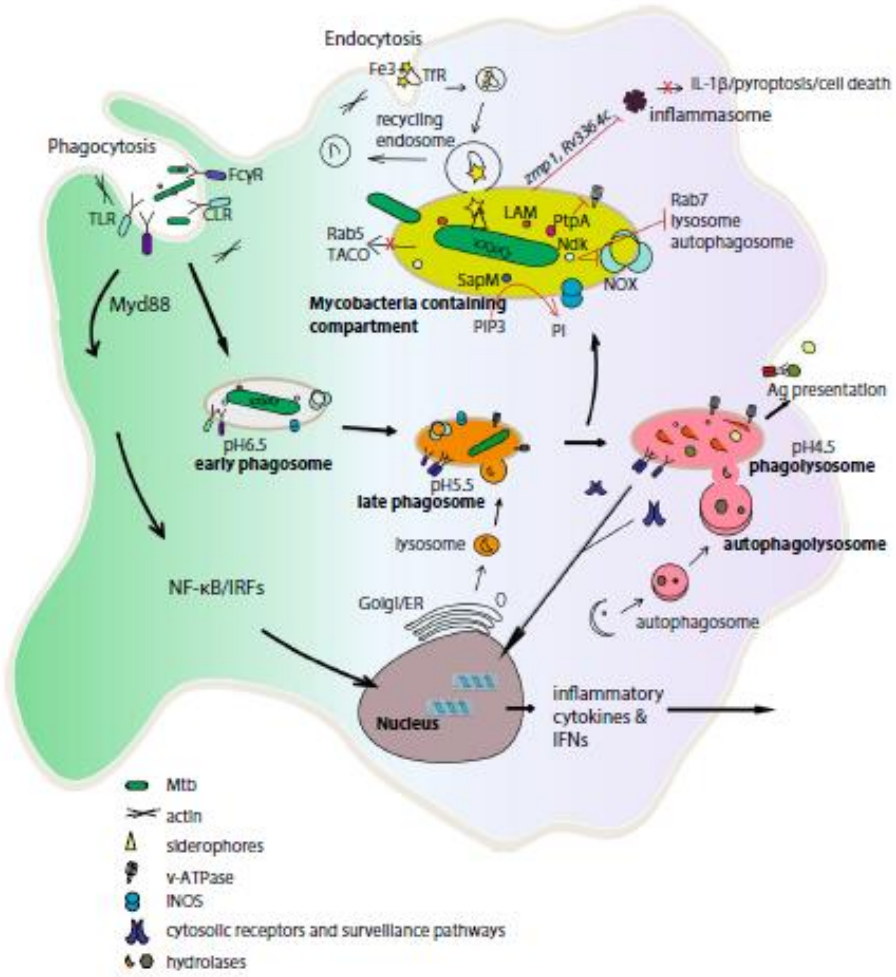

Figure 1.2: Mycobacterial evasion strategies in macrophages. Mtb is phagocytosed by a myriad of recognition receptors and directed to lysosomal degradation through phagosomal maturation and acidification. Virulent mycobacteria are known to interfere with maturation and phagolysosome fusion. Mtb faces iron starvation once inside the phagosomes; however, can access through transferrin receptor in recycling endosomes. Mtb detection by various cytosolic and membrane-associated sensors can activate autophagy to eliminate the bacteria through encapsulating Mtb-containing compartment or free cytosolic Mtb by a double membrane, i.e. autophagosome which later merges with lysosomes [66].

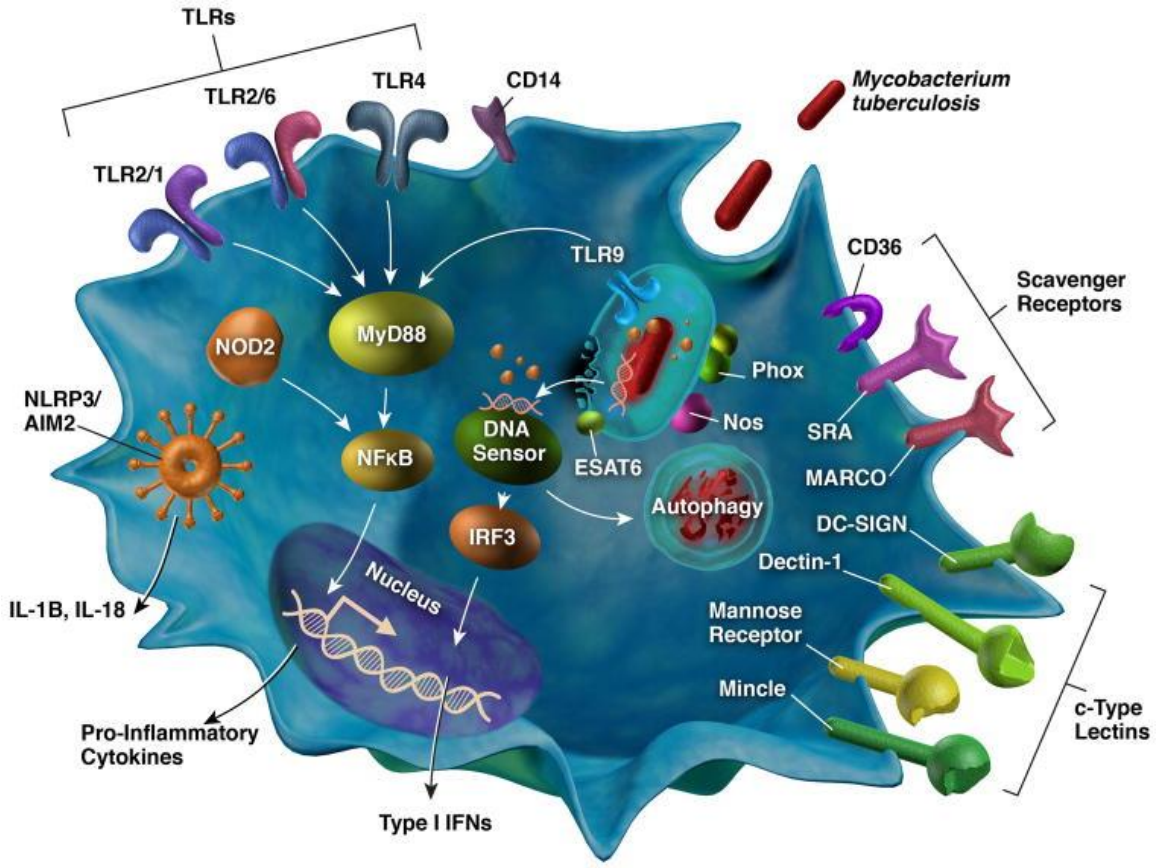

Figure 1.3: Pattern recognition receptors involved in Mtb sensing. Membrane-associated receptors include Toll-like receptor (TLR), C-type lectin and scavenger receptor classes. Cytosolic receptors sense secreted Mtb virulence factors, cell wall components or mycobacterial DNA accessed to cytosol after phagosomal rupture by ESAT6. IRF3 and NFκB are major transcription factors activated by these surveillance pathways. Inflammasome and autophagy activation are also shown as crucial macrophage responses to limit bacterial replication [67].

Macrophages employ myriad ways of killing processes to ingest invading microorganisms. The hallmark of these functions is phagosome maturation that phagosomes interact with lysosomes and endosomes resulting in an exchange of solute materials and membrane components. Fusion of these organelles allows acidification of pathogen-containing phagosomes through the acquisition of v-ATPase hydrogen pumps, accumulation of proteolytic lysosomal hydrolase enzymes and reactive oxygen species. Mtb is able to evade killing machinery and contrive to persist in

macrophages [68]. The two essential ways are circumventing acidification of phagosomes and the fusion of phagosomes with lysosomes. Although there has been much debate before, it is now widely accepted that Mtb escapes phagosomal milieu and translocates to the cytosol [69]. Phagosome maturation blocking permits Mtb to thwart lysosomal degradation and downstream immunologic events like antigen presentation to mount an adaptive immune response.

Mtb secreted phosphatases, PtpA and SapM, is shown to block phagosome maturation by interfering with host signaling cascades. PtpA is indispensable for the pathogenesis of Mtb in macrophages. Host vesicle trafficking protein vesicular protein sorting 33B (VPS33B) was captured to be the target of PtpA by immunoprecipitation methods [70]. VPS33B is a subunit of Class C vacuolar protein sorting (VPS) complex and dephosphorylation of VPS33B by PtpA induces phagosome maturation arrest. Another target of PtpA is subunit H of macrophage v-ATPase. PtpA binds in a non-catalytic manner and deranges phagosome pump assembly [71]. Lysosomes deliver v-ATPase to phagosomes amidst phagosome maturation which regulates proton transport across the membrane and decreases phagosomal pH from 6.5 to around 4.5. SapM is a lipid phosphatase and it hydrolyzes phosphatidylinositol 3-phosphate (PI_3P). PI_3P provides a signature membrane tagging signal, designating phagosomes into maturation [72]. It is no surprise that this evolutionarily successful pathogen developed multiple ways to interfere with the hallmark killing mechanism of macrophages.

Reactive oxygen species (ROS) are effective microbicidal agents that can kill intracellular pathogens. ROS are synthesized by NADPH oxidase (NOX2) which consists of phagosomal transmembrane proteins $gp91^{phox}$, $gp22^{phox}$, catalytic subunits $p40^{phox}$, $p47^{phox}$, $p67^{phox}$ and small GTPase Rac1. For NOX2 to be functional all members need to be translocated into phagosome and assembly around $gp91^{phox}$ which later transfer electrons from cytosolic NADPH to phagosomal oxygen and resulting in superoxide. Superoxide can be converted into active microbicidal agents hydrogen peroxide, hydroxyl radicals and peroxynitrite when reacts with reactive nitrogen intermediates. NOX2 is a crucial innate response enzyme, still, it has found to be linked with macrophage apoptosis which paves the way for adaptive immunity. It has been recently found that a GTPase activating protein of Mtb, nucleoside diphosphate kinase (Ndk) interacts with Rac1 and blocks NOX2 assembly which in turn increases Mtb survival in phagosomes. nuoG is found to be another virulence factor of Mtb which interferes with the NOX2 generation of phagosomal ROS and TNF-mediated apoptosis of infected macrophages [73].

To evade adaptive immune surveillance, Mtb targets antigen presentation on macrophages. $CD4^+$ T cell activation is mediated through the presentation of Mtb antigenic peptides on MHC II molecules that later induces the release of pro-inflammatory cytokines from T cells and enhances microbicidal functions of macrophages. A recent paper controversially claimed that cytokine diffusion from $CD4^+$ T cells is dispensable for Mtb control *in vivo*; however direct recognition of MHC II-antigen complexes are required. Researchers used MHC II bone marrow chimeras to compare bacterial burden in myeloid cells that can be recognized ($MHCII^{+/+}$) or incapable of recognition ($MHCII^{-/-}$) by $CD4^+$ T cells. In their experimental setup $MHCII^{+/+}$ cells had the significantly lower bacterial burden and $CD4^+$ T cell depletion increased the burden in $MHCII^{+/+}$ cells but not in $MHCII^{-/-}$ cells [74]. The results actually implicate that TB vaccine development should focus on augmenting direct recognition of infected cells by CD4 effector T cells rather than inducing polyfunctional (multiple cytokine secreting) CD4 effector T cells. Indeed, Mtb has developed different strategies to down-modulate macrophage-T cell interaction.

Attenuated expression of MHC II molecules is the primary strategy of Mtb is to diminish antigen presentation and alter CD4 T cell priming. Interestingly, Mtb lysate can downregulate MHCII expression, meaning that Mtb viability is not requisite. Cell wall lipoproteins LpqH (also known as 19 kDa lipoprotein), LprG and LprA were shown to down-modulate MHC II expression [75]. These lipoproteins function as TLR2 agonists and chronic TLR2 stimulation leads to MHC II expression inhibition. The most detailed studied one is LpqH that targets and suppresses transcription factor C/EBP mediated MHC II transcriptional transactivator (CIITA) expression [76]. Intriguingly, the much earlier study found that LpqH is exported from Mtb-containing phagosomes through cytosol which would make it available for sustained TLR2 stimulation and prolonged MHC II downmodulation [77]. Another Mtb virulence factor, a DNA methyltransferase Rv2966c is also shown to target transcription of C/EBP through translocation into the nucleus, methylation of non-CG DNA, interacting with histone H3 and H4 tails thereby repressing transcription of host protective genes [78]. These evasion strategies are not limited to macrophages; a recent study found that Mtb cell envelope associated serine hydrolase Hip1 impairs antigen presentation and maturation of dendritic cells which are the professional antigen-presenting cells [79].

Along with MHC II gene expression, Mtb also interferes with maturation and trafficking of MHC II molecules to diminish antigen presentation. Earlier studies showed that IFN-γ induced

cell surface expression of HLA-DR in human monocytic cell line THP-1 was attenuated in Mtb infection and this interference occurred in the transport of class II molecules from trans-Golgi network to endosomal and lysosomal vesicles [80]. Cathepsin S was later found to play important role in maturation and surface expression of MHC II. Cathepsin S is a lysosomal hydrolase that is responsible for removal of invariant chain (Ii) and processing into class II-associated Ii peptide (CLIP). When THP-1 cells were infected with BCG, IL-10 expression was induced, thereby limiting expression of cathepsin S [81]. IL-10 is an anti-inflammatory cytokine that dampens excessive Th1 responses to minimize tissue damage. However; overabundant IL-10 expression can be favored for Mtb to evade immune responses, the maturational arrest of class II molecules in this case.

Autophagy is a conserved cellular process that digests potentially harmful macromolecules and organelles which are not possible to be degraded by proteasomes. It plays a dual role in defense against Mtb by both inhibiting intracellular Mtb growth and restricting excessive inflammatory responses; in other words antibacterial and anti-inflammatory. Atg5 is one of the central genes in the execution of autophagy and by utilizing $LysM^{cre}Atg5^{flox/flox}$ mice (macrophage and neutrophil-specific deletion of Atg5 gene), researchers concluded that autophagy is bona fide protection mechanism against tuberculosis. When infected with Mtb, $LysM^{cre}Atg5^{flox/flox}$ mice showed increased release of IL-1α from macrophages, elevated Th17 response, neutrophilic infiltration, tissue necrosis and higher bacterial burdens in the lungs compared to littermate controls [82]. IFN-γ induces Interferon Response Genes (Irg) that are mainly involved in autophagy and reduction of intracellular bacillary load. Many autophagic markers are found to be associated Mtb-containing phagosomes. Induction of autophagy by starvation increases the acidification and maturation of phagosomes [83]. While IFN-γ and TNF-α induce autophagy, Th2 cytokines IL-4 and IL-13 inhibits starvation-induced autophagy, autophagic phagolysosome maturation and autophagy-dependent bacterial killing in Mtb-infected human and mouse macrophages [84]. Counteracting on autophagy pathway is a means of action for Th2 cytokines to inhibit Th1-mediated protection in Mtb infection. Mtb also targets autophagy pathway by its virulence factors. It is shown that ESX-1 secretion system is responsible for the arrest of autophagosome maturation in dendritic cells [85]. Since autophagy promotes MHC Class I and MHC Class II-dependent antigen presentation and activation of T cell responses, targeting autophagy pathway is a valuable immune

evasion mechanism for Mtb. Vaccines that are enhancing macrophage autophagy pathway can be advantageous against latent TB infection.

Peroxisome proliferator-activated receptor (PPAR) family is a group of transcription factors in the superfamily of nuclear hormone receptors. The family consists of PPARα, PPARβ/δ and PPARγ [86]. PPARγ is abundant in alveolar macrophages and the deletion of PPARγ in alveolar macrophages results in increased expression of proinflammatory genes, i.e iNOS, IFNγ, Il12p40, Ccl3 and Cxcl10 in bronchoalveolar lavage cells [87]. The virulent H37Rv strain induces PPARγ upregulation in human monocyte-derived macrophages through mannose receptor which in turn increase Il8 and PGE_2 production. The knockdown of PPARγ increases TNF production and decreases bacterial replication [88]. The increased resistance of PPARγ knocked-down macrophages can also occur through reduction of lipid body formation since PPARγ antagonists are shown to inhibit lipid body formations in BCG-infected mouse peritoneal macrophages [89]. Modulation of PPARγ pathway through selective molecules has been pursued in type II diabetes with a recent ongoing interest in host directed adjunct therapies in tuberculosis [90].

microRNAs are endogenous, small (~22 nucleotides) non-coding RNA species transcribed in primary miRNA (pri-miRNA) form in inter- or intragenic regions of the chromosome. They are highly conserved among mammals and mediate crucial gene regulatory events by pairing with target mRNA of protein coding genes which result in a decrease in mRNA abundance or translational efficiency [91]. There are myriad of miRNA targets and functions identified during Mtb infection. let-7f is downregulated in Mtb-infected macrophages in ESAT-6 dependent manner. let-7f targets a deubiquitinating enzyme A20 which is a negative regulator NFκB activity, thereby fine tuning inflammatory signals in infected macrophages [92]. miR-17 is found to regulate autophagy by targeting autophagy suppressor Mcl-1 and its transcriptional activator STAT3 [93]. miR-155 is also found to regulate autophagy by targeting autophagy suppressor protein Rheb and promote maturation of mycobacterial phagosomes [94]. miR-124 targets TLR6, Myd88, TRAF6 and TNF in murine alveolar macrophages to alleviate pathogen-induced inflammatory responses [95]. miR-132 and miR-26a target transcriptional coactivator p300 which is a mediator of IFN-γ response genes in Mtb-infected human macrophages [96]. On the other hand, miR-29 is found to directly target IFN-γ transcripts in T lymphocytes and natural killer cells. The transgenic mice with sponge miR-29 sequence (miR-29 knockdown mice) show increased resistance to BCG and H37Rv strain [97]. miR-223 directly regulates CXCL2, CCL3 and Il6

transcript levels which modulate inflammatory cell chemotaxis to lung and ablation of miR-223 renders mice susceptible to Mtb infection [98]. Modulation of miRNA expression levels during Mtb infection can help researchers to discriminate between healthy individuals, latently infected or active TB patients in whole blood or sputum samples [99-102]. miRNA mimics and anti-miRs (antagomir) based approaches also provide novel options for host-directed therapy.

Exosomes are small, 30-100 nanometer, extracellular vesicles that can play role in communication between cells or in pathogen dissemination. Exosomes can serve as disease biomarkers since they can be isolated from various body fluids like serum, bronchoalveolar lavage, urine, saliva and they can act on modulation of host immune response [103]. Exosomes released from Mtb-infected macrophages can have both innate and adaptive immune modularity activities. Over 40 immuno-dominant mycobacterial proteins including antigen 85 complex, ESAT-6, LpqH are found in these exosomes which can activate CD4 and CD8 T lymphocytes in vivo [104]. It is not well proven yet how naïve T cell activation occurs in vivo, however, the immune modularity effects of exosomes can occur by the presence of antigen-loaded major histocompatibility complex (MHC) Class II molecules on the surface of exosomes. Mtb infection augments ATP-triggered shedding of MHC-II molecules into microvesicles and exosomes which in turn present antigen to naïve T cells [105]. Exosomes from Mtb-infected macrophages can also transport mycobacterial RNA and biologically active host RNA. Exosomal RNA from Mtb-infected macrophages can elicit different immune responses than exosomal RNA from naïve macrophages in recipient macrophages. Interestingly Mtb-infected exosomal RNA also induces apoptosis in recipient cells possibly through the presence of mycobacterial RNA [106]. Exosomes can also provide cell-free vaccine opportunity in TB research since exosomes from Mtb culture filtrate protein treated macrophages can have similar efficacy as BCG vaccine and have better protection when boosting BCG-primed mice in low dose aerosol infection [107]. Nevertheless, the immune modulatory effects of exosomes in human tuberculosis still await further clarification.

TB pathogenesis is highly controlled by the bacilli's ability to subvert the macrophage innate responses. Mtb uses multiple and even overlapping strategies to hide and replicate within the human host. Manipulation of the macrophage response to Mtb is a promising new avenue for the treatment of infection and development of vaccines.

CHAPTER II

TRANSCRIPTOMICS OF MTB INFECTED MACROPHAGES

1. ROLE OF FUNCTIONAL GENOMICS TO UNDERSTAND IMMUNE RESPONSES

Whole genome sequencing of organisms, advancements in microarray technologies, RNA sequencing and proteomics have offered to scrutinize complex interactions in the cells that control essential biological processes. The emergence of "big data" has revolutionized the view in molecular biology from reductionism to non-reductionist systematic view of biological phenomena in the last decade. Reductionism tries to reduce the characteristics of a living organism to simpler constituents, as it was applied in early years of molecular biology. However; the biological phenomenon can only be explained as long as the components and the physiochemical interaction between these components are defined with unambiguous axioms [108]. As the popular statement indicates that the scientists are becoming to know "more and more about less and less". The colossal information gathered from various –omics technologies brings about the challenging question how best to understand complex biological systems. A new field, systems biology, has emerged as a consequence of -omics revolution to handle high-throughput data which in turn can yield an in-depth understanding of complex cellular networks.

The research in innate immunity has increased immensely to understand its importance as the first line of defense against infectious pathogens and elucidate its intricate interactions with the adaptive immune system which made the immunologists realize that innate responses are tightly regulated. Innate immunity is a complex network of signal transduction pathways which are activated by various stimulators rather than a small set of pathogen recognition receptor pathways [109]. A single ligand can activate various signal transduction cascades, albeit it is hardly proven that a pathogen can bear single ligand to establish infection. Conventionally, multiple ligands can bind to various receptors simultaneously and induce several signaling pathways. These pathways frequently cross-talk, regulate each other through positive and negative feedback loops and display diverse regulatory mechanisms [110]. Transcription factors form a regulation network to activate transcription of specific response genes downstream of these pathways. The significance of post transcriptional regulation; e.g. RNA splicing, polyadenylation, RNA editing, micro RNAs and long noncoding RNAs mediated regulation, and post translational regulation; e.g. ubiquitination,

phosphorylation, acetylation, glycosylation, and proteolysis, are also becoming increasingly appreciated. The physiological location and the environment of innate cells can also affect their responses to stimuli to a great extent. Stimulation by various cytokines and chemokines, growth factors or small lipid signaling molecules, and contact by neighboring immune and non-immune cells can have a profound effect on innate responses [111]. The presence of single nucleotide polymorphisms (SNP) can change the expression levels of specific genes or protein-protein interactions which add an extra layer of complexity in innate immunity at population genetics level [112]. The innate immune response does not solely depend on the regulatory pathways in host immunity. The pathogen can induce many virulence factors or alter its phenotype to resist in harsh environments. It is known that there are distinct differences in the whole transcriptome when macrophages are encountered with viable and nonviable Mtb underlining the fact that viable Mtb manipulating host responses through various virulence factors [113]. The interaction of Mtb with host microbiome can also change the innate response exhibited by the host [114]. The complex nature of innate immunity entails an elaborate and in-depth analysis presented by diverse systems biology techniques, in a nutshell. Systems biology includes approaching the scientific question in genomic, epigenetic, transcriptomic, proteomic, metabolomic, and interactomic level, collecting the data in a scientifically sound manner, incorporating bioinformatics and computational biology approaches and scrutinizing the perturbations in biological systems.

Whole transcriptome microarrays and RNA sequencing (RNA–Seq) are routinely used to analyze gene expression profiling. Microarrays have been the benchmark method to measure the gene expression levels simultaneously in a specific cell population, though they are limited by the probes deposited on the microarray chip. The seminal paper in tuberculosis field employing microarray is the first comparison of whole blood transcriptome of healthy individuals and active tuberculosis patients which revealed previously underestimated neutrophil driven Type I Interferon signaling in TB patients [115]. Rapid genome-wide sequencing provided by next generation sequencers have become favorable in recent years. In a recent South African study, the blood samples of latently infected adolescents were collected every 6 months and disease progression was monitored prospectively [116]. Whole blood transcriptome through RNA-Seq revealed a 16-gene disease progression signature which can be used a diagnostic tool to predict which latently infected individual is more likely to progress active TB. The full transcriptome sequencing approach remains expensive, demands rather larger amount of RNA and necessitates

a validation step through quantitative PCR (qPCR) for genes of interests. As in delineation of TB biomarkers, a signature panel of genes is tolerable rather than complete transcriptome to handle specific questions. Therefore, high throughput multiplex gene expression systems like Fluidigm and nCounter can offer cheaper alternatives to full transcriptomics approaches with low amounts of sample in TB diagnostics [117].

Transcriptomics at a single cell level brought attention to the matter of heterogeneity in homogenous populations that were considered to be uniform. Single cell RNA sequencing (scRNA-Seq) can allow the study of rare cell populations in the immune system by clustering whole transcriptomics profiles of immune cells and cataloging similar sets [118]. scRNA-Seq on bone marrow-derived dendritic cells revealed that there is considerable bimodality in gene expression, alternative splicing and regulatory circuit activation in response to lipopolysaccharide (LPS) [119]. These previously unobserved levels of heterogeneity can reveal new cell states and markers that can differentiate within the seemingly homogenous population. The limiting factor in scRNA-Seq is that processing of single cells is relatively time-consuming which require various sequential methods, hence the risk of batch effect. The scalability of scRNA-Seq has been dramatically improved by utilizing droplet micro fluidics in which single microparticles coated with poly (T) barcodes and single cells encapsulated together in nanoliter-scale droplets [120].

Recent breakthroughs with next generation sequencing and the establishment of large sequencing consortiums such as Encyclopedia of DNA Elements (ENCODE) or Functional Annotation of Mammalian Genome (FANTOM) unveiled substantial numbers of non-coding RNAs in mammalian genome [121, 122]. microRNAs are usually profiled with small RNA sequencing or specific miRNA arrays, and later miRNAs of interest are validated by qPCR. Profiling of circulating miRNAs in serum in Chinese cohort identified numerous miRNAs that are differentially expressed, with mir29a as the most promising marker, between active TB patients and healthy controls [123]. Increasing availability and affordability of miRNA profiling and growing interest in TB field has deemed miRNAs as potential biomarkers and targets of therapeutic interventions [124]. Another non-coding RNA species in the spotlight is long non-coding RNAs (lncRNA) which are longer than 200 nucleotides, expressed in nearly all cell types and regulates transcription, splicing, RNA degradation, translation and epigenetic modifications [125].Profiling of lncRNA expression generally rests on data from RNA-Seq to choose lncRNAs of interest followed by qPCR step. These studies have led to numerous roles of lncRNAs in

immunity including differentiation and activation of T cells, regulation of innate response, differentiation of monocytes into macrophages and dendritic cells, chromatin remodeling during variable, diversity and joining (V(D)J) in antigen receptors in T and B lymphocytes [126]. In terms of lncRNAs in host-pathogen interactions lncRNA-CD244 is found to be upregulated in $CD244^{+}CD8^{+}$ T cells during active disease. CD244 is a costimulatory molecule and modulates IFNg and TNF release from $CD8^{+}$ T cells through upregulation of lncRNA-CD244 levels. LncRNA-CD244 is shown to recruit polycomb protein enhancer of zeste homolog 2 (EZH2) to promoters of IFNg and TNF leading to trimethylation at H3K27 and repressive chromatin states [127]. In a recent study, maternally expressed gene 3 (MEG3) lncRNA is shown to negatively regulate IFNg induced autophagy in BCG infected macrophages [128]. Genetic deletion of LncRNA-EPS (lncRNA-erythroid pro-survival) in mice revealed that lncRNA acts as a transcriptional repressor of IRGs (immune response genes) in macrophages in response to LPS stimulation by recruiting ribonucleoprotein complexes to promoters of its target genes [129].

Epigenetics relate to long-term or heritable changes in gene expression which can change the phenotype without altering genotype of the cell. Epigenetics profiling is routinely performed by chromatin immunoprecipitation (ChIP) which is to precipitate modified histones by specific antibodies and analyze DNA sequences that are bound to histone complexes. Another widely used epigenetics method in immunology is DNAse hypersensitivity assay to detect loosely packed genomic sites by nucleosomes with the concept that active transcription occurs in hypersensitive sites. Integration of these techniques with next generation sequencing methods advanced the sensitivity and specificity of uncovering epigenetic modifications in a given cell state. The significance of epigenetics in regulating immune response has been established in recent reports. It is shown that after BCG vaccination monocyte phenotype is changed through H3K4 trimethylation on the promoters of several cytokines and immune activation genes and these "trained" monocytes respond better to unrelated pathogens such as *Candida albicans* and *Staphylococcus aureus* [130]. In a recent effort, genome-wide methylation sites are mapped in Mtb infected human monocyte derived DCs. The data suggests that there is a strong demethylation pattern occurring in distal regulatory elements, mainly in enhancers of key transcription factors of the innate response, e.g. REL, NFKB1, IRF2, and IRF4 [131]. H3K4 monomethylation ChIP Sequencing in Mtb infected macrophages revealed that Alu repeats (ancestral short interspersed elements) are enriched in these enhancer regions and contain putative

transcription factor binding sites for MEF2, ATF, LXR and RAR which are involved in macrophage differentiation, survival and response to infection [132]. Deciphering of epigenetic factors or markers that are involved in Mtb pathogenesis can be key to understand immune modulation and pave the way for novel therapeutic interventions or biomarkers.

With the advent of next-generation sequencing methods and their decreasing costs, there is an increasing number of datasets that harbor exhaustive host and pathogen genome sequences. These datasets can be mined to pertain genomic information to immune system functions. Genome-wide association studies (GWAS) compare genomic sequences to find a relation between single nucleotide polymorphisms (SNP) and specific traits such as disease outcome. There have been many studies that are linking polymorphisms in host innate immune genes, e.g. major histocompatibility complex (MHC), tumor necrosis factor (TNF) and its associated receptors, toll like receptors, vitamin D receptor (VDR), soluble C-type lectins, cytokines and chemokines to host susceptibility to TB [133]. Despite genetic association studies have partly explained why some individuals are more susceptible to TB, they do not report the underlying mechanisms. ChIP assays can be helpful to pinpoint whether these polymorphisms are on regulatory sites such as transcription factor binding sites. Accordingly, there has been increasing interest in expression quantitative trait loci (eQTL) which influence the gene expression, as a greater number of polymorphisms associated with diseases map to regulatory regions in lieu of protein coding regions [134]. Mapping of eQTL in Mtb infected primary human dendritic cells identified dual-specificity phosphatase 14 (DUSP14), receptor-interacting serine/threonine-protein kinase 2 (RIPK2) and V-type proton ATPase 116 kDa subunit an isoform 2 (ATP6V0A2) as novel candidates to affect susceptibility to TB [135]. Dissecting eQTLs can help to understand molecular mechanisms which may be an important weapon to fight against TB.

2. CAP ANALYSIS GENE EXPRESSION (CAGE) SEQUENCING

Quantifying transcript abundance is a fundamental approach to investigate gene regulation, the molecular principle of complex biological systems. RNA-Seq and CAGE-Seq are two major technologies that have emerged with next-generation sequencing platforms to measure transcript abundance. The advantage of RNA-Seq over CAGE-Seq is that full length of RNA sequence can be identified since RNA-Seq focuses on sequencing random fragments of RNA or cDNA which are later mapped to reference transcriptome. RNA-Seq allows alternative splicing and gene fusion discovery as an upper hand over CAGE-Seq. On the contrary, CAGE is devised originally to

construct full-length cDNA libraries by identifying 5' ends of capped RNAs through chemically labeling with biotin residues which was termed cap trapping [136]. Initially, CAGE sequencing protocol was consisting of cDNA synthesis with oligodT primers, cap trapping of full length cDNAs with linkers (contains recognition site for restriction enzymes) attached to 5' ends, digestion with class II restriction enzymes where they cleave 20 nucleotides downstream of the recognition site, amplification of these tags by PCR, ligation of the tags to form concatamers, cloning into plasmids followed by Sanger sequencing method [137]. cDNA synthesis with oligodT primers was later changed with random primers to detect non-polyadenylated RNA transcripts (Figure 2.1). CAGE Sequencing allowed precise mapping of transcription start sites (TSS) and their associated core promoters by its very nature. However; with Sanger sequencing only approximately 48500 tags per mouse cell were sequenced which was not reflecting the complexity of the transcriptional landscape. Conventional sequencing method was changed with high throughput sequencer from 454 Life Sciences which did not require cloning of concatamers in bacteria and DeepCAGE method was developed. DeepCAGE on hippocampus dramatically increased the sampling depth with 1.4 million tags mapped to mouse genome [138]. Over the years, CAGE sequencing was improved by introducing *Eco*P15I restriction enzyme which cleaves 27 nucleotide downstream thereby increasing CAGE tag lengths and their mapping efficiency to reference genome. Optimization of linkers and ligation reactions decreased required RNA amount from 50 μg to 1-5 μg and it was adapted to Illumina Sequencers. Barcoding of CAGE linkers allowed to pool 4 to 6 libraries to a single lane and reduced cost of sequencing [139]. CAGE method was further simplified when it was adapted to third generation sequencer from Helicos Biosciences. The single molecule sequencer, HeliScope Genetic Analyses, avoids PCR amplification of CAGE tags, thereby preventing potential biases introduced during library production. HeliScopeCAGE also does not need second strand synthesis of cDNA that it directly sequences poly(A) tailed single strand cDNA for the first time [140]. The HeliScopeCAGE protocol has been broadly employed in Functional Annotation of Mammalian Genome 5 (FANTOM5) project in order to provide transcription initiation network over 1000 mammalian cells. FANTOM5 can provide transcriptional initiation activities in a single base pair resolution from very diverse states of mainly primary human and mouse cells [122]. The extensive profiling across samples allows digging up genes, transcription factors, and noncoding RNAs and analyzing

their activation states across biological states. TSS profiles also provide the opportunity to correlate transcription factor activity with motifs and epigenetic features when it is compared with

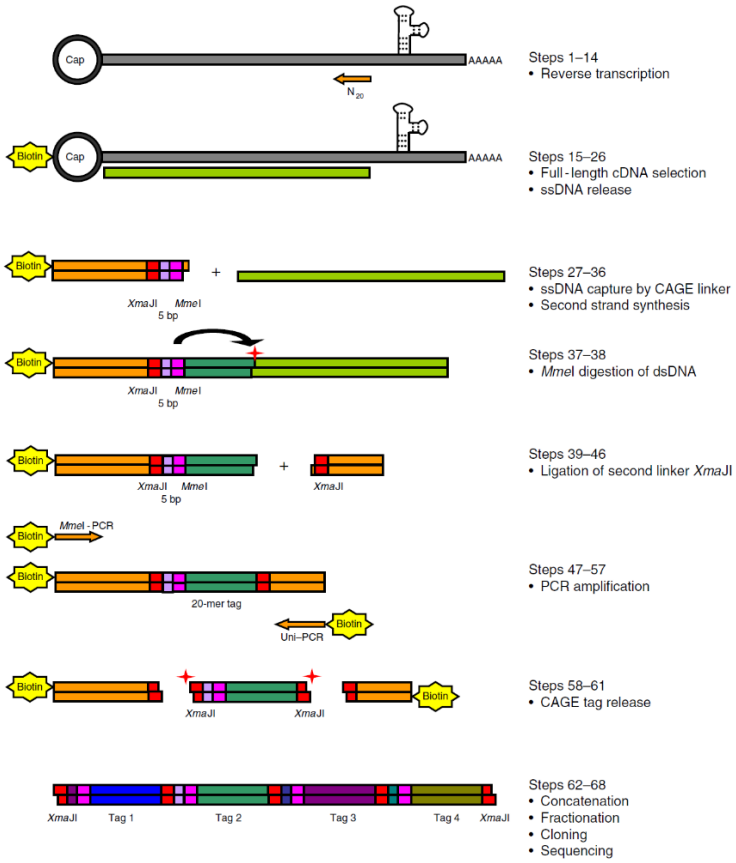

Figure 2.1: Procedure of CAGE protocol. RNA is reverse transcribed into cDNA with random primers. Both ends of cDNA are later biotinylated which is followed by RNase I treatment. RNase I is not effective against RNA-cDNA hybrids, however, it cleaves single stranded RNAs and biotinylated 3' end is removed from RNA-cDNA hybrid. Biotinylated RNA-cDNA hybrid is captured on streptavidin beads and single stranded DNA (ssDNA) is purified after Tris-HCl neutralization and fractionation. ssDNA is later ligated to biotinylated CAGE linkers which introduce *MmeI* recognition site to 5' end of ssDNA. The second strand of ssDNA is synthesized, followed by *MmeI* digestion of double stranded DNA. *MmeI* digestion creates 2bp overhang which is optimal for ligation of a second linker containing *Xma*JI recognition sites. Double stranded CAGE construct is amplified by PCR and later digested by *Xma*JI which leads to compatible ends for concatenation of CAGE tags. Concatamers are subsequently cloned into plasmids and finally sequenced under conditions befitting to GC-rich regions and secondary structures[141].

available ChIP-Seq data. FANTOM5 CAGE Expression Atlas also provided the means to catalog enhancers by virtue of the fact that RNA Polymerase initiates the transcription in enhancer regions bi-directionally and CAGE can detect balanced bi-directional capped RNAs which reveals enhancer activity [142].

3. EXPERIMENTAL DESIGN and REFINEMENT of CAGE DATA

Mouse bone marrow-derived macrophages (BMDM) are used to investigate the changes in the transcriptional landscape of the host after infection with clinical hypervirulent HN878 Beijing strain of Mtb. BMDMs are primary macrophages which are derived from bone marrow cells in the presence of a specific growth factor macrophage-colony stimulating factor (M-CSF). They are widely used in immunological studies because of the high yield and relatively homogenous population. We also scrutinized whether activation states of macrophages can alter their response to Mtb infection. BMDMs are stimulated with IFNg to direct them towards M1 polarization (classically activated macrophages, caMph) and IL-4, IL-13 or in a combination of IL-4, IL-13 for M2 polarization (alternatively activated macrophages, aaMph). Total RNA was extracted in an extensive time-kinetic manner from both infected and non-infected macrophages (Figure 2.2).

Initially, the goal was to obtain four replicates for each time point and macrophage state. Unfortunately total RNA of infected samples from replicate #3 and non-infected samples from replicate #4 was not sequenced because of the experimental drawbacks. Furthermore; a few libraries had less than 500.000 total tags which were removed from analysis to meet library depth criteria since shallow libraries can produce false positive gene expression data [122] (Table 2.1).

The full FANTOM5 mouse CAGE transcriptome consists of 158966 tags that are mapped to the mouse genome (Figure 2.3). From these tags, nearly 22.5% of them have TPM value over 10 in at least one mouse-Mtb infection dataset. Out of 35791 tags, nearly 54% of them were annotated to a gene or a transcript by FANTOM5 consortium through comparing with gene models from UCSC RefSeq, UCSC known gene, ENSEMBL transcripts and full-length mRNA tracks from UCSC genome database [122]. From nearly 19300 CAGE clusters, around 25% of them showed differential expression at 4 hours and 24 hours post infection in three different Mtb infected polarization states (non-stimulated, IFNg stimulated and IL4/IL13 stimulated). To simplify the analysis, these three different polarization states with their Mtb infection and non-infection datasets are used in this Chapter. The unannotated tag clusters generally have low TPM values and

lower proportion (10.6%) of them showed differential expression compared to annotated tags. When the differentially expressed (DE) clusters are looked into carefully, there is no skew towards upregulation or downregulation of CAGE clusters. In annotated DE CAGE tags 47.3% of them are upregulated; however, 56% of DE tags are upregulated in unannotated CAGE clusters.

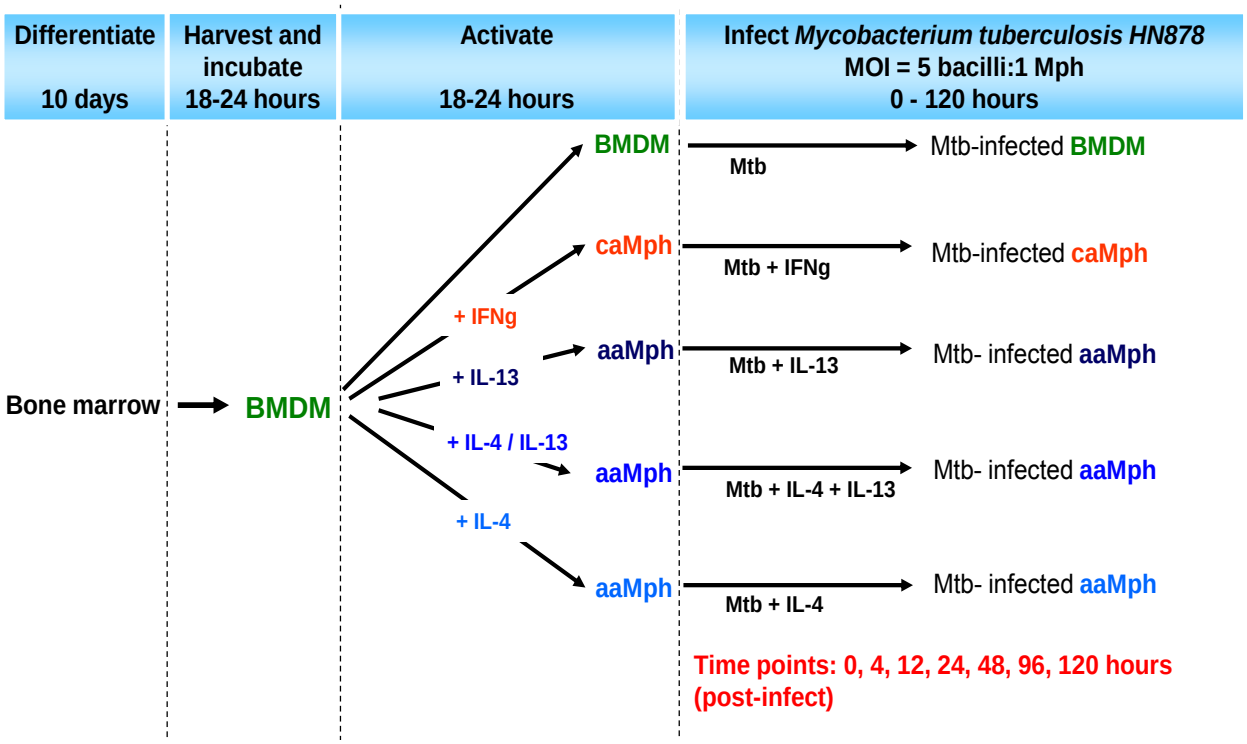

Figure 2.2: Layout of CAGE Experiment. Bone marrow cells from male BALB/c background mice are differentiated into BMDMs in M-CSF conditioned media for 10 days *in vitro*. BMDMs are harvested and seeded overnight in 6-well plates at 3x10^6 cells/well density. They are either left untreated or stimulated with recombinant mouse IFNγ (100U/ml), IL-4 (100U/ml), IL-13 (100U/ml) for overnight. They are infected with HN878 Mtb strain with a multiplicity of infection (MOI) 5 or left uninfected (uninfected macrophages are not shown in the figure for simplicity). Total RNA at 0hr, 4, 12, 24, 48 and 96 hours post infection is extracted for CAGE sequencing. These experiments were performed by Dr. Sugata Roy, Dr. Anita Schwegmann, and Dr. Reto Guler.

	STIMULATION					INFECTION				
	Non-stim	**Ifng**	**IL-13**	**IL-4**	**IL-4,IL-13**	**Non-stim**	**Ifng**	**IL-13**	**IL-4**	**IL-4,IL-13**
Rep1	✓	48h	✓	✓	✓	✓	✓	✓	✓	✓
Rep2	✓	✓	48h	✓	✓	36h	✓	✓	✓	✓
Rep3	✓	✓	✓	✓	✓	4h	4h	4h	4h	4h
						12h	12h	12h	12h	12h
						24h	24h	24h	24h	**24h**
						36h	36h	36h	36h	36h
						96h	96h	96h	96h	96h
Rep4	**4h**	4h	4h	4h	4h	✓	✓	12h	✓	✓
	12h	12h	12h	12h	12h			24h		
	24h	24h	24h	24h	24h					
	48h	48h	48h	48h	48h					
	96h	96h	96h	96h	96h					

Table 2.1: Missing datasets from transcriptomics analysis. Tick denotes the presence of full dataset in corresponding macrophage state. Time points shown are the missing datasets for that replicate and macrophage state.

Unsupervised hierarchical clustering of samples shows a distinct grouping of infection and non-infection samples except Mtb infection in non-stimulated macrophages at 24 hours post infection time point (Figure 2.4). In uninfected samples there is no strong pattern of clustering; however, there is a tendency that same polarization states cluster together. Interestingly, the clustering pattern differs at early time points after infection, i.e. the expression profiles at 4 and 12 hours post infection cluster together and not based on the polarization states. In later time points, it appears that IL4/IL13 stimulated Mtb infected samples and IFNg stimulated Mtb infected samples cluster within their group. PCA analysis of Mtb infection samples also revealed that early time points after infection tend to cluster together regardless of their stimulation state (Figure 2.5). 24 hours post stimulation (or 0h of infection) samples are clustered more closely than any other time point and as the infection progresses over time the samples that belong to same time point start to group away from each other. At later time points of infection, the samples look to cluster according to their polarization states rather than the time point group that they belong to which is also observed in heatmap figure.

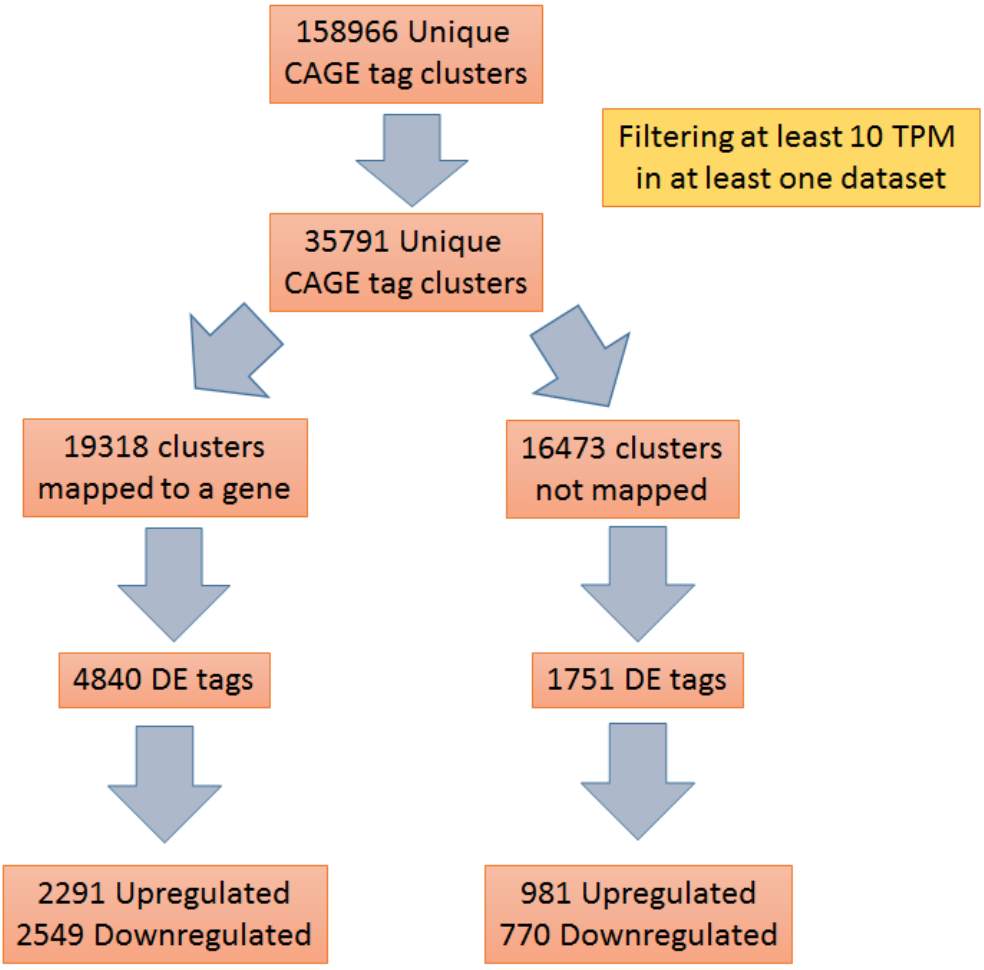

Figure 2.3: Refinement of CAGE tags. The full mouse-Mtb infection dataset is first filtered by removing out lowly expressed tags in all time points and activation states. Differential expression analysis is performed in Mtb infected non-stimulated, IFNg stimulated and IL-4/IL-13 stimulated samples compared to the non-infected counterparts.

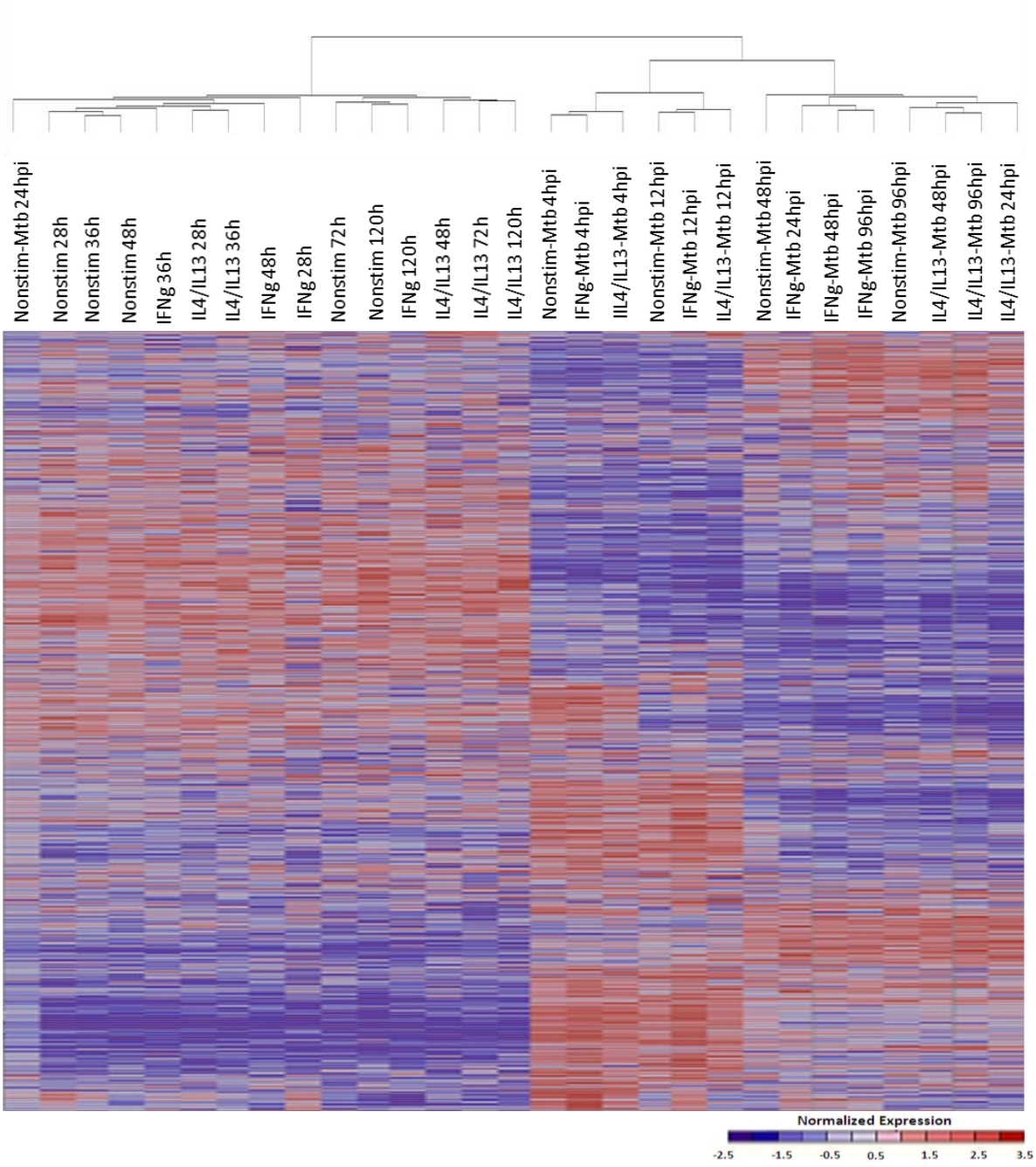

Figure 2.4: Unsupervised hierarchical clustering of Mtb infected and uninfected samples and heatmap of tag clusters. TPM values for each tag from replicate #1 (Rep1) and replicate #2 (Rep2) are averaged (replicate #3 does not have infection data and replicate #4 does not have non-infection data, see Table 2.1). Each row represents the individual tags with blue gradient showing downregulation and red gradient showing upregulation of these tags in corresponding samples. Unsupervised hierarchical clustering and heatmap are constructed by using HierarchicalClustering and HeatMapViewer modules in GenePattern [143].

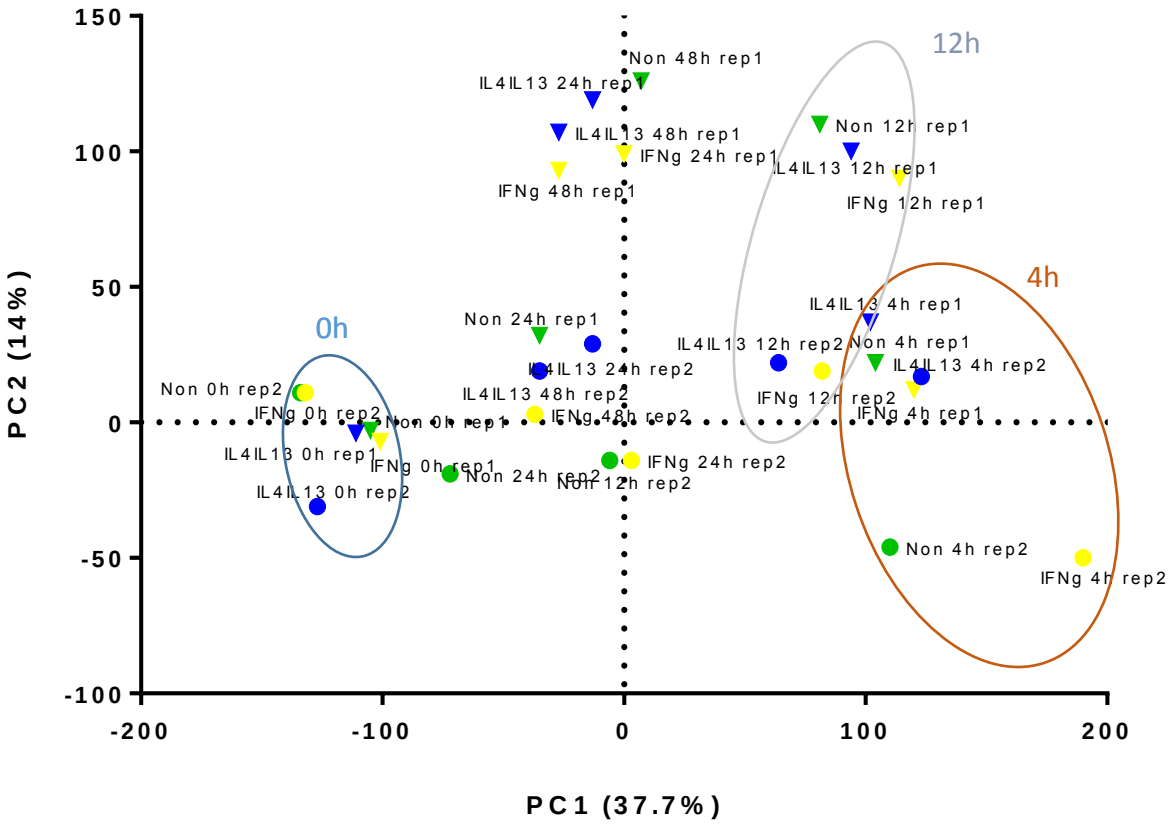

Figure 2.5: PCA Analysis of Mtb infected samples. Total CAGE tag expression values for Rep1 and Rep2 are analyzed for PCA in MultiExperiment Viewer (MeV) [144]. "●" represents Rep1 samples and "▼" represents Rep2 samples. Non-stimulated Mtb infected samples are shown in green, IFNg stimulated Mtb infected samples are shown in yellow and IL4/IL13 stimulated Mtb infected samples are shown in blue color. 0h, 4h, and 12h samples are encircled to show close clustering.

4. TRANSCRIPTIONAL CHANGES INDUCED by HN878 INFECTION

The infection of primary murine macrophages with hypervirulent Mtb strain changes the full transcriptome drastically at earlier time points, i.e 4 hours and 12 hours post infection (Figure 2.6). Although there are more downregulated tags than upregulated tags (3319 tags vs 3272 tags), the mean $\log_2$ fold change in early time points is over 0 meaning that the combinatorial magnitude of upregulation surpasses the combinatorial magnitude of downregulation. To give an example, interleukin-6 (Il6) is one of the highest upregulated genes with nearly 2400 fold induction at 4

hours post infection in IFNg stimulated macrophages and cannabinoid receptor 2 (Cnr2) is one of the highest downregulated genes with over 170 fold reduction at 4 hours post infection in non-stimulated macrophages. Mtb infection initiates such a drastic change in macrophage transcriptome (around 40% of annotated tags show common differential expression) that different macrophage states behave in similar fashion at transcriptional level (Figure 2.7). However; only 5.7% of unannotated tags (100 out of 1751) display common DE characteristic which implies that the response of these macrophage states can differ substantially in unannotated noncoding RNAs or unannotated alternative isoforms of coding RNAs.

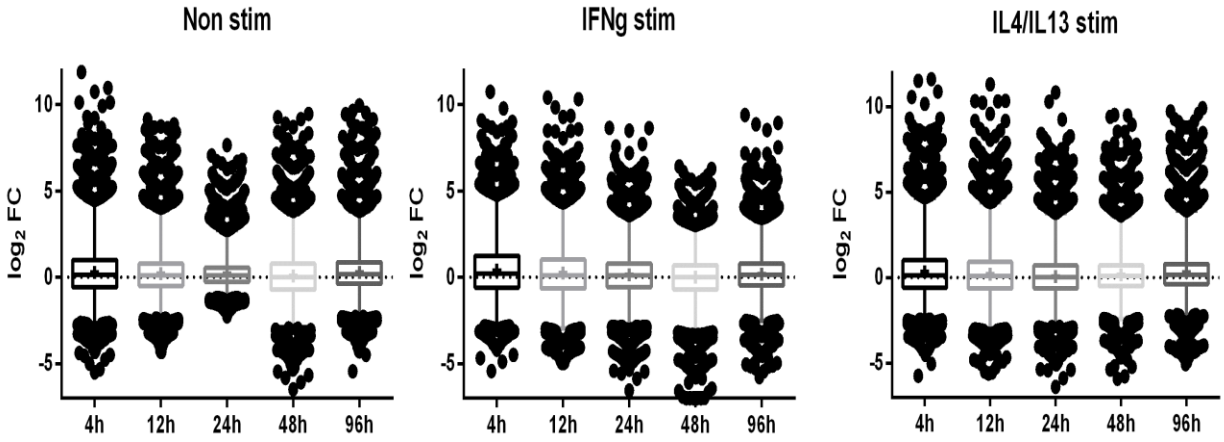

Figure 2.6: Fold change (FC) distribution of CAGE tags. Under three different stimulation conditions, the fold changes for each individual tags are calculated by comparing Mtb infected and non-infected samples at specified time points by averaging replicate #1 and replicate #2 TPMs. Log_2 FC values are drawn as a box-whisker plot with whiskers covering 1-99 percentile. Values below or above the percentile range are staggered as individual dots. The line in the box shows median value and "+" denotes mean value.

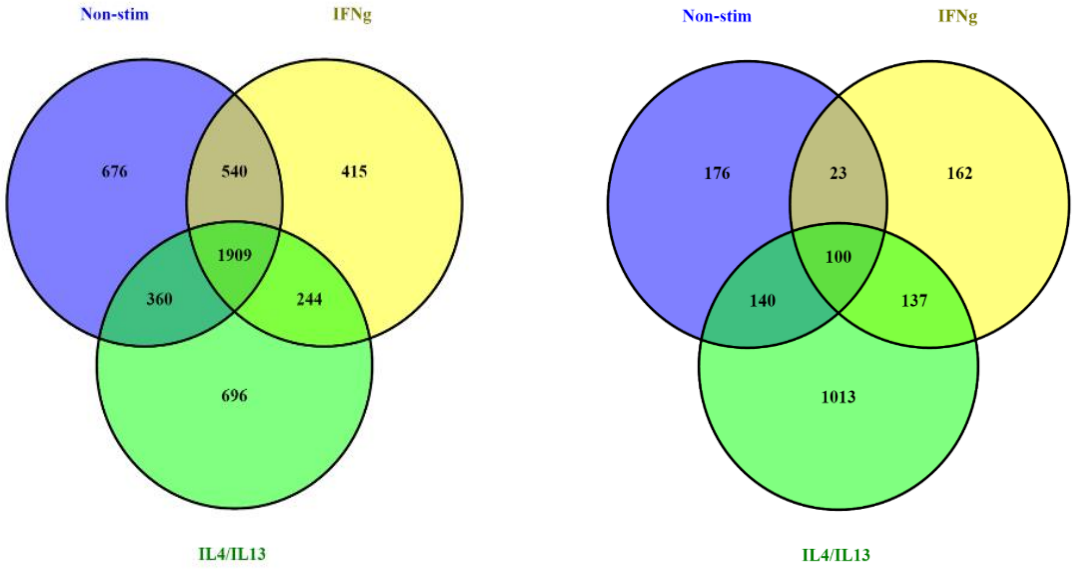

Figure 2.7: Venn diagrams of differentially expressed tags. Differentially expressed tags meeting threshold criteria (fold change ≥ 2, multiple comparisons testing with $p < 0.05$ and false discovery rate < 5%) are determined for annotated tags (left) and unannotated tags (right) for 4 hours and 12 hours post infection datasets compared to 0 hr dataset in three different macrophage states. Venn diagrams are constructed with Venny tool [145].

Additionally, the genes that respond the strongest to Mtb infection in each macrophage activation states are assessed. As expected, many cytokines and chemokines associated with the innate immune response including interleukin-6, inhibin B, Cxcl1, Cxcl2, Cxcl3, vascular endothelial growth inhibitor (Tnfsf15), interleukin-1 alpha, granulocyte colony stimulating factor (Csf3), interleukin-12 alpha and interleukin-27 were amongst the highest upregulated genes (Table 2.2). Prostaglandin synthase 2, endothelin 1, tissue factor (F3), signaling lymphocytic activation molecule (Slamf1), oxidized low density lipoprotein receptor (Olr1) and Phldb1 are also associated with various aspects of innate immune response; hence it is not surprising to find them in upregulated gene list. Whereas the strongest downregulated genes (Table 2.3) include various signal transduction genes (Sesn1, Rnf144b, and Lyl1), G-protein coupled receptors (Cnr2, Lpar5) and histone proteins (His1h3b and His1h3c) except a cytokine $CD4^+$ cell chemoattractant Il16 and chemokine receptor Ccr2 [146].

		Non-stim macrophages			IFNg-stim macrophages			IL4IL13-stim macrophages		
Tag Name	**Molecular Function**	**TPM**	**Fold Change**	**p-value**	**TPM**	**Fold Change**	**p-value**	**TPM**	**Fold Change**	**p-value**
p1@Edn1	Vasoactive, vasoconstrictor	0.5	**2208**	4.4E-25	0	3051	1.8E-18	0.5	3699	6.5E-22
p1@Ptgs2	Dioxygenase, oxidoreductase	7.8	**1979**	8.5E-30	26.2	1059	1.7E-18	11.9	1912	4.8E-23
p1@Il6	Cytokine, growth factor	0	**1935**	4.2E-27	0.9	2470	1.4E-19	0.5	2256	5.5E-20
p1@Inhba	Growth factor, hormone	0	**1156**	7E-19	0	2557	5.6E-10	0	2579	1.6E-16
p1@Cxcl1	Cytokine, growth factor	16.2	**1064**	2.8E-25	9.8	1080	1.4E-16	16.7	1192	1.5E-22
p1@Cxcl2	Cytokine	35	**798**	1.9E-24	63.5	729	9.6E-18	39.6	1014	6.5E-22
p1@Tnfsf15	Cytokine	0	538	1.4E-21	0	**1188**	1.1E-17	0	553	1.6E-15
p1@F3	Blood coagulation	0	285	1E-17	0	**976**	8.6E-17	0	857	3.3E-16
p1@Il1a	Cytokine	1.9	761	1.2E-25	2.5	**832**	2.4E-18	3.5	730	2.1E-21
p1@Cxcl3	Cytokine	4.2	539	3.3E-21	3.6	**743**	6.3E-09	15.4	293	1.8E-18
p1@Csf3	Cytokine, growth factor	0	518	3.7E-18	0	**531**	6.4E-14	0	490	3.3E-14
p1@Slamf1	Receptor	0.5	135	7.2E-13	0	448	1.9E-10	0	**828**	4.2E-16
p1@Olr1	Receptor	0	146	6.8E-14	0	174	3.4E-11	0.5	**296**	1.5E-15
p2@Il27	Cytokine	0.5	67	6.4E-22	0.4	380	1.1E-17	0	**146**	8.7E-15
p1@Phldb1	Cytoskeleton	0	45	6.9E-07	0	76	4E-06	0	**104**	3E-09
p1@Il12a	Cytokine	0	24	8.3E-10	0	42	3.9E-08	0	**104**	1.9E-08

Table 2.2: Highest upregulated genes common in three polarization states of macrophages after Mtb infection. Fold change shown in the table corresponds to highest fold change in early time points (4h and 12h pi) when the TPM values are averaged over replicates. The short molecular function of the genes is retrieved from UniProt database [147].

		Non-stim macrophages			IFNg-stim macrophages			IL4IL13-stim macrophages		
Tag Name	**Molecular Function**	**TPM**	**Fold Change**	**p-value**	**TPM**	**Fold Change**	**p-value**	**TPM**	**Fold Change**	**p-value**
p1@Cnr2	Receptor	38.1	**-171**	4.7E-10	26.9	-54	7.4E-10	62.2	-58	3.3E-08
p2@Lpar5	Receptor	30.7	**-82**	2.7E-10	44.7	-89	5E-10	55.3	-99	2.9E-08
p1@Sesn1	Oxidoreductase	41.9	**-67**	1.8E-12	72	-143	1.3E-10	87	-165	1.8E-09
p1@Gcnt1	Glycosyltransferase	98.3	**-28**	2.4E-09	70.7	-23	2.9E-08	64.6	-9	4E-04
p1@Ccr2	Receptor	27	-12	4.9E-05	46.9	**-94**	1.7E-09	32.4	-45	1.7E-07
p2@Kcnj10	Ion channel	17.4	-40	5.6E-11	28.8	**-58**	9.4E-10	17.1	-32	5.2E-08
p1@Rnf144b	Transferase	25.5	-31	6.1E-10	24.3	**-44**	5.3E-09	17.8	-17	7.4E-07
p1@Susd3	Membrane protein	57.6	-13	8.4E-08	84.2	**-42**	1.9E-08	68.1	-23	3.1E-06
p1@Hist1h3b	DNA binding	43.9	-6	0.02	17.2	-31	1.8E-08	55.1	-101	1E-12
p2@Hist1h3c	DNA binding	42.3	-19	0.002	12.7	-10	0.035	39.2	-78	2.7E-11
p1@Il16	Cytokine	16.1	-16	2.2E-09	32.6	-27	1.4E-09	31	-57	7.6E-10
p1@Lyl1	Transcription fact.	97	-16	3.7E-09	113.1	-28	2.5E-08	127.1	-14	2.6E-05

Table 2.3: Highest downregulated genes common in three polarization states of macrophages after Mtb infection. Fold changes shown in the table correspond to lowest fold changes in early time points (4h and 12h pi) compared to 0h when the TPM values are averaged over replicates.

Enrichment analysis of common upregulated genes reports anticipated Gene Ontology (GO) Biological Terms with high confidence including response to the bacterial origin, positive regulation of cytokine response, inflammatory response (Table 2.4). Gene list enrichment analysis is performed on a web-based software Enrichr which covers more than 100 gene set libraries ranging from metabolic pathways, ENCODE ChIP-Seq data, ontology resources to proteome maps [148]. Kinase enrichment analysis is a way to have an idea about which signal transduction pathways can be activated after perturbation. Here, we see that there is enrichment in mitogen-activated protein (MAP) kinase signaling pathways, the master macrophage innate immune response cascade NF-κB signaling and interferon regulatory factor 3 (IRF3) signaling (Table 2.5).

Enrichment analysis of transcription factor binding motifs in the promoters of genes of interest revealed that downstream master regulators of NF-κB signaling, i.e. Rela and Nfkb1, and MAP kinase signaling Egr1 and Tfap2a can be the major transcription factors that drive the gene expression in Mtb response in different macrophage states.

GO Term	Overlap	P-value	Adjusted P-value
response to molecule of bacterial origin (GO:0002237)	71/243	2.43E-33	1.02E-29
response to lipopolysaccharide (GO:0032496)	68/228	1.39E-32	2.91E-29
inflammatory response (GO:0006954)	82/376	1.75E-28	2.45E-25
regulation of cytokine production (GO:0001817)	88/482	1.14E-24	1.2E-21
cellular response to lipopolysaccharide (GO:0071222)	41/110	2.55E-24	2.15E-21
cellular response to molecule of bacterial origin (GO:0071219)	41/116	2.76E-23	1.93E-20
regulation of response to wounding (GO:1903034)	69/347	1.06E-21	4.94E-19
positive regulation of defense response (GO:0031349)	61/272	4.08E-22	2.14E-19
cellular response to biotic stimulus (GO:0071216)	43/132	9.75E-23	5.85E-20
positive regulation of cytokine production (GO:0001819)	66/327	3.57E-21	1.5E-18

Table 2.4: Top Gene Ontology Biological Process Terms Associated with Common Upregulated Genes. Genes that are commonly upregulated at early time points post Mtb infection in all three macrophage states are analyzed through Web-based tool Enrichr. Here top 10 most enriched GO biological process terms are shown in the table. Fischer's Exact Test is employed by Enrichr to rank the terms and compute statistical significance. Overlap is the ratio of a number of genes from the initial gene list inquired that are represented in a single GO term to the total number of genes in that specific GO term.

Kinase	Pathway Associated	Overlap	P-value	Adjusted P-value
Mapk14	p38 MAPK cascade	48/396	9.88E-08	2E-05
Mapk1	ERK1 and ERK2 cascade	40/326	8.33E-07	5.64E-05
Tbk1	IRF3 signalling	7/11	3.32E-07	3.37E-05
Gsk3b	Glucose homeostasis	52/527	1.51E-05	7.68E-04
Cdk2	Cell Cycle	52/553	5.49E-05	0.002
Ikbkb	NF-kB signalling	8/25	3.08E-05	0.001
Mapk4	Atypical MAPK signalling	9/34	5.33E-05	0.002
Abl1	Cell growth and survival	15/94	1.31E-04	0.003
Mapk9	JNK signalling	18/131	2.1E-04	0.005
Src	Cytoskeletal organization	27/259	7.11E-04	0.013

Table 2.5: Top Enriched Kinases Associated with Common Upregulated Genes. Kinase enrichment analysis (KEA) from Enrichr is employed to detect which kinases and their substrates are enriched in commonly upregulated genes at early time points post Mtb infection in all three macrophage states.

Transcription Factor (TF)	TF Full Name	Overlap	P-value	Adjusted P-value
Egr1	Early growth response protein 1	147/1617	7.17E-11	1.12E-08
Smad4	Mothers against decapentaplegic homolog 4	145/1580	5.02E-11	1.12E-08
Sp1	Transcription factor Sp1	194/2360	2.88E-10	2.99E-08
Rela	Transcription factor p65	134/1656	6.28E-07	3.92E-05
Nfkb1	Nuclear factor NF-kappa-B p105 subunit	229/3284	6.3E-06	3.28E-04
Prdm1	PR domain zinc finger protein 1	21/196	0.002	0.039
Tfap2a	Transcription factor AP-2-alpha	115/1663	0.002	0.045

Table 2.6: Enriched Transcription Factor motifs with Common Upregulated Genes. Enrichr employs position weight matrices from TRANSFAC and JASPAR databases to browse through -2000 bp upstream and 500 bp downstream of transcription start site of genes of interest to identify putative transcription factor binding sites. Only 7 mouse transcription factors are statistically found to be enriched after multiple comparisons test computed by Enrichr.

As it is seen in the fold changes of perturbed genes after Mtb infection, downregulated genes are also not enriched as strong as upregulated genes in terms of the kinase, TF motif enrichment and GO biological process terms (Table 2.7-2.9). Kinase enrichment and TF motif enrichment analysis report less number of statistically significant targets in downregulated genes. Gsk3b and Cdk2 kinases are present in both upregulated and downregulated gene enrichment analysis, yet lower coverage in downregulated genes. Another MAPK signaling member, Mapk12 substrates are found to be enriched in downregulated genes. The TF binding motifs that are enriched in downregulated genes are rather intriguing, since none of the four TFs, i.e. Sox10, Tead2, E2f1, and Myod1, are closely related to innate immune response. Interestingly, guanosine triphosphate hydrolase (GTPase) activity is over represented along with genes associated with B cell regulation and muscle cell differentiation. There are many GTPases that are associated with MAPK or NF-κB signal transduction which can explain enrichment of GTPase related terms, but hemostasis, DNA damage checkpoint and muscle cell differentiation terms are peculiar to be enriched in downregulated genes.

Kinase	Pathway Associated	Overlap	P-value	Adjusted P-value
Cdk2	Cell Cycle	43/553	6.6E-05	0.005
Mapk12	p38 MAPK cascade	6/15	1.84E-05	0.003
Gsk3b	Glucose homeostasis	38/527	7.5E-04	0.04
Akt1	Protein Kinase B signalling	19/210	0.001	0.051

Table 2.7: Top Enriched Kinases Associated with Common Downregulated Genes. Kinase enrichment analysis (KEA) from Enrichr is employed to detect which kinases and their substrates are significantly enriched in commonly down-regulated genes at early time points post Mtb infection in all three macrophage states.

Transcription Factor (TF)	TF Full Name	Overlap	P-value	Adjusted P-value
Sox10	Transcription factor SOX-10	41/451	2.49E-06	4.0E-04
Tead2	Transcriptional enhancer factor TEF-4	94/1591	3.0E-04	0.014
E2f1	Transcription factor E2F1	163/3056	4.0E-04	0.014
Myod1	Myoblast determination protein 1	96/1672	7.0E-04	0.023

Table 2.8: Enriched Transcription Factor motifs with Common Downregulated Genes. Enrichr employs position weight matrices from TRANSFAC and JASPAR databases to browse through -2000 bp upstream and 500 bp downstream of transcription start site of genes of interest to identify putative transcription factor binding sites. Only 4 mouse transcription factors are statistically found to be enriched in common down-regulated genes' promoters after multiple comparisons test computed by Enrichr.

Term	Overlap	P-value	Adjusted P-value
positive regulation of GTPase activity (GO:0043547)	54/482	3.72E-11	7.19E-08
positive regulation of GTP catabolic process (GO:0033126)	54/483	4.02E-11	7.19E-08
regulation of small GTPase mediated signal transduction (GO:0051056)	34/256	2.27E-09	2.71E-06
small GTPase mediated signal transduction (GO:0007264)	44/439	7.04E-08	6.3E-05
positive regulation of B cell activation (GO:0050871)	12/58	3.79E-06	0.003
regulation of Ras GTPase activity (GO:0032318)	33/349	1.05E-05	0.005
positive regulation of Ras GTPase activity (GO:0032320)	29/292	1.42E-05	0.006
muscle cell differentiation (GO:0042692)	17/119	8.65E-06	0.005
hemostasis (GO:0007599)	40/478	2.33E-05	0.008
mitotic DNA damage checkpoint (GO:0044773)	8/32	3.75E-05	0.0089

Table 2.9: Top Gene Ontology Biological Process Terms Associated with Common Downregulated Genes. Genes that are significantly downregulated at early time points post Mtb infection in all three macrophage states are analyzed through Web-based tool Enrichr. Here top 10 most enriched GO biological process terms are shown in the table.

Next, the unannotated tags, in other words, the tags that are not mapped to a gene by core FANTOM5 bioinformatics team, are investigated. Although there is a comparable number of annotated vs unannotated tags in mouse macrophages (Figure 2.3), there is more than one order of magnitude less differentially expressed unannotated tags compared to annotated tags shared by all three macrophage states (Figure 2.7). Additionally, the fold changes of the top upregulated and downregulated unannotated tags are dramatically lower compared to annotated tags since the range of TPM values of unannotated tags are dramatically smaller than annotated tags (Table 2.10).

When the genomic locations of these tags are scrutinized, there is no skew in frequencies between intergenic and intragenic locations (Table 2.11). Few of the tags show that they can be alternative transcription start sites for associated genes, a high possibility of transcription start site for mir339 for a specific tag and the high possibility of transcription start site of enhancer RNA for another tag since it is located at bi-directional transcription initiation region.

	Non-stim macrophages		**IFNg-stim macrophages**		**IL4IL13-stim macrophages**	
Tag Position	**Fold Change**	**p-value**	**Fold Change**	**p-value**	**Fold Change**	**p-value**
p@chr16:84703569,+	112	9.8E-05	114	1.07E-04	149	1.07E-06
p@chr2:136735887,+	42.6	9.5E-04	27.5	1.2E-04	26.2	0.001
p@chr1:58783008,+	32.2	2.9E-04	28.3	1.1E-05	34.4	1.2E-04
p@chr3:142224648,+	32	1.3E-04	26.7	3.9E-05	33.8	0.002
p@chr11:117839416,+	20.1	6.4E-04	17.8	4.4E-05	17.9	0.003
p@chr4:149942925,+	-12	2.9E-04	-12.2	4.6E-04	-15.4	0.002
p@chr15:103164241,-	-10.3	7.9E-11	-9.7	3E-04	-5.6	7.3E-05
p@chr19:17401449,-	-9.3	4.3E-04	-17.3	9.3E-04	-10.1	4.2E-04
p@chr16:78217402,+	-8.9	0.001	-7.2	8.5E-05	-5.9	0.001
p@chr5:139848167,-	-8.6	7E-04	-8.6	1.9E-04	-10.7	7.7E-07

Table 2.10: Top upregulated and downregulated unannotated tags common to different macrophage states. Fold change shown in the table corresponds to highest fold change in early time points (4h and 12h pi) when the TPM values are averaged over replicates. In the table, top 5 common upregulated and downregulated unannotated tags are shown.

Tag Name	Genomic Location
p@chr16:84703569..84703586,+	Intergenic,10 kb upstream of mir155 in an enhancer region
p@chr2:136735887..136735907,+	Intragenic TSS in Slx4ip gene
p@chr1:58783008..58783022,+	Intragenic TSS in Cflar gene (probably TSS for alternative isoform in Cflar)
p@chr3:142224648..142224710,+	Intragenic TSS in Gbp3 gene (probably TSS for alternative isoform in Gbp3)
p@chr11:117839416..117839490,+	Intergenic, 8.5 kb upstream of Pgs1
p@chr4:149942925..149942944,+	Intragenic TSS in Rere gene
p@chr15:103164241..103164267,-	Intragenic TSS in Zfp385a gene
p@chr19:17401449..17401453,-	Intragenic TSS in Gcnt1 gene, at 3' end of the transcript probably degradation product
p@chr16:78217402..78217433,+	Intragenic TSS in predicted Gm2311 gene
p@chr5:139848167..139848196,-	Probable TSS for mir339

Table 2.11: Genomic locations of tags shown in Table 2.10. The genomic coordinates of the tags are provided as in mouse genome data mm9 assembly.

5. DISCUSSION

The work described in this chapter focused on the global transcriptomic and single RNA level responses of different macrophage polarization states to hypervirulent Beijing strain of Mtb. Single molecule CAGE Sequencing is employed that substantially increases the depth of sequencing. It is evident that nearly 45% of the significantly expressed (at least 10 TPM in at least one dataset of Mtb infection) CAGE tag clusters were not associated with TSS of a gene. An increasing amount of transcriptomics studies in Mtb infected macrophages have been published; however, they are not as vast as the present study in terms of macrophage polarization states and time kinetics [113, 149-152]. The early response of M0 (non-polarized), M1 and M2 macrophages is more similar than expected, as both non-supervised hierarchical clustering and PCA analysis closely grouped same time points of different macrophage states instead of same macrophages states of different time points. While it may be somehow surprising, it shows that HN878 infection is such a strong perturbation of macrophage transcriptome, different polarization states respond in a similar fashion

in early time points. However; the response of M1 and M2 macrophages can be more sustained than M0 macrophages as it is seen in Figure 2.6. Another interesting fact is that M2 macrophages harbour more exclusive DE tags for both annotated and unannotated tags. It is more evident in unannotated tags since commonly DE tags account for 100 while M2 exclusive tags account for over 1000. The drastic increase in unannotated tags exclusively in M2 macrophages can be the result of alternative TSS in M2 macrophages since a higher proportion of unannotated tags are intragenic (Table 2.11). It has been shown that M1 and M2 activation of human macrophages can result in promoter switch and alternative TSS [153], although the authors report alternative TSS over 50 loci which is much less than expected. It is possible that Mtb infection can induce much higher promoter switch, since another level of RNA regulation, alternative splicing is shown to regulate transcriptional response to virulent and avirulent Mtb strains[154].

When we look at the gene expression changes at the single transcript level, endothelin 1 is surprisingly among the highest upregulated transcripts in macrophages. Edn1 primarily functions as a vasoactive peptide involved in hypertension and various vascular diseases [155]. Blockage of Edn1 signaling leads to augmented lung lesions and infiltration of neutrophils in Mtb infected mice; however, the detailed mechanisms are not elucidated further [156]. It is possible that Edn1 can stimulate the production of endothelial nitric oxide (eNOS) and in TB cavities which are generally characterized by a decrease in vascularization [157]. Highest upregulated transcripts include many genes that are studied in detail; such as prostaglandin synthase 2 is an enzyme that generates proinflammatory lipid signaling molecules, prostaglandins from arachidonic acid. Prostaglandins inhibit necrotic cell death in Mtb infected macrophages through plasma membrane repair processes to contain dissemination whereas competing lipid mediators, lipoxins mediate necrosis and facilitates immune evasion [158]. Interleukin-6 has distinct functions in tuberculosis pathogenesis; Il6 is shown to be crucial for protection when the mice are infected with high dose intravenously but dispensable in low dose aerosol Mtb infections [159, 160]. The release of Il-6 by Mtb infected macrophages can inhibit IFNg responsive genes at the transcriptional level [161]; however, it is critical for generating protective IFNg positive Th1 cells after immunization with a subunit vaccine against Mtb [162]. Cxcl1, Cxcl2, and Cxcl3 are major chemoattractants for neutrophils and share a single receptor Cxcr2. Yet, these ELR^{+} chemokines have additive roles rather than redundant in neutrophil recruitment to the site of infection [163]. The more interesting transcripts are actually harbored in top downregulated DE transcripts since only Ccr2 is studied in

Mtb infection [164]. The presence of NFκB and MAPK signaling members in both kinase and transcription shows that these pathways are integral to response to Mtb infection in all polarization states. However; the presence of novel various signaling pathways and transcription factors provide new targets to elucidate the mechanisms of macrophage response and immune evasion strategies.

CHAPTER III

BATF2: AN IMMUNE EVASION GENE IN VIVO

Classically activated macrophages are indispensable for the killing of Mtb, the release of proinflammatory cytokines and chemokines which in turn can drive adaptive immune response. M1 polarized macrophages are characterized by abundant expression of inducible nitric oxide synthase (iNOS) and production of nitric oxide (NO), production of proteolytic enzymes, the release of antimicrobial peptides, augmented phagocytosis and formation of the toxic intracellular environment [165]. Considering the hostile environment in M1 macrophages, it is intriguing to see that if transcription factors or molecular switches that govern M1 state can also take part in the killing of Mtb. Another facet of focusing on molecular mechanisms of M1 macrophages is to see whether prolonged M1 activation can be hindered by targeting M1 regulators in order to curtail destructive inflammatory responses. Accordingly, we concentrate on responses of M1 macrophages to HN878 infection in our transcriptomics data. We analyzed the transcription factors which are highly upregulated after Mtb infection to understand their role mechanistically in the control of Mtb infection (Table 3.1). Top 20 upregulated TF-associated tags consist of mainly novel TFs that are not studied in Mtb infection before; except NF-κB family (Nfkbiz, Nfkbid, Rel, Nfkbib, and Nfkb1) which is a master transcription factor in bacterial infections. The comparison of our list with the TFs known to be involved in M1 polarization [166] revealed that only Maff, Zfp800 and Batf2 are common. Maff and Zfp800 are novel TFs for M1 polarization and Mtb response which are interesting to investigate further. However; we have recently published that Batf2 heterodimerizes with interferon regulatory factor 1 (Irf1) upon stimulation by IFNg and TLR2, TLR4 ligands and activates the expression of proinflammatory mediators; Nos2, Tnf, Ccl5 and Il12b [167]. In a recent TB biomarker study, authors report that Batf2 signature alone is strong enough to distinguish pulmonary and extrapulmonary TB patients from healthy controls [168]. Hence, we seek to understand the role of Batf2 in Mtb infection both *in vivo* and *in vitro*. To our surprise, deletion of Batf2 renders the mice protected against H37Rv and HN878 Mtb strains. The manuscript presented below shows our collaborative work to elucidate the mechanism of action of Batf2 in Mtb infected mice and observational studies of human blood transcriptome. The PhD candidate performed validation experiments by RT-PCR from whole blood of healthy, latently infected and active TB individuals presented in Figure 1, RT-PCR experiments that shows

increased Batf2 expression *in vivo* following infection with Mtb presented in Figure 2 by himself; mortality experiments presented in Figure 3 and RT-PCR of various immune related genes from Mtb infected sorted cells presented in Figure 6 with Dr Reto Guler; immunohistochemistry, flow cytometry, bacterial burden and lung homogenate ELISA experiments presented in Figure 4 and Figure 5 with Dr Reto Guler and Dr Suraj Parihar; *in vitro* CFU assays and supernatant ELISA experiments presented in Figure 7 with Dr Suraj Parihar.

TF Cluster ID	TF Protein Name	Fold Change	p-value
p1@Maff	Transcription factor MafF	213	1.6E-12
p1@Nr4a1	Nuclear receptor subfamily 4 group A member 1	143	9.8E-08
p2@Nfkbiz	NF-kappa-B inhibitor zeta	98.7	7.5E-14
p2@Nr4a3	Nuclear receptor subfamily 4 group A member 3	86.9	6.7E-08
p1@Id3	DNA-binding protein inhibitor ID-3	80.8	1.6E-08
p1@Egr1	Early growth response protein 1	77.3	1.4E-10
p1@Mxd1	Max dimerization protein 1	67.1	1.8E-10
p1@Hivep2	Transcription factor HIVEP2	59	5E-06
p2@Nfkbid	NF-kappa-B inhibitor delta	58.6	2.4E-06
p1@Fosl1	Fos-related antigen 1	45.2	2.3E-07
p5@Tgif1	Homeobox protein TGIF1	43.6	1.6E-06
p1@Bhlhe40	Class E basic helix-loop-helix protein 40	43.3	3.7E-08
p1@Zc3h12a	Endoribonuclease ZC3H12A	30.5	1.3E-07
p10@Zfp800	Zinc finger protein 800	28.6	8.4E-09
p1@Id2	DNA-binding protein inhibitor ID-2	25	7.4E-07
p2@Rel	Proto-oncogene c-Rel	24.3	4.7E-07
p2@Batf2	**Basic leucine zipper transcriptional factor ATF-like 2**	**17.6**	**5.8E-06**
p2@Nfkbib	NF-kappa-B inhibitor beta	14.2	1.1E-06
p1@Nfkb1	Nuclear factor NF-kappa-B p105 subunit	11.8	3.5E-06
p1@Ets2	Protein C-ets-2	11.5	5.3E-06

Table 3.1: Top TF-associated tags in Mtb infected IFNg stimulated macrophages. A full list of mouse TFs are downloaded from TcoF-DB v2 [169] and all the transcripts associated with TFs are analyzed for differential expression. Highest upregulated 20 tags are shown in the table.

BATF2 CAUSES INFLAMMATION IN MICE AND IS A PREDICTIVE HUMAN MARKER FOR TUBERCULOSIS DISEASE PROGRESSION

Reto Guler[1,2#], Mumin Ozturk[1,2#], Suraj P. Parihar[1,2], Santosh Kumar[1,2], Sugata Roy[5], Thomas J. Scriba[2,3], Willem A. Hanekom[2,3], Adam Penn-Nicholson[2,3], Daniel E. Zak[4], Harukazu Suzuki[5*], Frank Brombacher[1,2*]

[1]International Centre for Genetic Engineering and Biotechnology, Cape Town Component, Cape Town 7925, South Africa

[2]Division of Immunology, Institute of Infectious Diseases and Molecular Medicine, Health Science Faculty, University of Cape Town, Cape Town 7925, South Africa

[3]South African Tuberculosis Vaccine Initiative, Institute of Infectious Disease and Molecular Medicine, Department of Pathology, University of Cape Town, Cape Town 7925, South Africa

[4] The Center for Infectious Disease Research, Seattle 98109, WA, USA

[5]RIKEN Center for Life Science Technologies, Division of Genomic Technologies, 1-7-22 Suehiro-cho, Tsurumi-ku, Yokohama 230-0045, Japan

* Correspondence: Frank Brombacher, frank.brombacher@icgeb.org and Harukazu Suzuki, harukazu.suzuki@riken.jp

#equal contribution

Running title: BATF2 biomarker for TB disease progression

ABSTRACT

We have previously shown that basic leucine zipper transcription factor (Batf2) regulates inflammatory responses in Mycobacterium tuberculosis (Mtb)-infected murine macrophages. Here, we show that BATF2 mRNA is highly expressed in peripheral blood from adolescents who progressed from infection to tuberculosis disease, and is a predictive human biomarker for incident tuberculosis disease. Subsequent infection studies with the clinical hypervirulent Mtb HN878 strain in wild-type mice resulted in Batf2 up-regulation in lung macrophages, with increased proinflammatory responses and subsequent mortality. In contrast, Batf2-/- mice survived acute tuberculosis with reduced lung inflammation and histopathology compared to wild-type mice. This was due to reduced recruitment of inflammatory macrophages, diminished pro-inflammatory cytokines (Il1a, Il1b, Tnf) and immune effectors (Il12a and Nos2) in infected Batf2-/- lung macrophages. Conclusively, Batf2 increases tissue inflammation and tuberculosis immunopathology in mice. Hence, targeting BATF2 and its transcriptional pathway for possible adjunctive host-directed therapy may reduce pathological inflammation during Mtb infection.

INTRODUCTION

Mycobacterium tuberculosis (Mtb), the causative agent of tuberculosis (TB), causes 1.5 million deaths per year globally [37]. Hence, there is a critical need to better understand host-protective immunological responses, define more robust pre-clinical biomarkers for TB disease and subsequently develop more sensitive bioassays to detect Mtb early in the host [170, 171]. Identification of correlates of risk of TB will contribute to early intervention therapies to prevent TB disease. Previous transcriptomic studies in whole blood from participants living in TB endemic areas have identified unique transcriptional signatures distinguishing between active, latent, recurrent TB and uninfected individuals [115, 172-174]. These gene expression results were mapped to different functional pathways and revealed diverse modules including cytokines, chemokines, receptors, specific immune cells and inflammation markers. The identification of novel inflammatory biomarkers could be of particular interest since uncontained infection with Mtb in the host is accompanied by an inflammatory response contributing to the pathogenesis of the disease. Excessive inflammatory immune responses to Mtb infection results in tissue pathology, and if left untreated, can result in organ dysfunction and death. For example, excessive TNF production greatly contributes to the immunopathogenesis of TB disease by inducing necrosis

in Mtb-infected macrophages [55]. Therefore a protective therapy for TB should reduce inflammation, and adjunctive host-directed therapies for TB targeting inflammatory effectors may become biologically relevant to reduce TB pathogenesis [68, 175, 176]. It is imperative to identify novel inflammatory biomarkers, which are induced during the early stages of infection before developing active disease, as correlates of risk for TB.

We previously identified Batf2 as a transcriptional inducer of inflammatory responses in Mtb-infected murine macrophages in vitro [167]. Recently, we identified BATF2 among a 16 human gene signature of risk that predicted tuberculosis progression in adolescents [116]. With the goal of better understanding the biology behind TB disease progression, we searched for other transcription factors (TFs) among this gene set as potential master regulators of TB progression. Out of the 16 signature genes, three were TFs (BATF2, ETV7, and STAT1). The protective role of Stat1 during mycobacterial infection is well-defined [177], while the role of ETV7 and BATF2 in TB disease progression is poorly defined. Unlike ETV7, BATF2 has a known mouse orthologue [178]. Moreover, a recent meta-analysis comparing 16 datasets among differentially expressed genes distinguishing active TB from controls, revealed a five gene signature that included BATF2 [179].

Batf2 is a transcription factor that belongs to the basic leucine zipper transcription factor family, which includes Batf and Batf3 family members [180, 181]. We previously reported that Batf2 associates with Irf1 to induce inflammatory responses in IFN-γ and LPS-activated macrophages [167]. Knockdown of Batf2 by shRNA in IFN-γ or LPS-activated macrophages caused significant reduction of important early immune response genes (Tnf, Ccl5, and IL12b) including the bacterial effector killing gene Nos2. In this study, using human whole blood transcriptomics, we identified elevated expression of BATF2 as an early correlate for TB disease progression in adolescents with latent Mtb infection. We further explored the role of Batf2 in a loss of function approach using Mtb-infected Batf2 deficient mice in comparison to infected wild-type mice. Interestingly, Batf2-/- mice were highly resistant to tuberculosis disease exhibiting reduced tissue inflammation, pulmonary histopathology, and subsequently increased survival during acute infection. Mechanistically, we identified Batf2 as a transcriptional inducer of inflammatory responses during Mtb infection in mice and showed that BATF2 is a predictive biomarker for TB disease in humans in a prospective cohort study in adolescents.

RESULTS

Increased BATF2 gene expression correlates with human TB disease progression

Recently, we identified a TB risk signature profile of 16 human genes (Fig. 1a) in whole blood that differentiated infected adolescents who progressed to TB disease from adolescents who remained healthy [116]. Among these 16 genes, three transcription factors, BATF2, ETV7, and STAT1, significantly increased during progression from latent Mtb infection to TB disease (Fig. 1b). The difference in expression became more pronounced during progression, but significant upregulation in progressors, relative to non-progressor controls, was detected approximately 600 days before TB was diagnosed. Little information is available on the functional role of BATF2 in TB disease progression. Thus we focused on BATF family members and showed that BATF2 gene expression is highly induced during human TB disease progression. By contrast, BATF and BATF3 expression levels were not increased (Fig. 1c). We previously showed that BATF2 associated with IRF1 to induce inflammatory responses in macrophages [167]. Here we show that IRF1 was also significantly upregulated during TB disease progression, similarly to BATF2 (Fig. 1c). Validation experiments by RT- PCR confirmed that BATF2 expression was significantly increased (5-fold) in participants with active TB disease when compared to healthy controls (both QFT- and QFT+). Together, these data suggest that elevated BATF2 expression is a good indicator of host transcriptional inflammation that characterizes TB disease progression.

Increased Batf2 mRNA expression in murine lung macrophages following infection with Mtb

In a genome-wide transcriptomics analysis, we previously reported that Batf2 is induced in Mtb-infected and IFN-γ activated macrophages in vitro [167]. To evaluate Batf2 gene expression in an experimental TB disease model in vivo, Batf2 mRNA expression was determined in $CD11b^{med}CD11c^{low}$ FACS-sorted lung macrophages from Mtb-infected mice. Batf2 mRNA expression was significantly induced in wild-type lung macrophages at 3 weeks post infection with the laboratory strain H37Rv (Fig. 2a), as well as 11 and 21 days, post infection with the clinical hypervirulent Beijing Mtb strain HN878 (Fig. 2b). As expected Mtb-infected Batf2 deficient (Batf2-/-) mice did not express Batf2 mRNA in lung macrophages. Taken together, these data show that Batf2 is highly upregulated in lung macrophages during acute Mtb infection.

Batf2-/- mice are resistant to the hypervirulent HN878 strain of Mtb

To explore the in vivo consequence of Batf2 deficiency in Mtb infection, a lethal dose of hypervirulent Mtb HN878 (350 CFU/mouse) was intranasally administered to Batf2-/- mice, heterozygous littermates (Batf2+/-) and control littermates (WT). Early weight loss (Fig. 3a) and subsequent mortality (Fig. 3b) was observed in control littermates, whereas no evident weight loss was observed in Batf2-/- and Batf2+/- mice. Strikingly, 71.4% of the control littermates and 40% of the heterozygous mice died during the experiment, whereas all infected Batf2-/- mice survived 18 weeks post infection, at the time point where the experiment was terminated. Kaplan-Meier analysis demonstrated significant survival differences ($P = 0.0015$) between WT and Batf2-/- but also significant survival differences ($P = 0.029$) between heterozygous Batf2+/- and Batf2-/-, revealing a gene dose effect. Of interest, control mice started to die early at 4 weeks post infection with high pulmonary bacterial burden from $1\text{-}2x10^9$ CFU. Infected heterozygous Batf2+/- mice died between 7 and 18 weeks with $2\text{-}70x10^5$ CFU. The remaining Batf2-/- mice at the termination of the experiment had pulmonary bacterial burden from $2\text{-}20x10^5$ CFU. Early during infection at 11 days post HN878 inoculation, Batf2-/- had significantly reduced lung burden when compared to WT and Batf2+/- mice (Fig. 2c). Together, this demonstrates that absence of Batf2 in mice reduces early bacterial burden and increases resistance to acute and chronic Mtb infection, suggesting that Batf2 may be detrimental in tuberculosis disease.

Mtb-infected Batf2-/- mice show reduced acute lung inflammation

To further analyze the role of Batf2 in TB, a sublethal dose (100 CFU/mouse) of Mtb HN878 was used. Batf2 deficient and heterozygous mice showed a tendency for reduced bacterial burden in the lung at week 3 and 6 post infection, compared to wild-type controls, (Fig. 4a), with slightly reduced lung weight index (Fig. 4b), pulmonary cell infiltration (Fig. 4c) and iNOS expression (Fig. 4d) compared to WT littermate controls. However, lesion size (Fig. 4e), histological score (Fig. 4f) and histopathology of lungs (Fig. 4g) at week 3 were significantly reduced in Batf2-/- and Batf2+/- mice compared to infected WT littermate controls. These results suggest that the presence of Batf2 during sub-lethal infection does not significantly influence early bacterial burden but strikingly increases histopathology due to increased pulmonary inflammation and lesion size.

Batf2 increases lung TNF levels and cellular lung infiltration of inflammatory macrophages

To better define cellular infiltration in the lungs we analyzed lung cell populations by flow cytometry, 3 weeks post infection with 1000 CFU/mouse of Mtb H37Rv. Although CFU counts were similar between WT and Batf2-/- mice (Fig. 5a), Mtb infection resulted in slightly lower total lung weight and significantly reduced lung cell numbers in Batf2-/- mice compared to WT mice (Fig. 5b and 5c). In particular, the percentage and total cell numbers of recruited $CD11b^{med}CD11c^{low}$ inflammatory macrophages were significantly lower in Batf2-/- mice (Fig. 5d, e). Cell numbers but not the percentages of $CD11b^{low}CD11c^{high}$ alveolar macrophages were significantly reduced in Batf2-/- mice. TNF, an important pro-inflammatory cytokine mainly produced by activated macrophages in the lungs during Mtb infection, was significantly reduced in Batf2-/- mice when compared to WT mice (Fig. 5f). Together, these data suggest that the presence of Batf2 leads to increased inflammation, demonstrated by enhanced TNF production and increased recruitment of inflammatory macrophages at the site of pulmonary infection.

Batf2 induces pro-inflammatory responses in lung macrophages following Mtb infection

To examine the consequence of Batf2 deletion on inflammatory responses in lung macrophages, mRNA expression of various inflammatory effectors was measured by RT- PCR in $CD11b^{med}CD11c^{low}$ inflammatory lung macrophages isolated from mice infected with Mtb H37Rv for 3 weeks (Fig. 6). Batf2 deficient lung macrophages had significantly reduced transcription of several pro-inflammatory cytokines, such as Il1a, Il1b, Tnf, and Il12a. Moreover, Nos2, the enzyme producing the anti-mycobacterial effector molecule NO, was significantly reduced in Batf2-/- compared to WT lung macrophages. In the absence of Batf2, Il10, an anti-inflammatory cytokine along with a suppressor for cytokine signaling (Socs1) was also significantly reduced. We previously reported that Batf2 associates with Irf1 to induce inflammatory macrophage responses [167]. Here we show that Irf1 is also significantly reduced in the absence of Batf2 in lung macrophages. Together, these results suggest that Batf2 is important in the regulation of inflammatory responses in lung macrophages following Mtb infection.

Batf2 induced TNF and NO production in bone marrow-derived macrophages (BMDM)

We previously reported in BMDM that Batf2 is essential for IFN-γ and LPS-induced Nos2 and Tnf expression by using shRNA mediated Batf2 knockdown [167]. Here we extend these data

and show that Batf2 deficient BMDM stimulated with IFN-γ and IFN-γ/LPS produce significantly reduced levels of TNF following H37Rv Mtb infection compared to WT BMDM (Fig. 7a). In the absence of Batf2, TNF levels were also significantly reduced in IFNγ-stimulated Batf2-/- BMDM following infection with the HN878 strain of Mtb (Fig. 7b). Nitrite levels were significantly reduced in IFN-γ/LPS stimulated BMDM following H37Rv infection and in IFNγ-stimulated BMDM following HN878 infection. Together, these results show that Batf2 induces TNF and NO production in BMDM following in vitro infection with Mtb, suggesting that Batf2 directly regulates macrophages in vivo.

DISCUSSION

In this study, we demonstrated that the basic leucine zipper transcription factor (Batf2), which we [167] and others [182] recently identified in IFN-γ activated classical macrophages, was induced during Mtb infection in macrophages. Subsequent in vivo loss of function studies, comparing Mtb-infection of Batf2 deficient mice and wild-type mice, demonstrated that Batf2 induced inflammatory macrophages to produce pro-inflammatory cytokines in the lung. This response resulted in early pulmonary inflammation and subsequent mortality post Mtb- infection in wild-type mice compared to Batf2 deficient mice. Hence, this demonstrated that Mtb-induced Batf2 expression is detrimental in pulmonary murine tuberculosis. This is also of relevance for human TB as we, in a recent South African adolescent cohort study [116], identified increased BATF2 expression by RNA sequencing in whole blood of asymptomatic individuals who progress to active TB disease (Fig. 1). This matches our mouse studies and conclusions and implies that BATF2 can be used as an urgently needed predictive marker for disease progression in populations living in TB endemic areas

Batf2 is a basic leucine zipper transcription factor of the Batf family, with various immune regulatory functions [180]. Little is known about the functional role of the Batf family in TB disease development. Previously it was reported that Batf3 deficient mice had similar survival rates to Mtb infection compared to wild-type mice [182]. We recently reported that Batf2 is essential in macrophage activation and showed that lentivirus-mediated knockdown of Batf2 resulted in reduced inflammatory macrophage responses during stimulation with LPS, IFN-γ or heat-killed Mtb [167]. This suggests that upon cell stimulation the presence of Batf2 transcriptionally polarizes macrophages towards an inflammatory activation status. Mtb induces

pro-inflammatory responses in the host and the presence of BATF2 in individuals developing progressive pulmonary TB (Fig. 1) could be an indication of an increased inflammatory response in active TB disease patients. Indeed, we showed that Batf2 expression in lung macrophages progressively increased during Mtb infection in mice inoculated with the hypervirulent HN878 strain of Mtb, a clinical isolate known to induce inflammation in the host [183, 184]. BATF2, also known as SARI, was also detected in human lung tissue but interestingly its expression decreased during clinical stage of lung cancer [185]. Upon infection with the HN878 strain of Mtb that induces a hyper-inflamed immune response in rabbits [183], we showed that Batf2 deficiency in mice resulted in survival when compared to control mice that succumbed to infection. Survival correlated with reduced pulmonary inflammation. The observed lung granulomas were reduced but more compact, and the lungs maintained the bacillary load as shown by similar CFU counts among the groups. Uncontrolled excessive lung pathology can lead to TB disease progression. Ill-defined granuloma formation and uncontrolled pulmonary lesion sizes can lead to an aggressive TB pathology, tissue damage, and death. Infecting mice with a high inoculum dose of Mtb H37Rv resulted in significantly diminished lung inflammatory macrophages and decreased lung TNF levels in Batf2 deficient mice. However, infected Batf2-/- mice were still able to control the bacillary loads. Although TNF is important for inducing protective immune responses against Mtb infection [186], TNF was also reported to mediate TB pathogenesis [55]. Therefore, the inflammatory response observed during Mtb infection needs to be balanced and an over-inflamed state of immune activation may lead to TB disease and tissue pathology. For example, this balance between pro- and anti-inflammatory signals can be observed spatially within lung granulomas during Mtb infection [187]. In our study, we show that blocking Batf2 could dampen this over-inflamed state and lead to resistance to Mtb infection. We demonstrated that Batf2 exerts its action in lung macrophages, as isolated pulmonary Batf2-/- macrophages during Mtb infection had a significantly reduced pro-inflammatory chemokine and cytokine response when compared to macrophages from wild-type mice (Fig. 6). The increased resistance of Batf2-/- to Mtb infection is similar to mice lacking the receptor for type 1 IFN [188]. For example, the absence of IFNar1 in mice resulted in reduced early lung inflammation with smaller pulmonary inflammatory foci. Similar to our results in Batf2 deficient mice, IFNar1-/- mice displayed a reduced recruitment of inflammatory macrophages with decreased lung chemokines, pro-inflammatory cytokines such as Il1a, IL1b, Tnf, Il6 and decreased nitric oxide killing effector function. Although the lung bacterial

burden reached a level close to 10^5 CFUs, IFNar1-/- mice were highly resistant to Mtb infection. The mechanisms of increased resistance of Batf2-/- mice could be explained by reduced recruitment of inflammatory macrophages to the site of infection. It seems that Mtb intensifies inflammation to develop a persistence replication niche in the host. As TB disease progresses, the accumulation of inflammatory cells drives lung tissue pathology and allows for a permissive state where Mtb can replicate. Indeed, granulocyte depletion significantly extended the survival of Mtb-infected mice [189] and TB susceptibility is determined by increased accumulation of a permissive monocyte/macrophage population in the lung [190].

Taken together, our results implicate BATF2 as a possible key transcription factor that regulates the inflammation that characterizes progression from infection to TB disease and as a potential adjunctive host-directed drug target against TB. In a scenario where Mtb infection leads to excessive lung pathology, blocking BATF2 could reduce inflammation, limit pulmonary pathology and subsequently ameliorate TB disease outcome.

METHODS

Mouse strains

Batf2 deficient mice (Batf2-/-) were generated in 129S6/SvEvTac-derived EDJ22 embryonic stem cells [182] and heterozygous mice (Batf2+/-) were purchased from Jackson Laboratories (600 Main Street Bar Harbor, Maine 04609 USA), subsequently intercrossed to generate Batf2-/-, Batf2+/- and littermate control Batf2+/+ 129S6/SvEv mice at the Animal Research Facility, University of Cape Town, Cape Town, South Africa.

Ethics Statement

All animal experiments were performed in accordance with the South African National Standard (SANS 10386:2008) and University of Cape Town of practice for laboratory animal procedures. The protocol (Permit Number: 012/036) was approved by the Animal Ethics Committee, Faculty of Health Sciences, University of Cape Town, Cape Town, South Africa. The human adolescent cohort study (Permit Number: 045/2005) was approved by the Human Ethics Committee, Faculty of Health Sciences, University of Cape Town, Cape Town.

Mtb infection in mice

Anesthetized mice were infected intranasally by inoculation with 25 µl of viable HN878 or H37Rv Mtb bacilli into both nasal cavities. Inoculum dose was determined at one day post infection. Bacterial loads, histopathological and flow cytometry analyses in lungs of Mtb-infected mice were determined as previously described [191].

BMDM generation and in vitro Mtb infection

Bone marrow-derived macrophages were generated from 8-12 week old wild-type and Batf2 deficient male mice as described previously [167]. After differentiation, BMDM were plated into 96-well plates (Nunc, Denmark) at 2 x 10^5 cells per well. Following overnight adherence, macrophages were stimulated with IFN-γ (100 U/ml, BD Biosciences, San Jose, CA), a combination of IFN-γ + LPS (20 ng/ml, Sigma Aldrich) or left unstimulated overnight. Activated BMDM were then infected with Mtb HN878 or H37Rv (MOI=5) for 4 hours. BMDM were washed once with pre-warmed culture media to remove extracellular bacteria and incubated with media containing fresh activators and 50 µg/ml of gentamycin. At 4 days post infection, the supernatant was collected to measure Tnf and $NO2^-$ levels.

Quantitative real-time RT-PCR

Total RNA (30 ng from each sorted murine cell populations) was reverse transcribed by Transcriptor First Strand cDNA Synthesis Kit (Roche) by using both random hexamer primer and anchored oligo dT primers according to manufacturer's instructions. Real-time PCR was performed with LightCycler® 480 SYBR Green I Master mix in LightCycler® 480 II (Roche). Absolute quantification method for each gene was used and normalized to Hprt. From the human adolescent cohort study [192], RNA was extracted from whole blood from healthy QFT- (n=16), healthy QFT- (n=16) and TB disease progressors (n=8). Here 100 ng of total RNA was extracted from PAXgene tubes and cDNA synthesis was performed with SuperScript II Reverse Transcriptase (Life Technologies). Real time PCR was performed as described for murine cell populations.

Measurement of nitric oxide and TNF in culture supernatants

BMDM culture supernatants were analyzed for the production of $NO2^-$ using the Griess reagent assay and TNF by standard sandwich ELISA using PNP (4-nitrophenyl disodium salt-hexahydrate) substrate solution (Sigma Aldrich).

The Adolescent Cohort Study

To examine gene expression during human progression from Mtb infection to TB disease, we analyzed whole blood gene expression data from a prospective epidemiological cohort study in adolescents with latent Mtb infection and TB disease, aged 12-18 years, from the Western Cape of South Africa [192]. 6,363 high school adolescents were recruited and monitored for 2 years for the development of TB disease. Latent Mtb infection was diagnosed by tuberculin skin test or QuantiFERON Gold TB in Tube assay and whole blood was collected in PAXgene tubes at enrollment and end of study (24 months) in all, and in an active follow-up group also at 6, 12 and 18 months [116]. Participants suspected of having either prevalent or incident TB were investigated through sputum smears, culture, and chest X-ray. A protocol- defined incident case of TB was any case confirmed by two or more sputum smears positive for acid-fast bacilli and/or one positive sputum culture for M. tuberculosis [116]. Non-progressor controls were matched to progressors by age, gender, ethnicity, high school and previous history of TB disease.

RNA-Seq

RNA-Seq was performed on whole blood samples from 46 progressors and 107 non-progressor controls as previously described [116]. Briefly, RNA was extracted and globin transcript depletion (GlobinClear, Life Technologies) was followed by cDNA library preparation using Illumina mRNA-Seq Sample Prep Kit. RNA-Seq was performed by Expression Analysis Inc., at 30 million 50bp paired-end reads, on Illumina HiSeq-2000 sequencers. Read pairs were aligned to the hg19 human genome using gsnap [193]. Mapped read pairs were assigned to genes by collapsing all transcripts into a single gene model and counting the number of reads that fully overlap the resulting exons using htseq (v. 0.6.0) [194] with strict intersection and including strand information. Gene models for protein-coding genes were downloaded from Ensembl (GRCh37.74). Reads that mapped to multiple locations were only counted once and those mapping to ambiguous regions were excluded. Log2-transformed values of counts normalized by adjusted

library counts were computed using the cpm function of the edgeR package [195]. Gene-level log2 fold changes comparing each TB progressor sample to the average of demographically matched healthy control samples were computed using the Adolescent Cohort Study metadata [116], and assigning "days before TB disease" values for each sample according to the original definitions. The gene expression fold changes for all TB progressor samples were modeled as a nonlinear function of "days before TB disease" for the entire population using the smoothing spline function in R with three degrees of freedom. Ninety-nine percent confidence intervals for the temporal trends were computed by performing 2000 iterations of spline fitting after bootstrap resampling from the full dataset.

Statistical analysis

All data were analyzed using GraphPad Prism v 6.0, a student t-test (two-tailed with unequal variance) or unless otherwise stated in figure legends. A 'p' value of less than 0.05 was considered significant.

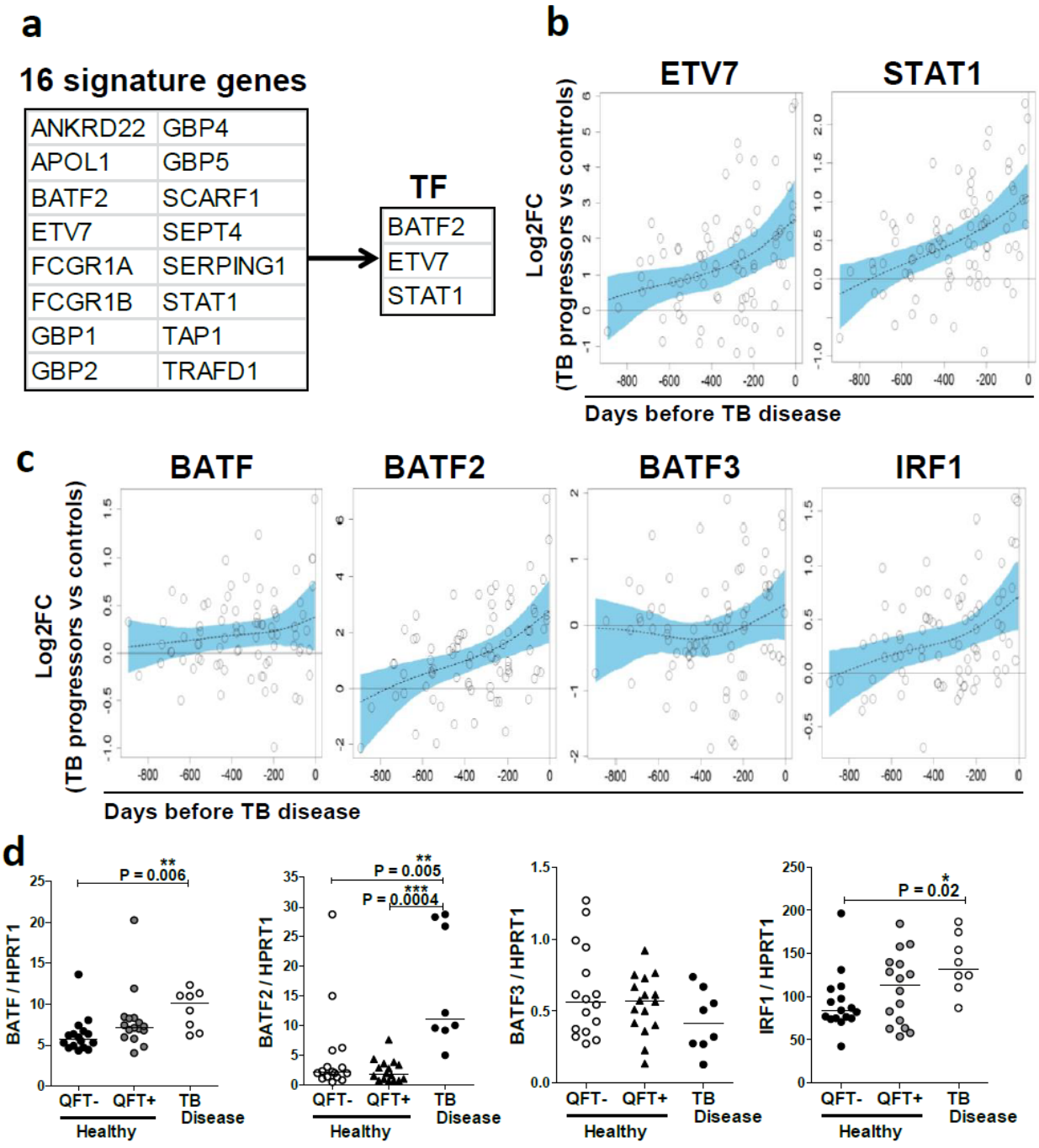

Figure 1. Increased Batf2 expression in human whole blood as a correlate for TB risk progression. (a) Whole blood RNA sequencing and qRT-PCR was employed to define risk signature profiles of 16 genes to predict TB progression that contains three transcription factors, adapted from [116]. (b) ETV7, STAT1 (c) BATF, BATF2, BATF3 family members and IRF1 expression was determined by RNA sequencing in TB progressors in comparison to healthy non-

progressor participants and plotted as log2 fold changes (FC) versus days before TB disease. The dotted line represents spline fit to the overall dataset, and the shaded blue areas represent 99% bootstrap confidence intervals for the spline fits to the fold change of gene expression, as determined by RNA-Seq, in TB progressors vs. healthy non-progressor controls. (d) BATF, BATF2, BATF3 and IRF1 mRNA expression relative to HPRT1 housekeeping gene was determined by RT-PCR from whole blood of healthy, QuantiFERON Gold TB In-Tube negative (QFT-) and positive (QFT+) adolescents, and participants diagnosed with active tuberculosis (TB) disease (One-way ANOVA with Tukey's multiple comparison tests).

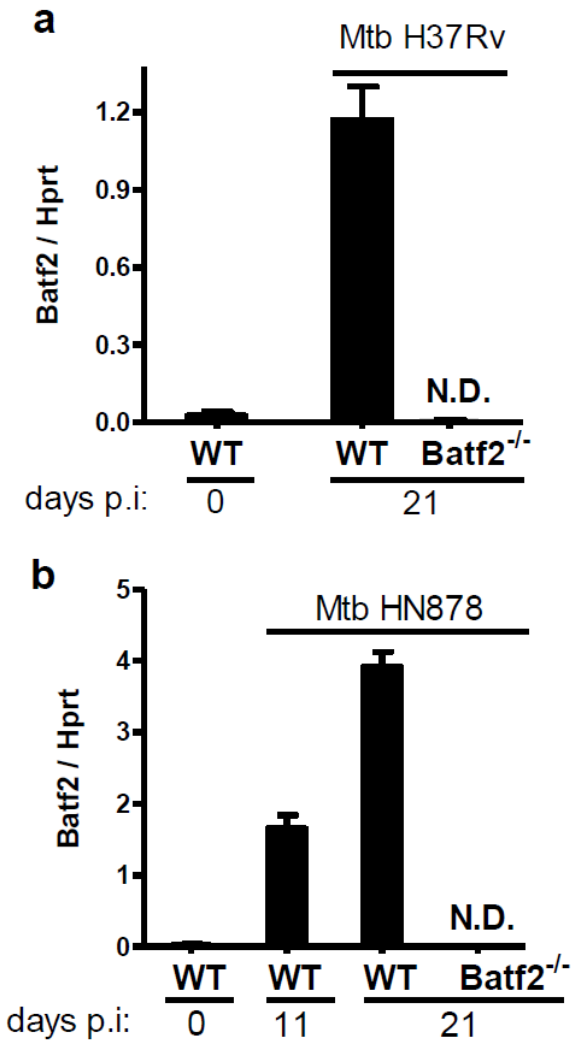

Figure 2. Enhanced Batf2 mRNA expression in murine lung macrophages during acute Mtb infection. Control littermates (WT) and Batf2-/- mice were infected intranasally with (**a**) 1000 CFU/mouse of H37Rv Mtb (n=5 mice/group) and (**b**) 350 CFU/mouse of HN878 Mtb (n=5 mice/group). Mice were sacrificed at (**a**) 21 days and (**b**) 11 and 21 days post infection to sort $CD11b^{med}CD11c^{low}$ lung macrophages by flow cytometry. *Batf2* mRNA expression relative to *Hprt* housekeeping gene was determined by RT-PCR in isolated macrophages (N.D. = not detected).

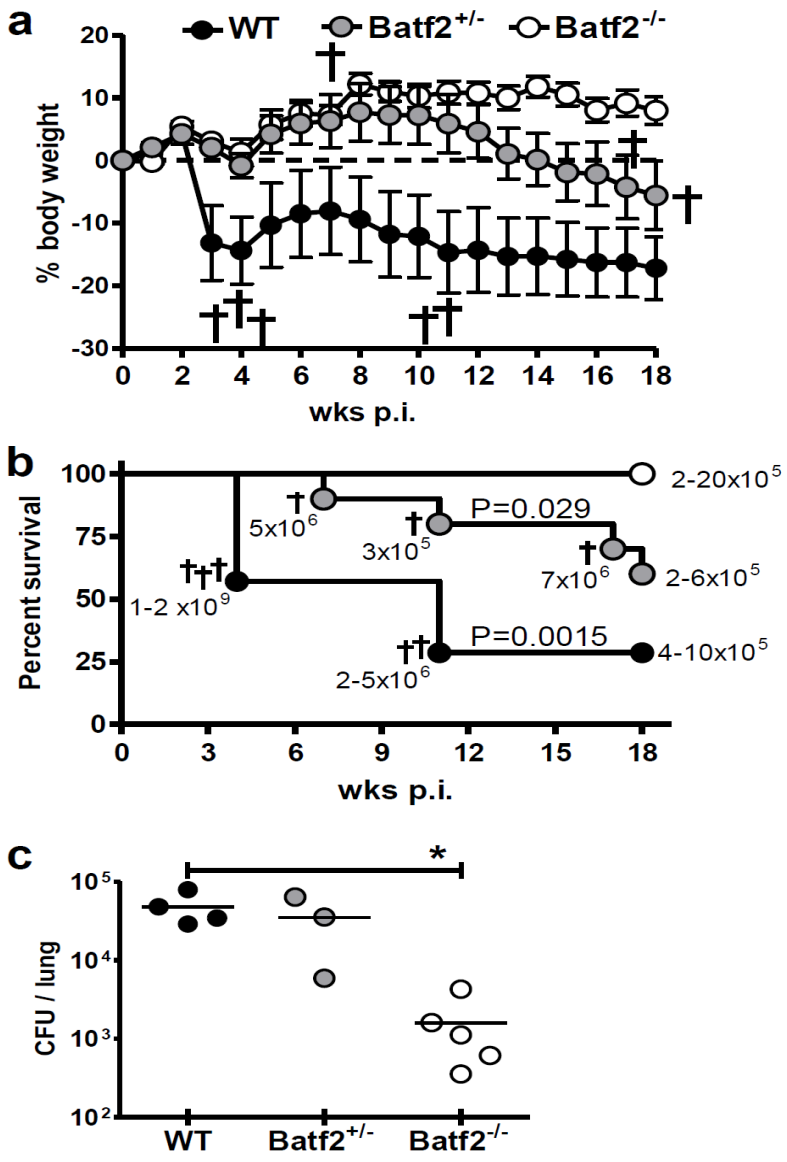

Figure 3. Batf2 deletion renders mice resistant to hypervirulent Mtb HN878 infection. Control littermates (WT), heterozygous littermates (Batf2$^{+/-}$) and Batf2$^{-/-}$ mice were infected intranasally with 350 CFU/mouse of Mtb HN878 (n=7-10 mice/group). (**a**) Body weight change in percentages and (**b**) survival of infected mice are shown with indicated CFU/lung from moribund mice and mice that were sacrificed at the termination of the experiment. Kaplan-Meier survival analysis with log rank test $P = 0.0015$, WT vs. Batf2$^{-/-}$ and $P = 0.029$, Batf2$^{+/-}$ vs. Batf2$^{-/-}$ (**c**) Lung bacterial burden was determined at 11 days post infection following infection with 350 CFU/mouse of Mtb HN878 (n=3-5 mice/group). Data shown in **a** and **b** are representative of three independent experiments (* $P < 0.05$).

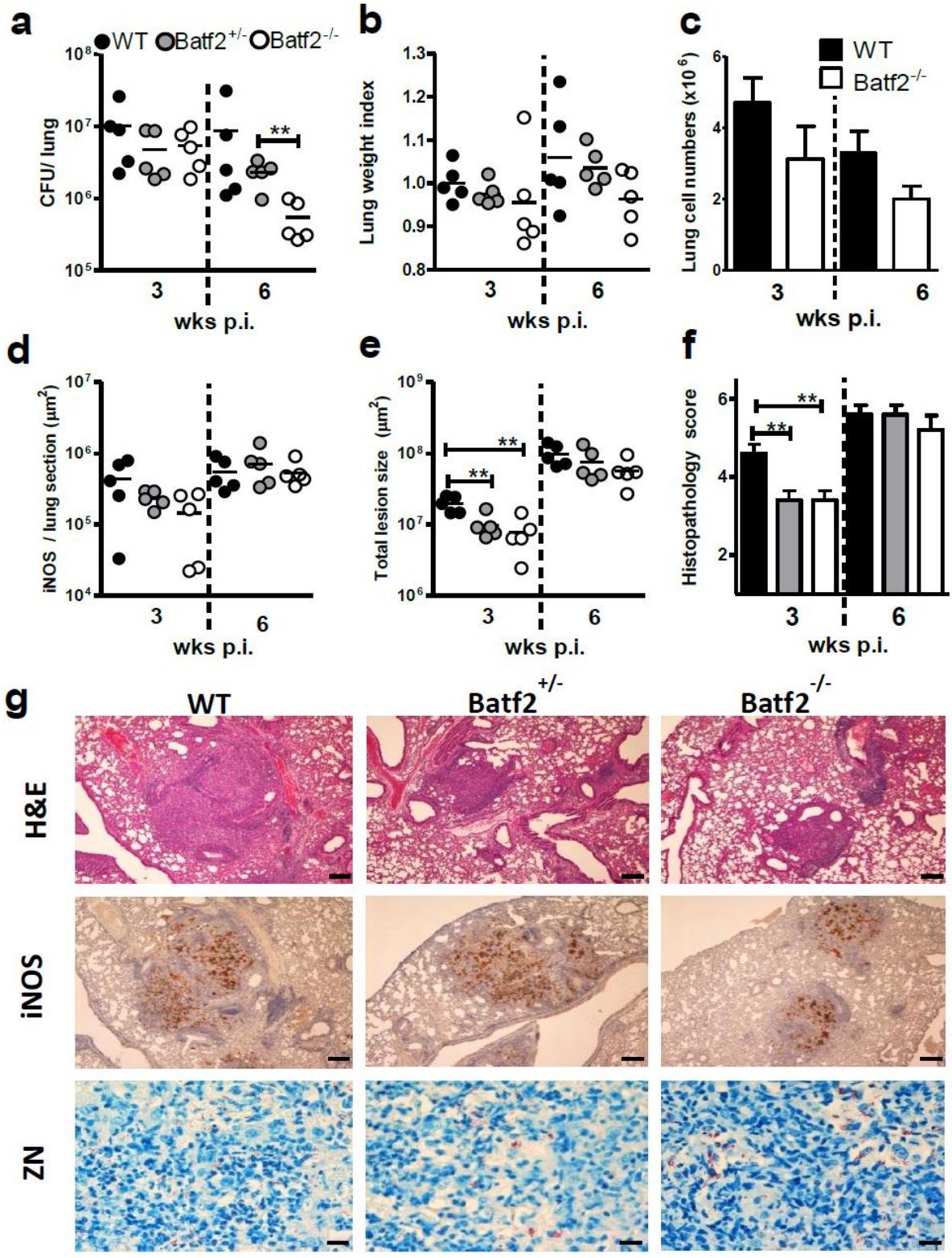
a
WT Batf2+/- Batf2-/-
CFU/ lung
wks p.i.
b
Lung weight index
wks p.i.
c
WT
Batf2-/-
Lung cell numbers (x10 6)
wks p.i.
d
iNOS / lung section (µm2)
wks p.i.
e
Total lesion size (µm2)
wks p.i.
f
Histopathology score
wks p.i.
g
WT
Batf2+/-
Batf2-/-
H&E
iNOS
ZN

Figure 4. Reduced lung inflammation in Batf2 deficient mice during acute Mtb HN878 infection. Control littermates (WT), heterozygous littermates (Batf2+/-) and Batf2-/- mice were infected intranasally with 100 CFU/mouse of hypervirulent Mtb HN878 (n=10 mice/group). Mice were sacrificed at 3 and 6 weeks post infection to determine (**a**) bacterial burden, (**b**) lung weight index and (**c**) lung cell numbers. Pulmonary histopathology was determined at 3 and 6 weeks post infection with H&E, iNOS, and Ziehl-Neelsen (ZN) staining. (**d**) iNOS staining (brown color) per lung section quantified as area in μm2. (**e**) Total H&E lesion size was quantified from ten deep cut lung sections (30 μm apart). (**f**) Lung histopathology scores graded from 1-10 based on perivascular/ peribronchiolar lymphocytic infiltrates, reduced ventilated alveolar spaces and extensive pulmonary lesions (** $P < 0.01$). (**g**) Representative histopathology sections at 3 weeks post infection for H&E, iNOS (scale bar = 50 μm) and ZN (scale bar = 5 μm).

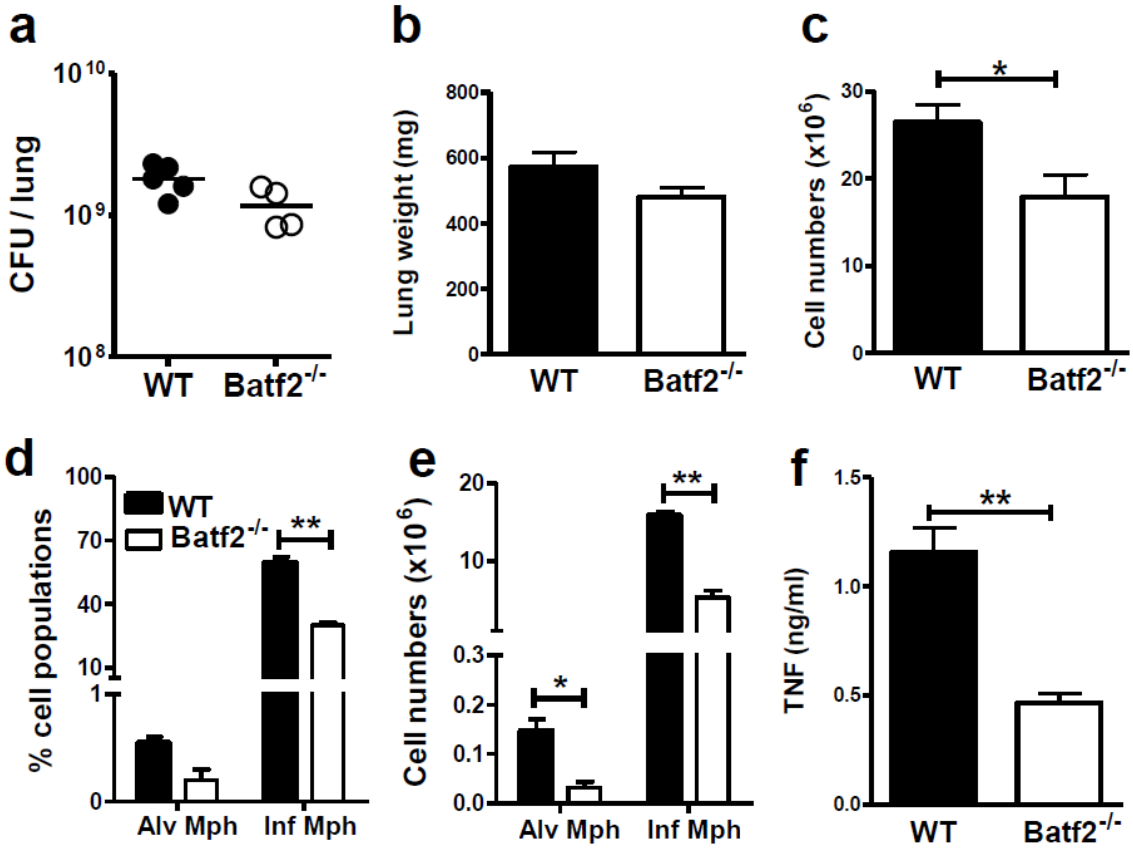

Figure 5. Reduced inflammatory macrophages in Batf2-/- lungs following infection with the Mtb strain H37Rv. Control littermates (WT) and Batf2-/- mice were infected intranasally with 1000 CFU/mouse of H37Rv Mtb (n=4-5 mice/group). Mice were sacrificed at 3 weeks post infection to determine (**a**) CFU loads in the lungs, (**b**) lung weight and (**c**) lung cell numbers. (**d-e**) The percentage and total number of alveolar macrophages ($CD11b^{low}CD11c^{high}$) and recruited inflammatory macrophages ($CD11b^{med}CD11c^{low}$) were determined by flow cytometry. TNF levels in lung homogenates were determined by ELISA (* $P < 0.05$, ** $P < 0.01$).

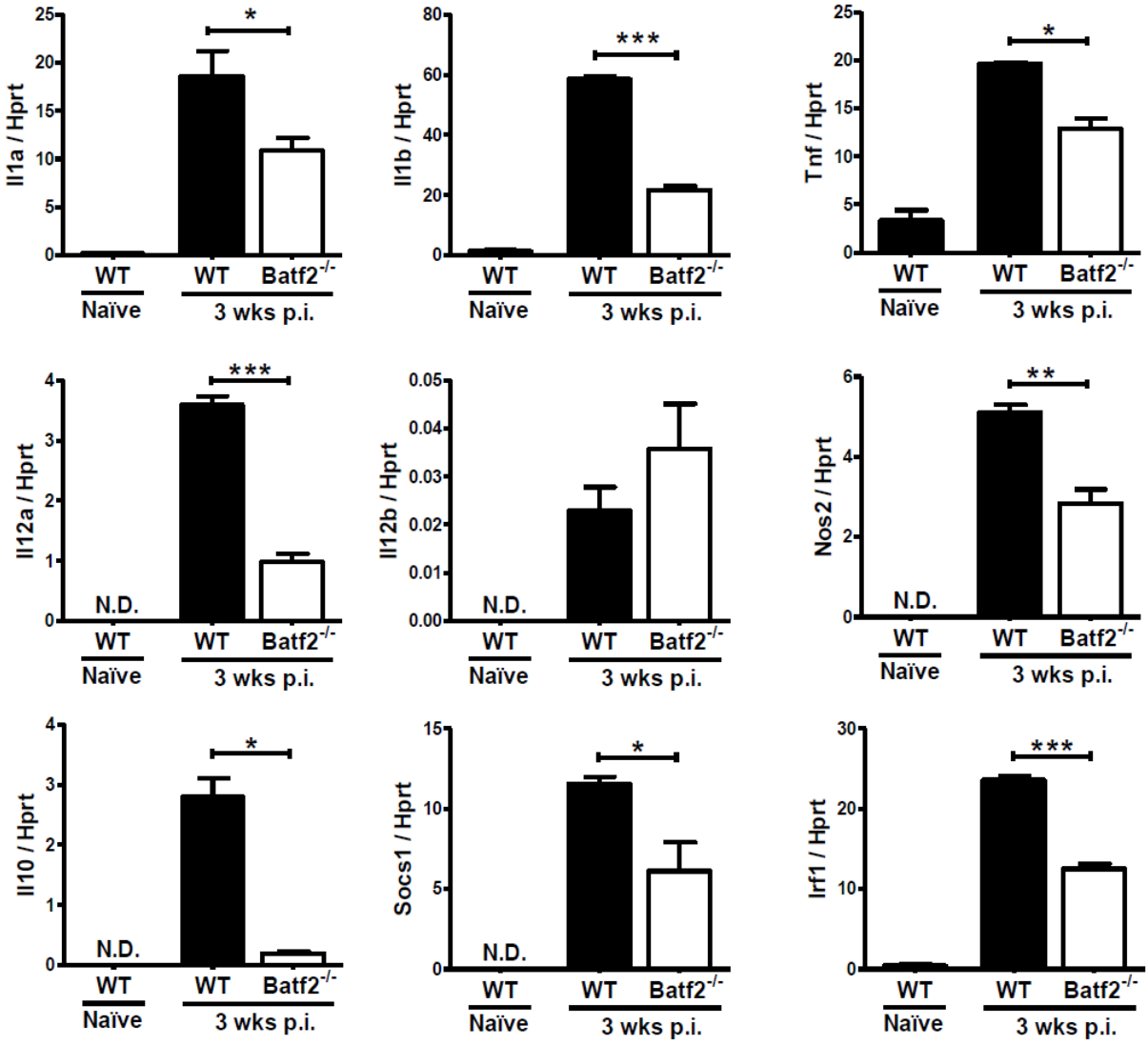

Figure 6. Reduced expression of pro-inflammatory mRNA in isolated lung Batf2-/- macrophages following infection with H37Rv at 3 weeks post infection. Control littermates (WT) and Batf2-/- mice were infected intranasally with 1000 CFU/mouse of H37Rv Mtb (n=5 mice/group). Mice were sacrificed at 3 weeks post infection to sort $CD11b^{med}CD11c^{low}$ inflammatory lung macrophages in the lungs by flow cytometry. mRNA expression was determined by RT-PCR in sorted cells from naïve and 3 weeks Mtb-infected mice (* $P < 0.05$, ** $P < 0.01$, *** $P < 0.001$; N.D. = not detected).

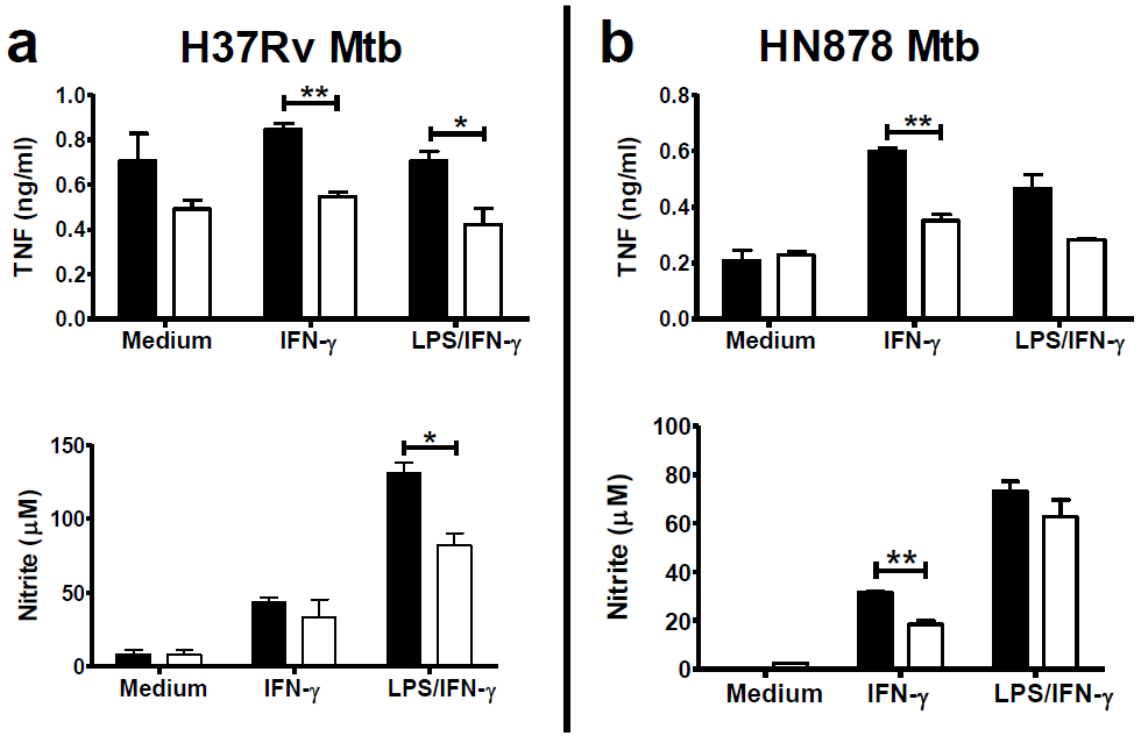

Figure 7. Reduced TNF and NO production in classically activated Batf2-/- macrophages following Mtb infection. Control littermates (WT) and Batf2-/- BMDM were stimulated with IFN-γ (100 Units/ml), a combination of LPS (20ng/ml) + IFN-γ (100 Units/ml) or left unstimulated overnight followed by infection with either (**a**) H37Rv or (**b**) HN878 strain of Mtb. Supernatants were collected at 4 days post infection to measure TNF and NO2- levels (* $P < 0.05$, ** $P < 0.01$).

CHAPTER IV

PRKCD: A HOST PROTECTIVE GENE IN VIVO

Alternatively activated macrophages play a role in various tasks including dampening inflammation, tissue remodeling and wound repair and parasite killing. Best action of play for Mtb to evade classically activated macrophage killing is to shift them towards alternative phenotype. Increased levels of M2 activation correlates with susceptibility to TB [149, 196] and type 2 environment can change back towards type 1 environment after successful anti-TB treatment [197]. Similarly, IFNg mediated type 1 response dominates first three weeks in Mtb infected mice, later shifted towards type 2 immune response with high IL-4 levels [198]. Type 2 response polarized macrophages towards M2 phenotype which is immunomodulatory and have poor bacterial killing capabilities [199]. Additionally, they harbor less nitric oxide and higher availability of iron that results in a permissive niche inside macrophages [149]. M1 macrophages retain iron in the cytosol, away from phagosomal compartments which result in bacteriostasis of Mtb [200], hence it is interesting to see whether Mtb manipulates host transcriptome to induce M2 associated pathways. For this reason, we ask to find kinase associated tags that are upregulated in M2 macrophages after Mtb infection however not liberally upregulated in M1 macrophages (Table 4.1). We choose kinases to focus on since they take crucial roles extensively to regulate complex processes and they are easier to target for future intervention approaches. This approach yielded only two kinases TSSs out of top 10 upregulated TSSs in M2 macrophages. Protein kinase, cGMP-dependent, type I (Prkg1) is a novel kinase to study since it is studied neither in M2 macrophages nor in responses to Mtb infection. We select protein kinase C delta (Prkcd) to further pursue our studies in order to understand extensively its role during Mtb infection. Prkcd has actually been studied in our lab with different infectious disease models. Mice deficient with PKCδ is highly susceptible to *Listeria monocytogenes* infection because of the increased escape of the pathogen from phagosomes into the cytosol, hence increased bacterial burden [201]. PKCδ deficient mice are also shown to be more susceptible to *Leishmania major* infection since PKCδ deficient macrophages and DCs are unable to produce sufficient levels of IL12p40/p70 which results in less efficient T cell priming [202]. The manuscript presented below shows our collaborative work to elucidate the mechanism of action of PKCδ in Mtb infected mice and observational studies of human blood transcriptome and lung proteome. The PhD candidate performed qRT-PCR analysis

of PKCδ in human blood and Mtb-infected human macrophages presented in Figure 1 by himself, mortality study and *in vivo* bacterial burden studies presented in Figure 2 and 3, lung homogenate ELISA and FACS analysis presented in Figure 4, *in vitro* mycobacterial growth and killing effector function assays presented in Figure 6 and 7 with the lead author Dr. Suraj Parihar.

Kinase Cluster ID	Kinase Protein Name	M2 Fold Change	p-value	M1 Fold Change	p-value
p1@Rps6ka2	Ribosomal protein S6 kinase alpha-2	55.2	1.1E-07	26.4	1.2E-04
p2@Mapk6	Mitogen-activated protein kinase 6	39.4	1.7E-06	47.5	8E-06
p1@Met	Hepatocyte growth factor receptor	33.6	2.3E-08	15.8	3.8E-06
p1@Plk2	Serine/threonine-protein kinase PLK2	30.1	4.3E-07	58.8	1.8E-07
p1@Plk3	Serine/threonine-protein kinase PLK3	18.8	1.2E-05	20.8	8.2E-07
p1@Ripk2	Receptor-interacting serine/threonine-protein kinase 2	18.8	9.2E-07	23.2	1.7E-06
p2@Rps6ka3	Ribosomal protein S6 kinase alpha-3	11.8	6.5E-05	24.5	2.1E-04
p4@Irak3	Interleukin-1 receptor-associated kinase 3	11.2	3E-04	3.8	7.5E-06
p1@Jak2	Tyrosine-protein kinase JAK2	7.5	1.9E-04	5	0.002
p2@Prkg1	cGMP-dependent protein kinase 1	6.7	6.4E-04	1.8	>0.05
p3@Prkcd	**Protein kinase C delta type**	**4**	**3.9E-03**	**0.3**	>0.05

Table 4.1: Top kinase associated tags in Mtb infected IL4/IL13 stimulated macrophages

Full list of mouse kinome is downloaded from UniProt (Release: 15 Feb 2017) and all the transcripts associated with kinases are analyzed for differential expression. Highest upregulated 10 tags for Mtb infected M2 macrophages are chosen and shown with their FC in M1 macrophages in the table.

PROTEIN KINASE C-DELTA (PKCD), A MARKER OF INFLAMMATION AND TUBERCULOSIS DISEASE PROGRESSION IN HUMANS, IS IMPORTANT FOR OPTIMAL MACROPHAGE KILLING EFFECTOR FUNCTIONS AND SURVIVAL IN MICE

Suraj P. Parihar[1,2], Mumin Ozturk[1,2], Mohlopheni J. Marakalala[1], Du Toit Loots[3], Ramona Hurdayal[1,2,4], Derylize B. Maasdorp[3], Mari Van Reenen[3], Daniel E. Zak[5], Fatoumatta Darboe[7], Adam Penn-Nicholson[7], Willem A. Hanekom[7], Michael Leitges[6], Thomas J. Scriba[7], Reto Guler[1,2] and Frank Brombacher[1,2]

[1]Institute of Infectious Diseases and Molecular Medicine (IDM), Division of Immunology and South African Medical Research Council (SAMRC) Immunology of Infectious Diseases, Faculty of Health Sciences, University of Cape Town, Anzio Road, Observatory 7925, Cape Town, South Africa.

[2]International Centre for Genetic Engineering and Biotechnology (ICGEB), Cape Town-Component, Cape Town, South Africa.

[3]Human Metabolomics, North-West University, Hoffman Street, Potchefstroom, 2531, South Africa.

[4]Department of Molecular and Cell Biology, Faculty of Science, University of Cape Town, Rondebosch 7701, Cape Town, South Africa.

[5]Center for Infectious Disease Research, Seattle, WA, USA.

[6]PKC Research Consult, Hofstr. 31, 51061 Cologne, Germany.

[7]South African Tuberculosis Vaccine Initiative (SATVI), Institute of Infectious Disease and Molecular Medicine (IDM) & Division of Immunology, Department of Pathology, University of Cape Town, Anzio Road, Observatory 7925, Cape Town, South Africa.

Full correspondence: Professor Frank Brombacher, UCT campus, International Centre for Genetic Engineering and Biotechnology (ICGEB), Wernher & Beit South Wing, Room S1.27, Anzio Road, Observatory 7925, Cape Town, South Africa.

ABSTRACT

We previously demonstrated that Protein Kinase C-delta (PKC-δ) is critical for immunity against *Listeria monocytogenes, Leishmania major,* and *Candida albicans* infection in mice. However, the functional relevance of PKCδ during *Mycobacterium tuberculosis* (*Mtb*) infection is unknown. PKCδ was significantly upregulated in patients with active TB disease and lung proteomics further revealed that PKCδ was highly abundant in the necrotic and cavitory regions of TB granulomas in multi-drug resistant human participants. In murine *Mtb* infection studies, PKCδ$^{-/-}$ mice were highly susceptible to tuberculosis with increased mortality, weight loss, exacerbated lung pathology reflected by uncontrolled pro-inflammatory cytokine responses and increased mycobacterial burdens. Moreover, these mice displayed a significant reduction in alveolar macrophages and dendritic cells, reduced accumulation of lipid bodies (in lungs and macrophages) and serum fatty acids. Further, a peptide inhibitor of PKCδ in wild-type mice caused increased inflammation in the lungs similar to PKCδ$^{-/-}$ mice. Mechanistically, increased bacterial growth in macrophages from PKCδ$^{-/-}$ mice was associated with a decline in killing effector functions independent of phagosome maturation and autophagy. Taken together, these data suggest that PKCδ is a marker of inflammation during active TB disease in humans and required for optimal macrophage killing effector functions and host protection during *Mtb* infection in mice.

INTRODUCTION

Protein Kinase C-delta (PKCδ) plays a multitude of physiological roles through its ability to phosphorylate multiple target proteins involved in various cellular processes such as signal transduction [203], apoptosis [204], proliferation and survival [205], transcription [206], hormonal regulation [207] and immune responses [201, 202]. PKCδ$^{-/-}$ mice were originally characterized by two independent research groups, who highlighted the role of this kinase in B cell anergy [208] and B cell-mediated autoimmunity [209]. Furthermore, PKCδ$^{-/-}$ mice were protected against high-fat-diet-induced glucose intolerance by exhibiting reduced accumulation of liver triacylglycerol and impaired production of lipogenic enzymes [210].

Most studies on the role of PKCδ were performed using inhibitors *in vitro*, which lacked in specificity to a particular PKC isoform. A frequently used example is rottlerin, which is a non-specific inhibitor of PKCδ to block enzymatic reactions and intracellular signaling in pancreatic acinar cells [211]. Rottlerin was shown to reduce viral burdens in human monocyte-derived

macrophages during the early stages of HIV-1 infection [212]. Physiologically, inhibition of PKCδ, with either rottlerin or anti-PKCδ siRNA, resulted in increased cholesterol efflux in hamster kidney cells and a murine macrophage cell line RAW264.7 [213]. Moreover, PKC isoforms such as δ and ε, are required for phagocytosis in RAW264.7 macrophages [214], and PKCε also regulates the autocrine production of TNF, which in turn induces apoptosis in LPS-activated macrophages [215].

Studies have suggested a functional role for PKCδ in regulating immunity to infectious diseases *in vivo*. Previously, using PKCδ$^{-/-}$ mice, we demonstrated a crucial role of this kinase in macrophage-mediated phagosomal clearance of the intracellular bacterium, *Listeria monocytogenes* [201]. We further reported that PKCδ regulates the production of IL-12p40/70 in both macrophages and dendritic cells, required for protective Th_1 immune responses in a murine model of cutaneous leishmaniasis [202]. We also demonstrated that deletion of PKCδ renders mice susceptible to *Candida albicans* infection via Card9-mediated anti-fungal immunity [216]. These studies highlighted the key role of PKCδ in the immune response to infectious diseases. However, the functional significance of this PKCδ in tuberculosis infection has not been studied yet.

Here, we investigate the role of PKCδ in host immunity to *Mtb* in human participants and in a murine model of tuberculosis. We report that PKCδ mRNA expression is increased in peripheral blood of participants with active tuberculosis. Additionally, proteomic analysis of lung tissues from treatment-refractory tuberculosis patients reveals higher levels of PKCδ protein expression in caseous and necrotic regions of cavitory granulomas, highlighting that PKCδ might be an indicator of an inflammation. We further demonstrate that deletion of PKCδ in mice has a detrimental effect on host with increased bacterial loads, enhanced lung pathology, and mortality. Moreover, PKCδ is critical for the accumulation of lipid bodies in macrophages and lungs during *Mtb* infection. Mechanistically, PKCδ is important for optimal killing effector functions, independent of phagosome maturation and autophagy in macrophages.

RESULTS

Increased expression of PKCδ during active tuberculosis disease

Recently, we identified a transcriptomic signature that has the potential to distinguish latent infection from the development of active disease [116]. Given the pivotal role of PKCδ in signal

transduction, we asked whether expression of this kinase changed during the transition from *Mtb* infection to TB disease. We analyzed gene expression data in whole blood from a nested control study correlating risk of TB from 800 days prior to diagnosis. This included 46 adolescents with latent *Mtb* infection who progressed to active disease (progressors) and 107 adolescents with *Mtb* infection who remained healthy [116]. PKCδ was significantly upregulated in progressors when compared to latently infected healthy controls (**Figure 1a**). Although two PKC isoforms (θ and η) exhibited down-regulation during progression to active TB disease, the expression levels of other PKC isoforms (α, β, γ, ι, ε and ζ) remained constant (**Supplementary Figure S1**). This highlighted PKCδ as a possible marker of active TB disease which we sought to validate using qRT-PCR. PKCδ mRNA expression was significantly higher in whole blood from eight participants with pulmonary TB disease when compared to sixteen healthy controls with or without latent *Mtb* infection (QuantiFERON +/-) (**Figure 1b**). This finding was confirmed in whole blood of a larger independent Strategic Health Innovation Partnerships (SHIP) cohort of 30 active tuberculosis participants and 30 healthy individuals with latent *Mtb* infection, too (**Figure 1c**). Additionally, human monocyte-derived macrophages (MDMs) also upregulated PKCδ expression, following *Mtb* infection (**Figure 1d**). Collectively, these data indicate that PKCδ expression increases during active TB disease and *in vitro* Mtb infection of macrophages.

We then investigated whether anti-tuberculosis therapy would decrease PKCδ expression. We analyzed a publicly available dataset from an independent study [217], which reported whole blood expression profiles of 27 first-time TB patients before and after treatment. PKCδ was the most abundantly expressed isoform compared to other PKC isoforms. The expression decreased starting from week 1 to 26 weeks of successful treatment with antituberculosis therapy (**Figure 1e**). Of note, all other PKC isoforms remained unchanged before and after tuberculosis therapy except PKCθ, which was marginally increased only at completion of treatment (**Figure 1e**). This decline in PKCδ expression after treatment suggests that it can be an important component or mediator of the host immune response during active TB disease.

PKCδ is highly expressed in necrotic and cavitory regions of granulomas in patients with Multi-Drug Resistant tuberculosis

We recently characterized proteomic signatures in various regions of granulomas from treatment-refractory TB patients who had undergone pneumonectomy due to severe lung damage

[187]. Using the proteomics data, we determined the protein expression levels of various PKC isoforms. Our analysis revealed that only PKCδ was associated with the necrotic regions of both caseous and cavitory granulomas (**Figure 1f**) whilst other PKC isoforms were largely absent in the lung tissue samples (data not shown). This suggests an association of PKCδ within the regions of *Mtb*-specific host immune responses at the site of disease. The abundance of PKCδ protein at the sites of exaggerated disease strengthens our transcriptomic findings in whole blood, highlighting that PKCδ can be an important host factor that is induced during the transition of cellular to necrotic granulomas in humans.

PKCδ is critical for host survival against *Mtb* infection in mice

To further investigate how PKCδ influences host mortality during *Mtb*-infection, we compared PKCδ$^{-/-}$ mice [201, 202] with wild-type controls in a murine model of experimental tuberculosis. Deletion of PKCδ rendered mice highly susceptible to various doses of intranasal *Mtb* infection (**Figure 2a, d,** and **g**). Earlier and increased mortality was associated with rapid weight loss (**Figure 2b, e,** and **h**) and increased bacterial titers in the lungs and spleen determined at the time of euthanasia (**Figure 2c, f** and **i**). Thus, PKCδ deficiency in mice results in increased bacterial burdens and mortality during *Mtb* infection.

Exacerbated histopathology and reduced accumulation of lipid bodies in the lungs of PKCδ$^{-/-}$ mice during *Mtb* infection

Since PKCδ mice succumbed to *Mtb* infection as early as 4 weeks in mortality studies **(Figure 2)**, we performed an in-depth analysis of disease parameters at 4 and 8 weeks, using a dose of 1000 CFU. At 4 and 8 weeks post-infection, PKCδ$^{-/-}$ mice displayed higher lung and spleen burdens (**Figure 3a**), corroborating the mortality findings. Susceptibility to infection in PKCδ$^{-/-}$ mice was further accompanied by a significant increase in lung inflammation as revealed by lung weight index (**Figure 3b**), higher pulmonary cell recruitment (**Figure 3c**) and larger lesion area in H&E-stained lung sections at 4 and 8 weeks after infection (**Figure 3d**). Furthermore, immunohistochemistry revealed that iNOS production was significantly increased in the lungs of PKCδ$^{-/-}$ mice, concomitant with increased pulmonary tissue pathology indicating that PKCδ contributes to the control of lung pathology (**Figure 3e**). Given the importance of PKCδ in the accumulation of cholesterol in human monocyte-derived macrophages [218] we also investigated neutral lipid accumulation in the lungs of PKCδ$^{-/-}$ mice. We found at 4 and 8 weeks after infection,

PKCδ$^{-/-}$ mice displayed significantly reduced accumulation of lipids in lungs when compared to control animals revealed by Oil Red O staining of tissue sections. (**Figure 3f**). We next assessed whether inhibiting PKCδ in wild-type mice using a specific peptide inhibitor TatVδ1.1 [219] would recapitulate exaggerated lung pathology of PKCδ$^{-/-}$ mice following *Mtb* infection. Indeed, mice treated with TatVδ1.1 had significantly higher lung weight index, more inflamed lung sections and lesion size when compared to control animals (**Supplementary Figure S2a-c**). Together, these results demonstrate that absence of PKCδ in *Mtb* infection resulted in exacerbated pathology and reduced accumulation of lipids in the lungs.

Increased pro-inflammatory cytokine responses in the lungs of PKCδ$^{-/-}$ mice following *Mtb* infection

Following excessive lung pathology as a consequence of increased bacterial loads in PKCδ$^{-/-}$ mice (**Figure 3d**), we measured the proinflammatory cytokines profile in the lungs. Compared with wild-type, PKCδ$^{-/-}$ mice showed marked increases in pro-inflammatory cytokines including IFN-γ, TNF, IL-1β, IFN-β and IL-6 with minor effect on IL-10 at week 4 (**Figure 4a**) and week 8 (**Figure 4b**) after infection. The extent of proinflammatory cytokines response in the lungs of wild-type mice is, in fact, *Mtb* infection dose-dependent phenomenon (**Supplementary Figure S5f**). Furthermore, flow cytometric analysis of various pulmonary immune cell populations in PKCδ$^{-/-}$ mice after 4 and 8 weeks of infection, demonstrated that frequencies and total cell numbers of alveolar macrophages, (**Figure 4c, f, i** and **l**) and dendritic cells (**Figure 4d, g, j,** and **m**), were significantly decreased with concomitant increase in activated macrophages (**Figure 4g**) when compared to control mice. Of note, we observed no major differences in the frequencies and cell numbers of lymphocytes (CD4^{+} and CD8^{+} T and B cells) (**Figure 4e, h, k,** and **n**) or neutrophils (**Figure 4c, f, i** and **l**) infiltrating the lung during infection. Gating strategy to define alveolar macrophages and dendritic cells in the lungs are shown (**Supplementary Figure S2d, e**). Additionally, we show that percentage of T-cells were decreased whilst dendritic cells were increased in thoracic lymph nodes at 4 weeks (**Supplementary Figure S3a-d**) however no differences were observed at 8 weeks post infection (**Supplementary Figure S3e-h**). Higher mycobacterial burdens during TB infection along with increased proinflammatory cytokines might be responsible for the increased mortality observed in PKCδ$^{-/-}$ mice during *Mtb* infection.

Decreased fatty acids in serum of PKCδ$^{-/-}$ mice following *Mtb* infection

Decreased lipid accumulation in lungs of PKCδ$^{-/-}$ mice during *Mtb* infection prompted us to perform a total metabolome analysis of the serum in these animals. Principal Component Analysis (PCA) shows a clear differentiation between *Mtb*-infected (1000 CFU) wild-type and PKCδ$^{-/-}$ mice at 4 weeks (62% variance) and 8 weeks (64% variance) post infection, respectively (**Figure 5a** and **b**). Metabolite profiles of these two groups thus varied significantly to allow a natural grouping of the individual samples. Considering these results, *Mtb*-infected PKCδ$^{-/-}$ mice showed significantly decreased levels of all serum fatty acids when compared to wild-type mice, except for mead acid, an elevation of which is a well-known marker for fatty acid deficiencies [220]. Here, we selectively report that host protective (arachidonic acid, α-linoleic acid, and palmitic acid) [221] and host detrimental (behenic acid, cervonic acid or DHA and timnodonic acid or EPA) [221] fatty acids were significantly lower in the PKCδ$^{-/-}$ mice during *Mtb* infection (**Figure 5c** and **d**). To assess whether the observed effect was indeed PKCδ specific and not as a consequence of morbidity and pathology at this dose resulted in reduced food and water intake, we performed metabolomics at a low dose (70 CFU) and found similar results (**Supplementary Figure S5a-d**) to 1000 CFU. Moreover, we also confirmed that the changes in lipid profiles were not a function of bacterial loads in the lungs of wild-type mice (**Supplementary Figure S5e**). Thus, the absence of PKCδ led to a modest decrease in serum fatty acids of *Mtb*-infected mice.

Macrophages deficient in PKCδ exhibit reduced mycobacterial killing capacity and reduced accumulation of lipid bodies

Using our publically available dataset from CAGE sequencing of macrophages infected with a hypervirulent *Mtb* strain (HN878) [122], we report that PKCδ in the murine BMDMs was also upregulated, whereas other PKC isoforms (except Prkcb) remained largely unaffected (**Figure 6a**), PKCδ expression was also validated by qRT-PCR in murine macrophages (**Supplementary Figure S4a**). Given the entire study was performed with an H37Rv strain of Mtb, we also measured the expression of PKCδ in H37Rv-infected macrophages (**Figure 6b**), which had slightly different kinetics at 24 hours post infection when compared to HN878-infected macrophages (**Figure 6a** and **Supplementary Figure S4a**). This discrepancy in expression kinetics at the indicated time point was most likely due to the different strains of *Mtb*. We next investigated the intracellular growth of *Mtb* in primary macrophages deficient for PKCδ. Mycobacterial growth was

significantly increased in PKCδ$^{-/-}$ macrophages at 3 and 6 days after infection (**Figure 6c**) as well as in wild-type macrophages transfected with anti-PKCδ siRNA at 48 hours post-infection (**Supplementary Figure S4b**). In PKCδ$^{-/-}$ mice, we found a reduced accumulation of the lipid bodies in the *Mtb*-infected lungs. Likewise, PKCδ$^{-/-}$ macrophages displayed fewer lipid bodies following *Mtb* infection in a time-dependent manner as shown by the Oil Red O staining (red) in fluorescent microscopy concomitant with significantly higher bacterial numbers shown as green fluorescent protein-expressing *Mtb* (Rv-GFP) (**Figure 6d** and **e**). Unlike in the *in vivo* model, we found no differences in cytokine production by PKCδ$^{-/-}$ BMDMs except for a significant decrease in IL-6 (**Figure 6f-i**) suggesting other cell populations contributed in total cytokine production in the lungs or CFU difference between the groups is not substantial as *in vivo* which does not drive higher cytokine production. Thus, PKCδ is important for macrophage-mediated containment of mycobacteria and lipid accumulation.

Killing effector functions in *Mtb*-infected PKCδ$^{-/-}$ macrophages

The PKC isoforms including β [222] and α [223] were reported to be important for maturation of *Mtb*-containing phagosomes. In bacterial infection, we previously reported that PKCδ is critical for containment of *Listeria monocytogenes* in phagosomes of macrophages [201]. Surprisingly in *Mtb* infection, no differences in the analyzed phagosome markers including LAMP-1, LAMP-3, Cathepsin D and an autophagy marker LC3-II were observed between PKCδ$^{-/-}$ and control macrophages (**Figure 7a-b**). This result suggests that PKCδ is dispensable for phagosome and autophagy-mediated killing of *Mtb* in macrophages.

Since the intracellular killing of *Mtb* is enhanced by nitrogen and oxygen species [224], we measured the ability of macrophages to release reactive oxygen species (ROS), hydrogen peroxide (H_2O_2) and nitric oxide (NO). We report nitric oxide production was significantly decreased in PKCδ$^{-/-}$ macrophages at the protein level (**Figure 7c**) and confirmed at mRNA level using qRT-PCR (**Figure 7d**). To assess whether this led to concomitant increase in Arginase 1 (Arg1) expression since both iNOS and Arg1 utilizes same substrate (L-arginine). To our surprise, the expression of Arg1 was also significantly decreased in a time-dependent manner when compared to control macrophages (**Figure 7e**). Further, we also found that PKCδ is upregulated with IL-4 stimulation in *Mtb*-infected macrophages from our CAGE dataset (**Supplementary Figure S4c**).

In addition to NO, the release of H_2O_2 (**Figure 7f**) and reactive oxygen species (ROS) (**Figure 7g**) was also significantly decreased in the PKCδ$^{-/-}$ macrophages. Further, the absence of PKCδ in macrophages also renders them more prone to apoptosis, revealed by Annexin V and 7-AAD staining following *Mtb* infection (**Figure 7h**). Moreover, we also evaluated the possible effect of antimicrobial molecules secreted into the cell supernatant by *Mtb*-infected macrophages by treating infected PKCδ$^{-/-}$ cells with supernatants from wild-type cells, and *vice versa*. Supernatant from infected wild-type macrophages indeed reduced bacterial growth in *Mtb*-infected PKCδ$^{-/-}$ macrophages (**Figure 7j**). This indicates that a deficiency of PKCδ decreases optimal oxidative and nitrosative killing effector functions in macrophages thereby favors bacterial growth.

Oleic acid increased bacterial growth in PKCδ$^{-/-}$ macrophages

Of interest, from decreased lipids in lungs (**Figure 3f**), macrophages (**Figure 6d**) and serum fatty acids (**Figure 5c** and **d**) of PKCδ$^{-/-}$ mice. We asked whether foam cell formation using ox-LDL (oxidized low-density lipoproteins) would control the growth of *Mtb* in otherwise susceptible PKCδ$^{-/-}$ macrophages. We found no differences in bacterial growth in PKCδ$^{-/-}$ macrophages cultured in presence of ox-LDLs for 3 days when compared to untreated cells (**Figure 7i**). On the other hand, ox-LDL-treated wild-type macrophages revealed a significant increase in bacterial growth when compared to untreated cells (**Figure 7i**), most likely due to foam cell formation and alternative activation of macrophages (M2). Furthermore, we evaluated the effect of an unsaturated (Oleic Acid), saturated (Palmitic Acid) fatty acids and Native-LDLs on PKCδ$^{-/-}$ macrophages. In contrast to ox-LDL, we found a significant increase in growth of *Mtb* in PKCδ$^{-/-}$ macrophages (**Supplementary Figure S4d**) with concomitant decrease in production of nitric oxide (**Supplementary Figure S4e**) in presence of oleic acid and native-LDL but not with palmitic acid despite a modest decrease in nitric oxide production (**Supplementary Figure S4d-e**). This suggests that fatty acids have a differential effect on the role of PKC-delta in mycobacterial survival *in vitro*. Supplementation of PKCd KO macrophages with fatty acids did not reverse susceptibility of PKCd KO macrophages which means the role of PKCd on lipid accumulation might not be a major contributing factor on increased mycobacterial burdens *in vitro.*

DISCUSSION

We have demonstrated the functional role of PKCδ in host defense against *Mtb* infection. PKCδ is highly expressed in human whole blood during active tuberculosis disease progression as

well as within the *Mtb*-specific pro-inflammatory regions of necrotic and cavitory lung granulomas during TB disease. These regions of high pro-inflammatory signatures, are required for an early control of bacterial replication and could lead to necrotic damage (caseation) and consequent cavity formation if not appropriately regulated [225]. This was indeed evident in this study, where PKCδ was more abundant in the caseous and cavitory regions, colocalizing with antimicrobial signatures [187] and the regions of abundant lipids in granulomas [226]. Consistent with this, we found PKCδ as an indicator of lung inflammation in yet another whole blood transcriptome dataset from pulmonary infections such as sarcoidosis, tuberculosis, pneumonia, and lung cancer [227]. Given the non-specificity to TB and substantial overlap in PKCδ expression between healthy participants and TB patients, the gene offers a limitation to be used as a prognostic marker for tuberculosis. Mass spectrometry additionally confirmed that the expression of PKCδ varies within the regions of lung granuloma. Importantly, anti-tuberculosis therapy decreased PKCδ expression in whole blood of human patients, reflecting a potential role for this protein kinase as a host factor regulating *Mtb*-driven inflammation.

Our findings revealed that PKCδ is indeed associated with host defense against murine tuberculosis since PKCδ ablation enhanced mortality with rapid weight loss, high bacterial loads and exacerbated lung pathology in *Mtb* infected mice. In these mice, we found higher levels of lung proinflammatory cytokines during *Mtb* infection which was consistent with our previously published reports on the role of PKCδ in listeriosis [201] and cutaneous leishmaniasis [202]. Notably, inhibition of PKCδ using a specific peptide inhibitor-TatVδ1.1 [219] recapitulated aggravated lung inflammation in PKCδ$^{-/-}$ mice during *Mtb* infection; revealing a direct role of this kinase in regulation of *Mtb*-driven lung inflammation.

Consistent with the essential role of alveolar macrophages in controlling *Mtb* infection in mice [228], we found strikingly reduced numbers of these macrophages with concomitantly higher lung bacterial loads which could lead to necrosis in PKCδ$^{-/-}$ mice. To control infection, activated macrophages and monocytes would be recruited, perhaps contribute in excessive nitric oxide in the lungs, in contrast to reduced iNOS expression in PKCδ$^{-/-}$ macrophages. Notably, mice deficient for alveolar macrophages also result in higher accumulation of intracellular lipids in the lungs [229]. This effect on lipid homeostasis is unlikely to recapitulate in PKCδ$^{-/-}$ mice since the absence of this kinase would result in excess lipid efflux from the macrophages, therefore, decreased lipid

accumulation and diminished production of lipogenic enzymes. Our findings suggest that PKCδ is required for maintenance of an optimal inflammatory balance during *Mtb* infection, which is a key factor in limiting immunopathology to host lung tissue. We infer from these findings deletion of PKCδ in mice renders them hyper-susceptible to tuberculosis, therefore it is likely that increased expression (blood) and abundance (granulomas) of this kinase reflect its role as a host factor to contain inflammation in humans.

Host lipid bodies provide an excellent nutrient source for the survival of *Mtb* in host cells [45] thereby decreasing its own metabolism [230], which allows pathogenesis [231] and persistence of the bacterium [232-234]. Consistent with the necessity of triacylglycerol for slow-replication, a recent study demonstrated that deposition of excessive triacylglycerol in *Mtb* bacterium slowed down its growth as opposed to a *Mtb* strain capable of pumping out lipids [235]. Reports have indicated a critical role of PKCδ in the accumulation of cholesterol in human [218] and mouse macrophages [213]. Corroborating with these findings, we found that PKCδ is indeed critical for the accumulation of lipids in the lungs, macrophages and to a lesser extent in the case of fatty acids in sera following *Mtb* infection. Notably, it has been shown that in steady state absence of PKCδ is dispensable for the uptake of ox-LDL to induce foam cell formation in murine and human macrophages [236]. Further, our observations of *Mtb* in PKCδ$^{-/-}$ macrophages in presence of unsaturated, saturated fatty acids, oxidized and native LDL support that the type of lipid contributes to foam cell formation that may not necessarily contribute to the intracellular bacterial growth. Recently, a published report has shown that increased lipids in lungs and macrophages drive the polarization of macrophages (M2) involved in fibrosis [237]. In PKCδ$^{-/-}$ mice, the decreased availability of lipids and enhanced pro-inflammatory cytokines, in addition, reduced Arg1 expression in macrophages might have limited tissue repair processes in the lungs. Thus, lipid accumulation can be the consequence, rather than the cause of susceptibility to *Mtb* infection in PKCδ$^{-/-}$ mice. This *Mtb*-driven modulation of host lipids may be the means by which this highly evolved pathogen controls its replication rate *in vivo*. It is feasible that inability of PKCδ$^{-/-}$ mice to accumulate intracellular lipids hampers the ability of *Mtb* to undergo persistent, slow-replicative state during infection.

Intracellular *Mtb* can be eliminated by the induction of macrophage phagosome maturation [238] and autophagy [83]. The PKC isoforms including β [222] and α [223] were reported to be

important for maturation of *Mtb*-containing phagosomes. In contrast to PKCβ and α, our findings indicate that phagosome maturation and autophagy occurs independently of PKCδ in *Mtb*-infected macrophages. An alternative explanation is given PKCδ, unlike other isoforms (α, β and γ), is insensitive to calcium signaling [239] which is important for phagosome maturation. Another isoform PKCζ has been implicated as a key factor for ERK1/2 and TLR2 mediated secretion of TNF both in murine and human macrophages following *Mtb* infection *in vitro* [240]. Whilst a recent study has demonstrated that inhibition of PKCδ with rottlerin abrogates apoptosis in murine macrophages when cultured with cell-free supernatant of *Mycobacterium indicus pranni* (*Mw*) [241]. In contrast, we observed increased apoptosis in PKCδ$^{-/-}$ macrophages following *Mtb* infection. This observation strengthens accumulating evidence regarding the non-specific actions of rottlerin as a PKCδ inhibitor [211, 236].

It is well-established that within macrophages, *Mtb* can be successfully eliminated by oxidative (ROS, H_2O_2) and nitrosative (nitric oxide) killing functions [224]. Interestingly, IFN-γ activated macrophages synergistically increase nitric oxide production 5-fold upon PMA-mediated PKC activation in *M. bovis* (BCG) infected macrophages [242]. Indeed, this was confirmed in our study since the presence of PKCδ enhanced killing effector functions whereas the absence thereof inhibited these effector responses thereby reducing the mycobacterial killing capacity of PKCδ$^{-/-}$ macrophages. Interestingly, in addition to reduced iNOS, this study shows decreased Arg1 expression in PKCδ$^{-/-}$ macrophages. We also found increased expression of PKCδ in Mtb-infected macrophages stimulated with IL-4. This evidence provides support for the possibility that PKCδ has an important role in the macrophage plasticity. We infer from these findings that PKCδ has a role in macrophage polarization during lung infections *in vivo*.

Collectively, our data revealed that PKCδ is an indicator of inflammation in both systemic and local tissue compartments during active tuberculosis disease progression in humans. Global deletion of PKCδ worsens the disease outcome in mice which exaggerated mortality with a shift towards increased bacterial burdens, exacerbated pathology and excessive pro-inflammatory responses. To a lesser extent following *Mtb* infection, decreased lipids in lungs and macrophages of PKCδ$^{-/-}$ mice further eliminate the possibility for this bacterium to undergo persistence, however not the cause of increased burdens. Mechanistically, reduced killing effector functions in macrophages increased susceptibility to *Mtb* in the absence of PKCδ. Taken together, the onset of

active human *Mtb* disease correlates with PKCδ expression and conferring from our murine model, PKCδ might be a critical factor employed by the host to control exacerbation of *Mtb* infection.

METHODS

Whole blood mRNA signature of PKC

For whole blood transcriptomics, we analyzed the publicly available RNA-Seq data set from the Adolescent Cohort Study [116]. We determined expression profiles of all PKC isoforms from 800 days prior to diagnosis of tuberculosis disease.

A cross-sectional cohort of TB disease and healthy control participants

A cross-sectional study of 30 healthy HIV-negative adults with latent *Mtb* infection and 30 HIV-negative adults with active pulmonary TB disease, recruited from the Western Cape region of South Africa. The human Study protocol (HEC: 288/2008) was approved by the University of Cape Town, Human Ethics Committee. Participants were recruited following written informed consent prior to inclusion in the study. Latent *Mtb* infection was diagnosed by QuantiFERON TB Gold in-tube assay (Qiagen, IFN-γ levels > 0.35 IU/mL) and TB disease was diagnosed as sputum-positive positive Xpert MTB/RIF test (Cepheid). Whole blood in PAXgene blood RNA tubes (PreAnalytix) was collected from each participant.

Human PKCδ expression following treatment and lung proteomics from treatment-refractory tuberculosis patients

The blood gene signature from the publically available data set in the NCBI-GEO database, accession number GSE31348 was used to analyze PKC expression of all isoforms during tuberculosis treatment [217]. For human lung proteomics, we analyzed the publicly available data that have been deposited into the PRIDE partner repository with the dataset identifier PXD003646. The heat map plot was constructed by calculating z-scores of PKCδ abundance in different types of granulomas derived from multi-drug resistant TB patients who had undergone pneumonectomy. Details of the patients and surgical procedures have been described previously [187].

Mice

Protein Kinase C-delta ($PKC\delta^{-/-}$) deficient mice on the 129Sv genetic background (8-12 weeks) were maintained under specific-pathogen-free conditions in individually ventilated cages.

All experiments were performed in accordance with the South African National Guidelines and University of Cape Town practice for laboratory animal procedures. The protocol (AEC: 012/036) was approved by the Animal Ethics Committee, Faculty of Health Sciences, University of Cape Town, Cape Town, South Africa.

Mtb infection and determination of bacterial loads in mice

Mtb (H37Rv) was grown to log phase in 7H9 complete media, and stocks were prepared for infections via an intranasal route as described previously [243]. Bacterial loads in lungs and spleen of *Mtb*-infected mice were determined at different time points post-infection. Briefly, organs from euthanized mice were removed aseptically, weighed and homogenized in 0.04% Tween 80. Ten-fold dilutions were plated onto Middlebrook 7H10 agar plates supplemented with 10% OADC and 0.5% glycerol and incubated at 37°C for 21 days before colonies were counted.

Histopathology, immunohistochemistry and lipid staining of the lung sections

Formalin-fixed (10%) lung tissue from *Mtb*-infected mice was cut into 3-micron sections and stained with H&E for histopathological analysis. For iNOS staining, immunohistochemistry was performed using rabbit anti-mouse iNOS (Abcam) as described previously [191]. Neutral lipids were analyzed in lung sections of *Mtb*-infected mice or macrophages by Oil red O (Sigma) staining for 5 minutes following washing and then a rinse with 60% isopropanol [244]. Sections were mounted using the gelatine-based mounting medium. Image acquisition and quantification of lesion area, iNOS staining and area covered by lipid bodies were performed on a Nikon 90i microscope using NIS advanced software.

Cytokine responses and immune cell populations in lungs using FACS

Supernatants from lung homogenates were collected for the determination of cytokines. IFN-γ, TNF, IL-6, IL-10 (all BD Biosciences) and IL-1β (R&D Systems) and IFN-β (BioLegend) productions were quantified in these supernatants by ELISA. Single cell suspension of *Mtb*-infected was lungs was prepared following collagenase digestion as previously described [191]. Cells were then stained for lymphocytes ($CD4^+$ T cells, $CD8^+$ T cells and B cells) and myeloid populations (alveolar macrophages, activated macrophages, dendritic cells, and neutrophils). Surface phenotyping of various cell populations was performed using the following antibodies; CD3-FITC, CD4-PE, CD8-APC, CD19-PerCP, CD11c-APC, CD11b-PE, MHC II-FITC, Siglec-

F-PE and Gr-1-FITC (all BD Biosciences). Cells were acquired on a FACS Calibur and the data was analyzed using FlowJo software (v10.1, Tree star) as described previously [191].

Metabolome analysis in serum of PKCδ mice using GC-MS

Extraction of the collected serum samples from *Mtb*-infected PKCδ$^{-/-}$ and wild-type mice at 4 and 8 weeks post-infection was performed as previously described [245] using 50 µL of 0.45 µg/mL 3-phenylbutyric acid (Sigma-Aldrich), as an internal standard prior to GC x GC-TOFMS analyses.

Mtb* infection *in vitro

Murine BMDMs and human MDMs were generated as previously described [243]. Macrophages were either treated with ox-LDL (100µg/ml) or native-LDL (125µg/ml) or oleic acid (500µM) or palmitic acid (500µM) or left untreated overnight. Cells were then infected in presence of treatment(s) with *Mtb* (H37Rv, unless otherwise indicated) with MOI of 2 for 4 hours followed by two washes with the pre-warmed medium. At indicated time points, cells were lysed in 0.1% Triton-X-100 for determination of bacterial growth or fixed using paraformaldehyde (4%) for visualization of bacteria and Oil Red O staining. Images were acquired using a Carl Zeiss 510 confocal microscope and bright field images were analyzed for the area under the lipid stain as mentioned above.

Quantitative RT-PCR from whole blood, MDMs, and BMDMs

Sixteen RNA samples from QuantiFERON positive and negative and eight tuberculosis progressor subjects were validated for the expression of PKCδ using qRT-PCR from the Adolescent Cohort Study. As per manufacturer's instructions, RNA was extracted from whole blood (PAXgene blood RNA kit, Qiagen). cDNA was synthesized from RNA using Superscript II Reverse Transcriptase (Life Technologies). *Mtb*-infected BMDMs or MDMs were reverse transcribed by Transcriptor First Strand cDNA Synthesis Kit (Roche) according to manufacturer's instructions. Real-time PCR was performed with LightCycler® 480 SYBR Green I Master mix using a LightCycler® 480 II (Roche) for relative expression of PKCδ relative to HPRT housekeeping gene.

Western Blot Analysis

SDS-PAGE and Western Blot analysis was performed as previously described [243]. Briefly, macrophages ($3x10^6$) were infected with *Mtb* at MOI of two for 4 hours. Cells were washed and then lysed with ice-cold RIPA buffer containing protease inhibitors for 30 minutes at 4°C. Total cell lysates were analyzed for protein contents using BCA assay (ThermoFisher). An equal amount of protein (40 μg) were then electrophoresed on 12% SDS-PAGE and transferred to a nitrocellulose membrane (Sigma). The membrane was probed with anti-LAMP-1, LAMP-3, Cathepsin D, LC3-II and GAPDH primary antibodies diluted (1:200) in blocking buffer at 4°C overnight. The membrane was then incubated with the HRP-conjugated secondary antibody (1:10,000) for 1 hour at room temperature in blocking buffer. Immunoblots were developed using Super Signal West Dura substrate (Pierce).

Measurements of nitric oxide, hydrogen peroxide and reactive oxygen species in BMDMs

Cell supernatants from infected macrophages were collected for measurement of nitric oxide using Griess reagent. Hydrogen peroxide (H_2O_2) release from macrophages was measured using colorimetric detection kit (Amplex Red Hydrogen Peroxide Assay, ThermoFischer). Reactive oxygen species was determined in macrophages using nitroblue tetrazolium (NBT, Sigma-Aldrich), which is reduced to a dark-blue insoluble formazan. Cells were incubated for phosphate buffered saline containing 0.2% NBT for 90 minutes. Formazan was dissolved in 0.04% HCL in isopropanol, and the absorbance was determined at 560 nm [246].

Statistics

All data were analyzed using Graph Pad Prism v 6.0, a student t-test (two-tailed with unequal variance) unless otherwise stated. A 'p' value of less than 0.05 was considered significant.

FIGURE LEGENDS

Figure 1 Increased expression of PKCδ in human whole blood, lungs of TB patients and *Mtb*-infected macrophages. (**a**) PKCδ mRNA expression in TB progressors, expressed as log2 fold change over matched controls, from Adolescent Cohort Study (ACS) group. The dotted line represents the mean log2 fold change, nonlinear spline function in 46 progressors and 107 healthy QuantiFERON positive controls. The blue shaded area represents 99% confidence intervals. (**b**) mRNA expression of PKCδ measured in an independent QuantiFERON negative or positive

controls, or patients with active TB disease, from ACS group in **A** (n = 8-16). (**c**) PKCδ mRNA expression validated by qRT-PCR in whole blood from SHIP cohort in adults with active TB disease before the initiation of drug treatment (n = 30) or QuantiFERON positive healthy controls (n = 30, LTBI, latent *Mtb* infection). (**d**) PKCδ mRNA expression in MDMs of healthy donors after *Mtb* infection *in vitro* (n = 2). (**e**) mRNA expression of PKC isoforms following the onset of antitubercular treatment in human TB patients (n = 27). (**f**) Heat map of z-score and log2-transformed label-free quantification of PKCδ in different types of human granulomas, excised from patients infected with multi-drug resistant *Mtb* (n = 5). Data are represented as mean ± SEM, analyzed using unpaired, student t-test (**c**), One Way ANOVA (**b-e**), * $p < 0.05$, ** $p < 0.01$, *** $p < 0.001$, **** $p < 0.0001$ versus control.

Figure 2 PKCδ$^{-/-}$ mice displayed enhanced mortality and mycobacterial burdens. Mice were infected with a range of *Mtb* (H37Rv) doses via intranasal challenge for mortality studies. Survival curve, body weight change and lung bacterial burden determined at the time of euthanasia. (**a-c**) 5000 CFU after 6 weeks. (**d-f**) 1000 CFU after 8 weeks. (**g-i**) 350 CFU after 18 weeks. Mortality curves were analyzed by Kaplan-Meyer survival test, ** $p < 0.01$, *** $p < 0.001$ versus WT control mice. Data are represented as mean ± SEM of 9-10 mice/group, analyzed using unpaired, student t-test, * $p < 0.05$, ** $p < 0.01$, *** $p < 0.001$ versus control.

Figure 3 PKCδ$^{-/-}$ mice displayed increased lung pathology, nitric oxide and decreased lipid accumulation in the lungs. Mice were infected with *Mtb* (1000 CFU) via intranasal challenge. (**a**) Bacterial burden in lungs and spleens were determined at 4 and 8 weeks after infection. (**b-c**) Lung weight index, as a proxy for inflammation and a total number of cells harvested at 4 and 8 weeks after infection. (**d-f**) Representative images and quantification of (**d**) histopathology H&E staining and lesions, **(e)** immunohistochemistry for iNOS and **(f)** Oil Red O staining for lipids at the indicated time points. Data are represented as mean ± SEM of n = 4-5 mice/group and representative of two independent experiments. Data is analyzed using unpaired, student t-test, * $p < 0.05$, ** $p < 0.01$, *** $p < 0.001$, versus WT control.

Figure 4 Increased pro-inflammatory cytokine responses and the immune cell populations in the lungs of PKCδ$^{-/-}$ mice following *Mtb* infection. (**a-b**) Supernatants from lung homogenates were analyzed for IFN-γ, TNF, IL-1β, IL-10 and IFN-β using ELISA after 4 and 8 weeks of *Mtb* infection. Single cell suspension of lung tissue was analyzed for percentage and total cell numbers of immune cell populations at 4 weeks (**c-h**) and 8 weeks (**i-n**) after infection. Surface markers of

different cell populations as follows; B cells = $CD19^+CD3^-$, CD4 T cells = $CD3^+CD4^+$, CD8 T cells = $CD3^+CD8^+$, Alveolar macrophages = $SiglecF^+CD11c^+$, Activated Macrophages = $CD11b^+MHCII^+CD11c^-$, DCs = $CD11c^+MHCII^+CD11b^-$ and Neutrophils = $Gr1^+CD11c^-$. Data are represented as mean ± SEM of n = 4-5 mice/group and representative of two independent experiments. Data is analyzed using unpaired, student t-test, * $p < 0.05$, ** $p < 0.01$, *** $p < 0.001$, versus WT control mice.

Figure 5 Decreased serum fatty acids by metabolic analysis following *Mtb* infection. (**a-b**) PCA plots with percentage variation for each Principal Component is indicated in parenthesis on the respective axis at 4 weeks and 8 weeks after infection (1000 CFU). (**c-d**) Serum levels (µg/L) of selected host-protective (arachidonic acid, α-linolenic acid and palmitic acid) and detrimental fatty acids (behenic acid, DHA and EPA) during *Mtb* infection at 4 weeks and 8 weeks after infection. Data are represented as mean ± SD of n = 4-5 mice/group. Data is analyzed using univariate and multivariate statistical techniques (PCA powers > 0.5, PLS-DA VIP > 1.0, effect size > 0.8, and student t-test $p < 0.05$) versus WT control mice.

Figure 6 Increased mycobacterial growth and decreased lipid bodies in PKCδ-deficient macrophages. (**a**) Expression of PKCδ and other isoforms in BMDMs infected with an HN878 strain of *Mtb* from CAGE study. (**b**) PKCδ mRNA expression during H37Rv *Mtb* infection in BMDMs using qRT-PCR. (**c**) Increased growth of H37Rv *Mtb* (MOI=2) in macrophages deficient for PKCδ during the course of infection. (**d-e**) $PKC\delta^{-/-}$ and WT BMDMs were infected with GFP-expressing *Mtb* (green, H37Rv) and stained with Oil Red O (red) for visualization and determination of intracellular bacteria and quantification of lipid bodies (Insets is bright field view). (**f-i**) Supernatants from infected macrophages were analyzed for the production of TNF, IL-12p40, IL-6 and IL-1β at indicated time points after infection by ELISA. Data are represented as mean ± SEM of quadruplicate and representative of three independent experiments, Data is analyzed using unpaired, student t-test, * $p < 0.05$, ** $p < 0.01$, *** $p < 0.001$, versus WT control macrophages.

Figure 7 Decreased production of killing effector molecules in macrophages deficient for PKCδ but similar phagosome maturation and autophagy induction. (**a-b**) Western Blot and densitometry analysis of phagosome (LAMP-1, LAMP-3, and Cathepsin D) and autophagy (LC3-II) markers in total macrophage cell lysates following *Mtb* infection. (**c-d**) Impaired production of nitric oxide in PKCδ macrophages measured by Griess reagent assay and qRT-PCR. (**e**) Decreased

mRNA expression Arginase 1 measured by qRT-PCR in PKCδ$^{-/-}$ macrophages. (**f-g**) Deficiency of PKCδ resulted in decreased production of hydrogen peroxide and reactive oxygen species (ROS). (**h**) Percentage of macrophages live, dead and apoptotic after 3 days of infection determined by Annexin V and 7-AAD staining. (**i**) Macrophages from wild-type and PKCδ$^{-/-}$ mice were treated overnight with or without oxidized-LDL. Cells were then infected with *Mtb*-containing medium with Ox-LDL for 3 days to determine mycobacterial growth. (**j**) Supernatants from 3 days infected WT and PKCδ$^{-/-}$ macrophages were transferred on 4 hours infected PKCδ$^{-/-}$ (WT SN) and WT (PKCδ$^{-/-}$ SN) macrophages to determine bacterial growth at 3 days post infection. Data are represented as mean ± SEM of quadruplicate and representative of three independent experiments, Data is analyzed using unpaired, student t-test, * $p < 0.05$, *** $p < 0.001$, versus WT control macrophages.

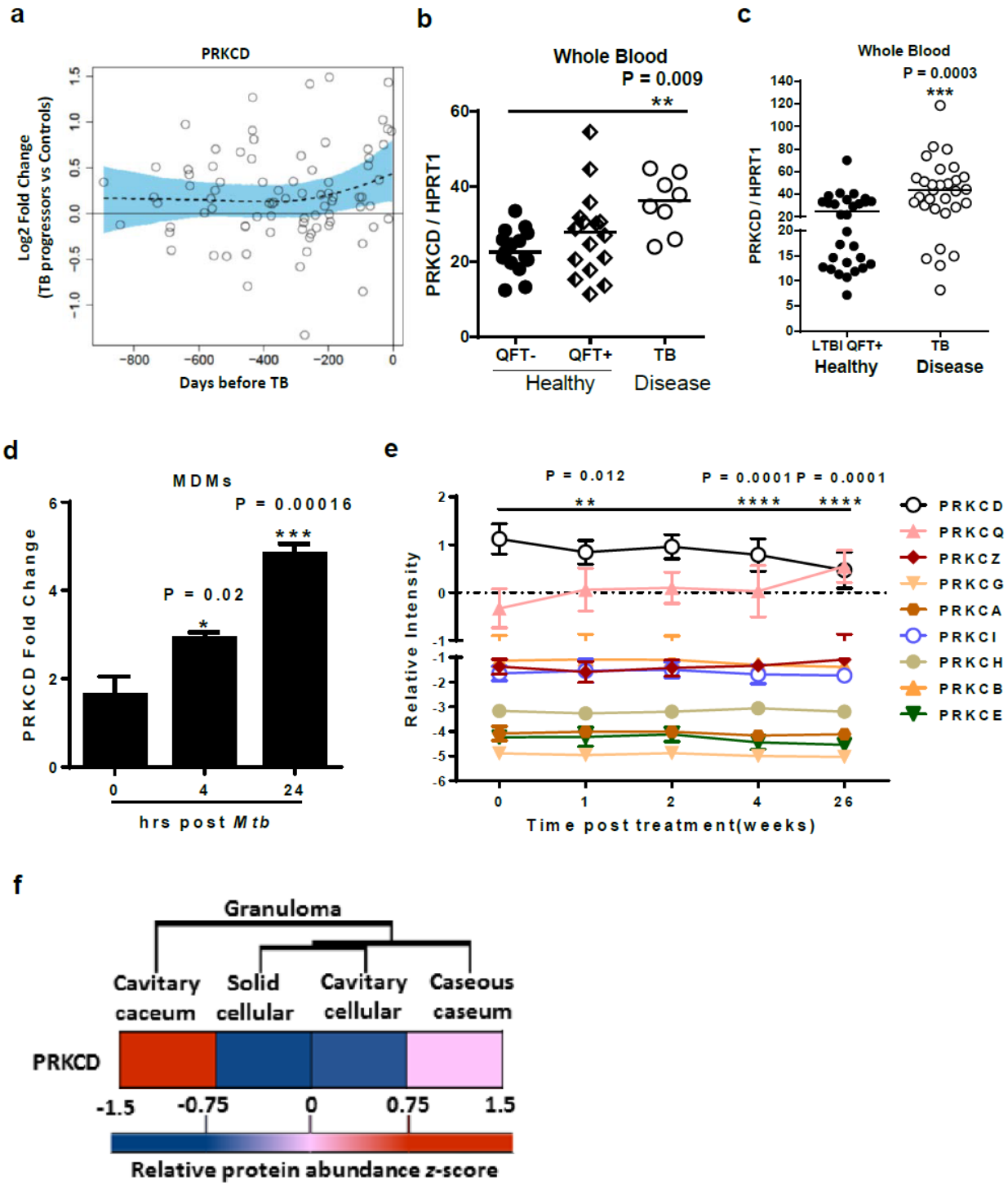
a
PRKCD
Log2 Fold Change (TB progressors vs Controls)
Days before TB
b
Whole Blood
P = 0.009
**
PRKCD / HPRT1
QFT-
QFT+
TB
Healthy
Disease
c
Whole Blood
P = 0.0003
***
PRKCD / HPRT1
LTBI QFT+
TB
Healthy
Disease
d
MDMs
P = 0.00016
***
P = 0.02
*
PRKCD Fold Change
hrs post Mtb
e
P = 0.012
**
P = 0.0001
****
P = 0.0001
****
Relative Intensity
Time post treatment(weeks)
PRKCD
PRKCQ
PRKCZ
PRKCG
PRKCA
PRKCI
PRKCH
PRKCB
PRKCE
f
Granuloma
Cavitary caceum
Solid cellular
Cavitary cellular
Caseous caseum
PRKCD
Relative protein abundance z-score

Figure 1

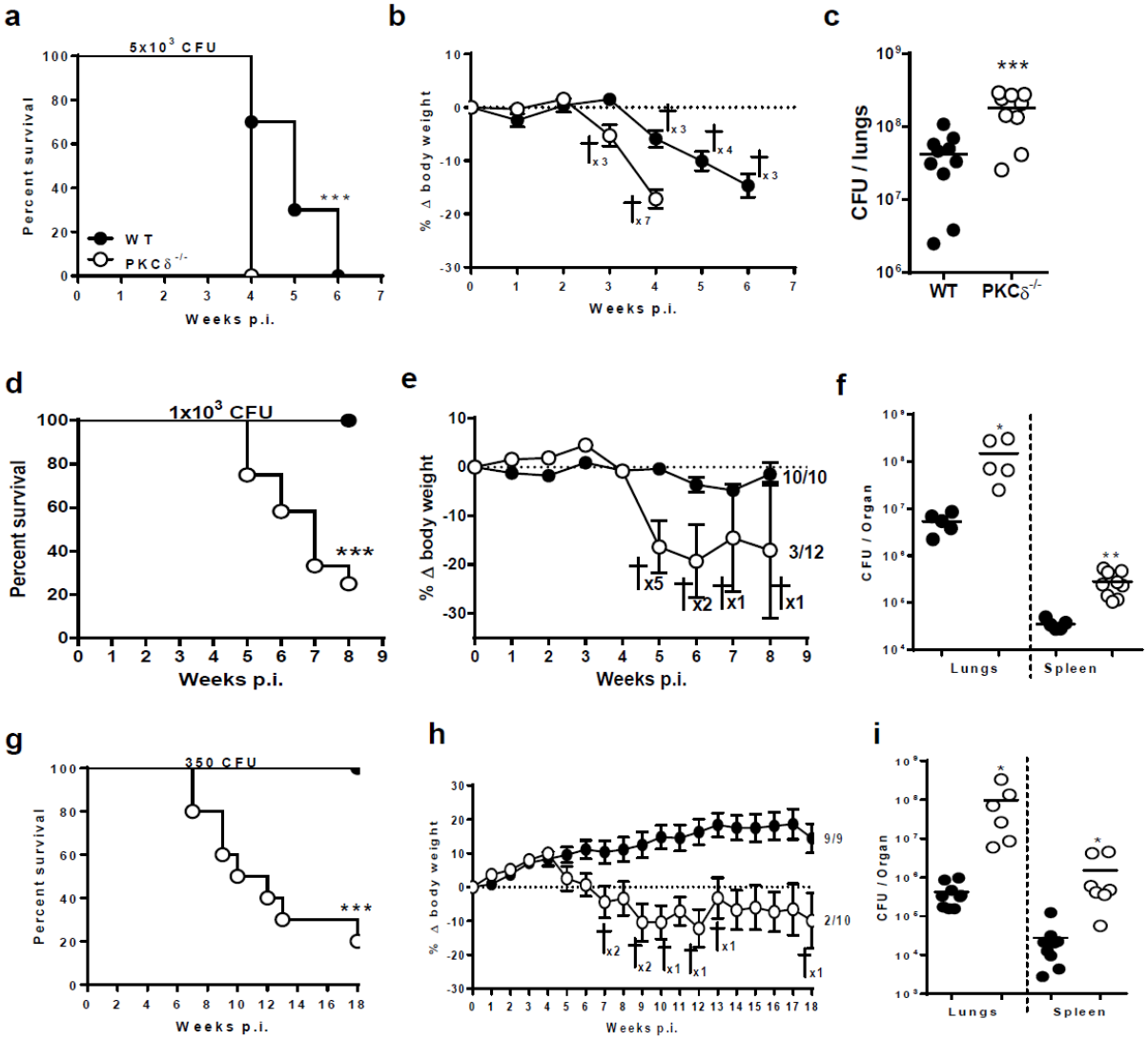
a
5x10^3 CFU
Percent survival
Weeks p.i.
WT
PKCδ -/-
***
b
% Δ body weight
Weeks p.i.
c
CFU / lungs
WT
PKCδ-/-
***
d
1x10^3 CFU
Percent survival
Weeks p.i.
***
e
% Δ body weight
Weeks p.i.
10/10
3/12
f
CFU / Organ
Lungs
Spleen
g
350 CFU
Percent survival
Weeks p.i.
***
h
% Δ body weight
Weeks p.i.
9/9
2/10
i
CFU / Organ
Lungs
Spleen

Figure 2

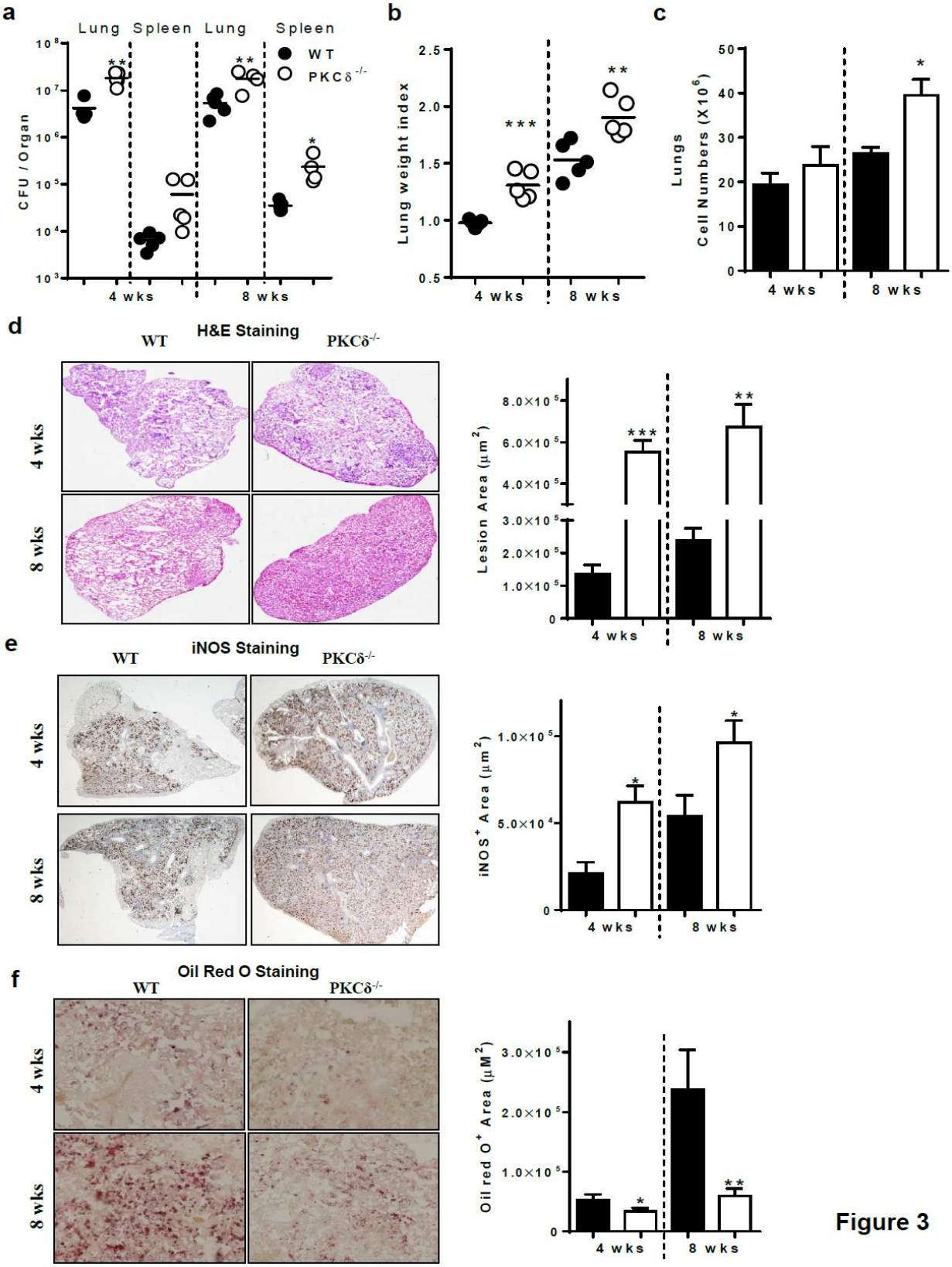
a
Lung Spleen Lung Spleen
WT
PKCδ -/-
CFU / Organ
4 wks
8 wks
b
Lung weight index
4 wks
8 wks
c
Lungs
Cell Numbers (X10 6)
4 wks
8 wks
d
H&E Staining
WT
PKCδ-/-
4 wks
8 wks
Lesion Area (μm 2)
4 wks
8 wks
e
iNOS Staining
WT
PKCδ-/-
4 wks
8 wks
iNOS+ Area (μm 2)
4 wks
8 wks
f
Oil Red O Staining
WT
PKCδ-/-
4 wks
8 wks
Oil red O+ Area (μM 2)
4 wks
8 wks

Figure 3

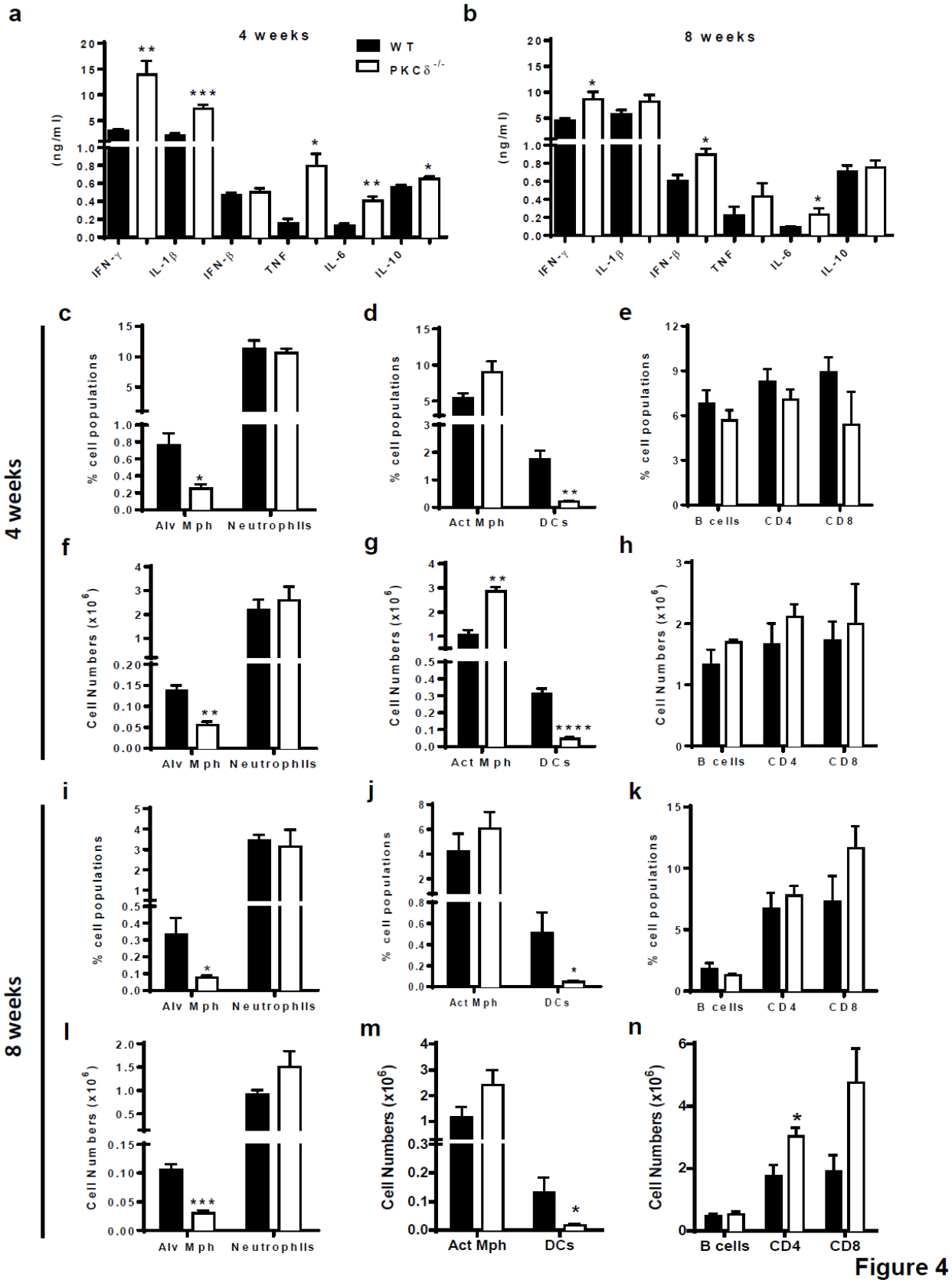
a
4 weeks
WT
PKCδ -/-
(ng/ml)
IFN-γ
IL-1β
IFN-β
TNF
IL-6
IL-10
b
8 weeks
4 weeks
8 weeks
c
d
e
f
g
h
i
j
k
l
m
n
% cell populations
Cell Numbers (x10^6)
Alv Mph
Neutrophils
Act Mph
DCs
B cells
CD4
CD8

Figure 4

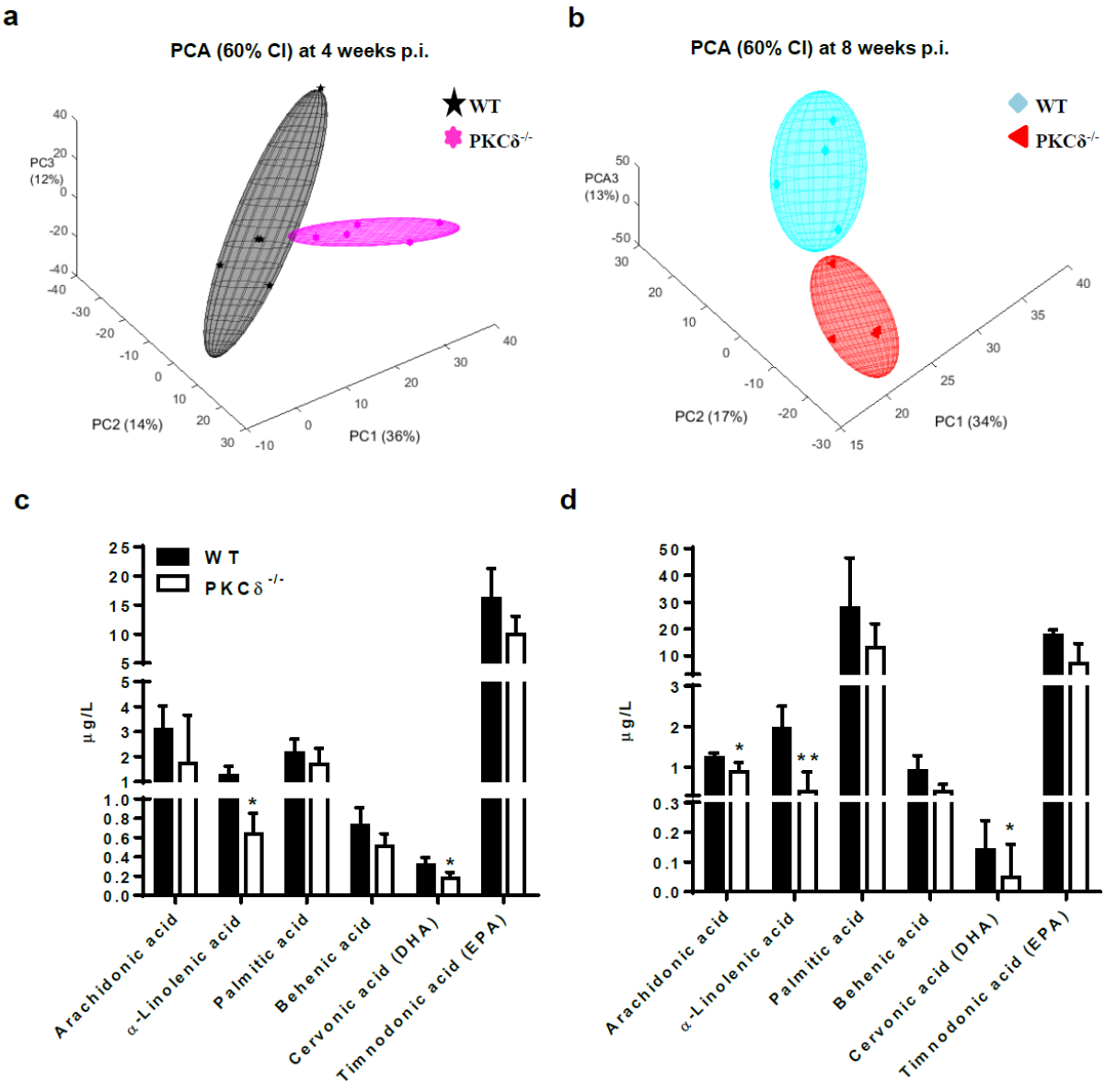
a
PCA (60% CI) at 4 weeks p.i.
WT
PKCδ-/-
PC3 (12%)
PC2 (14%)
PC1 (36%)
b
PCA (60% CI) at 8 weeks p.i.
WT
PKCδ-/-
PCA3 (13%)
PC2 (17%)
PC1 (34%)
c
WT
PKCδ-/-
µg/L
Arachidonic acid
α-Linolenic acid
Palmitic acid
Behenic acid
Cervonic acid (DHA)
Timnodonic acid (EPA)
d
µg/L
Arachidonic acid
α-Linolenic acid
Palmitic acid
Behenic acid
Cervonic acid (DHA)
Timnodonic acid (EPA)

Figure 5

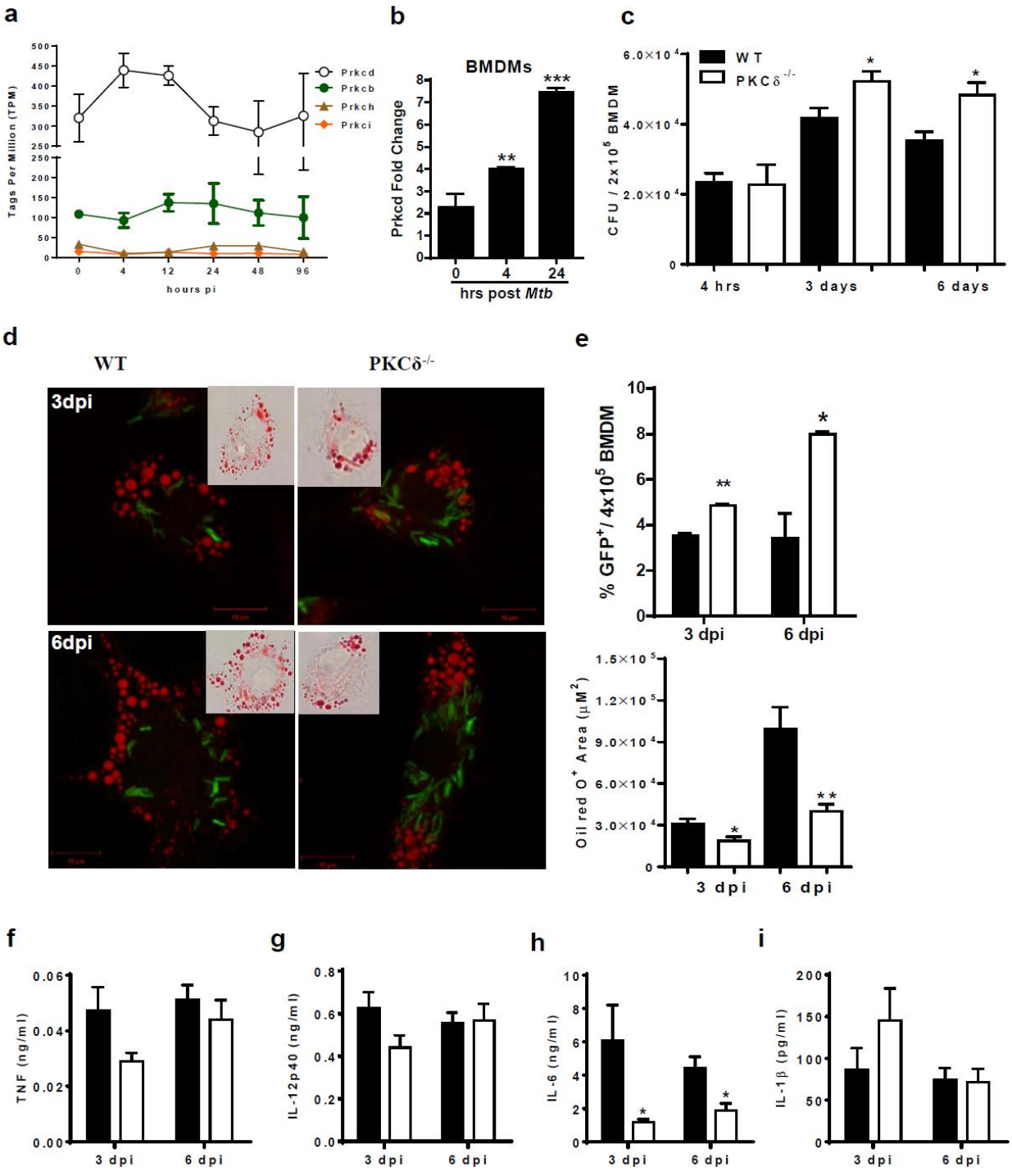
a
Tags Per Million (TPM)
Prkcd
Prkcb
Prkch
Prkci
hours pi
b
BMDMs
Prkcd Fold Change
hrs post Mtb
c
WT
PKCδ -/-
CFU / 2x10^5 BMDM
4 hrs
3 days
6 days
d
WT
PKCδ-/-
3dpi
6dpi
e
% GFP+/ 4x10^5 BMDM
3 dpi
6 dpi
Oil red O+ Area (μM2)
f
TNF (ng/ml)
g
IL-12p40 (ng/ml)
h
IL-6 (ng/ml)
i
IL-1β (pg/ml)

Figure 6

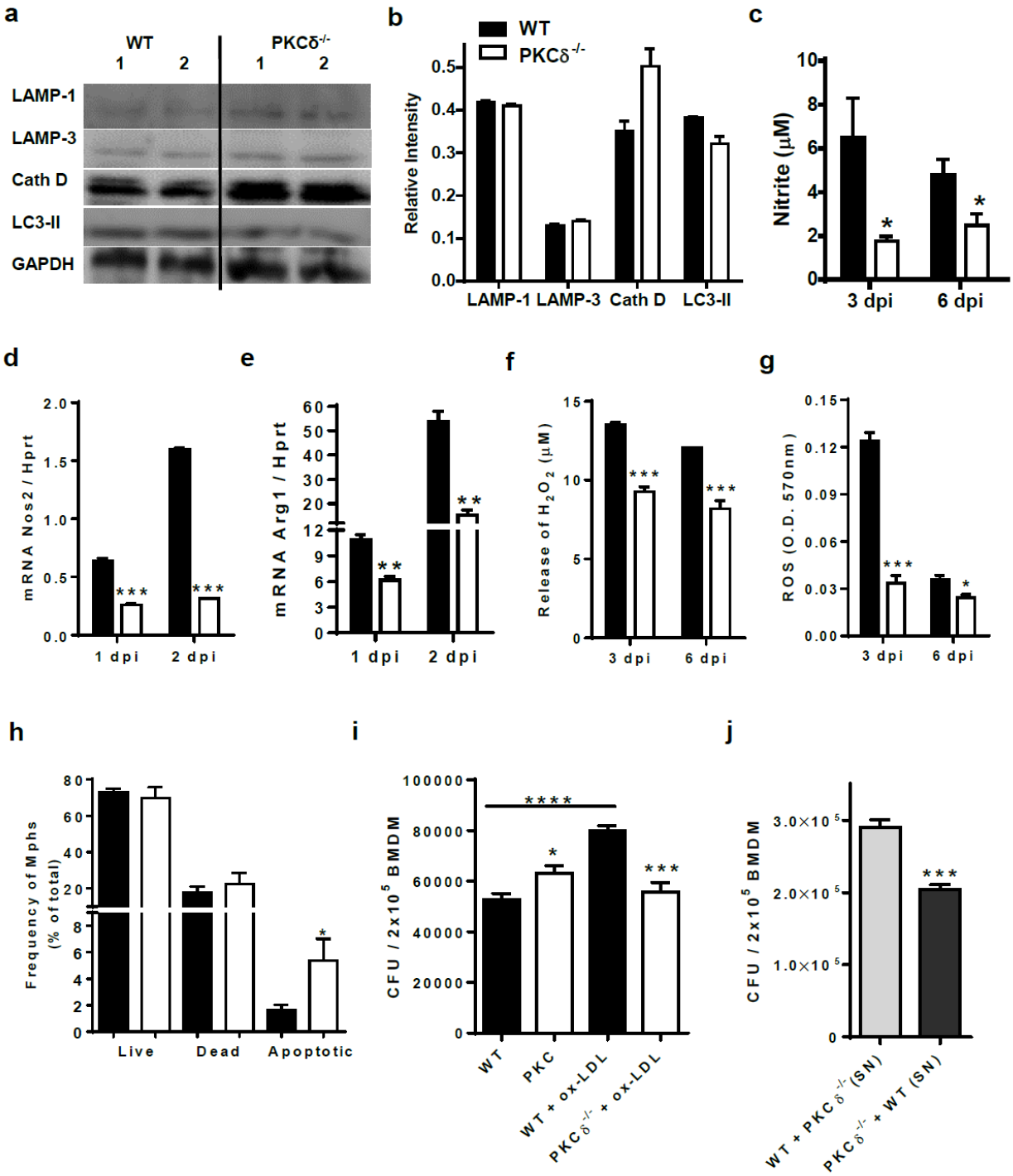
a
WT
PKCδ-/-
1
2
1
2
LAMP-1
LAMP-3
Cath D
LC3-II
GAPDH
b
WT
PKCδ-/-
Relative Intensity
LAMP-1 LAMP-3 Cath D LC3-II
c
Nitrite (μM)
3 dpi
6 dpi
d
mRNA Nos2 / Hprt
1 dpi
2 dpi
e
mRNA Arg1 / Hprt
1 dpi
2 dpi
f
Release of H2O2 (μM)
3 dpi
6 dpi
g
ROS (O.D. 570nm)
3 dpi
6 dpi
h
Frequency of Mphs (% of total)
Live
Dead
Apoptotic
i
CFU / 2x10^5 BMDM
WT
PKC
WT + ox-LDL
PKCδ-/- + ox-LDL
j
CFU / 2x10^5 BMDM
WT + PKCδ-/- (SN)
PKCδ-/- + WT (SN)

Figure 7

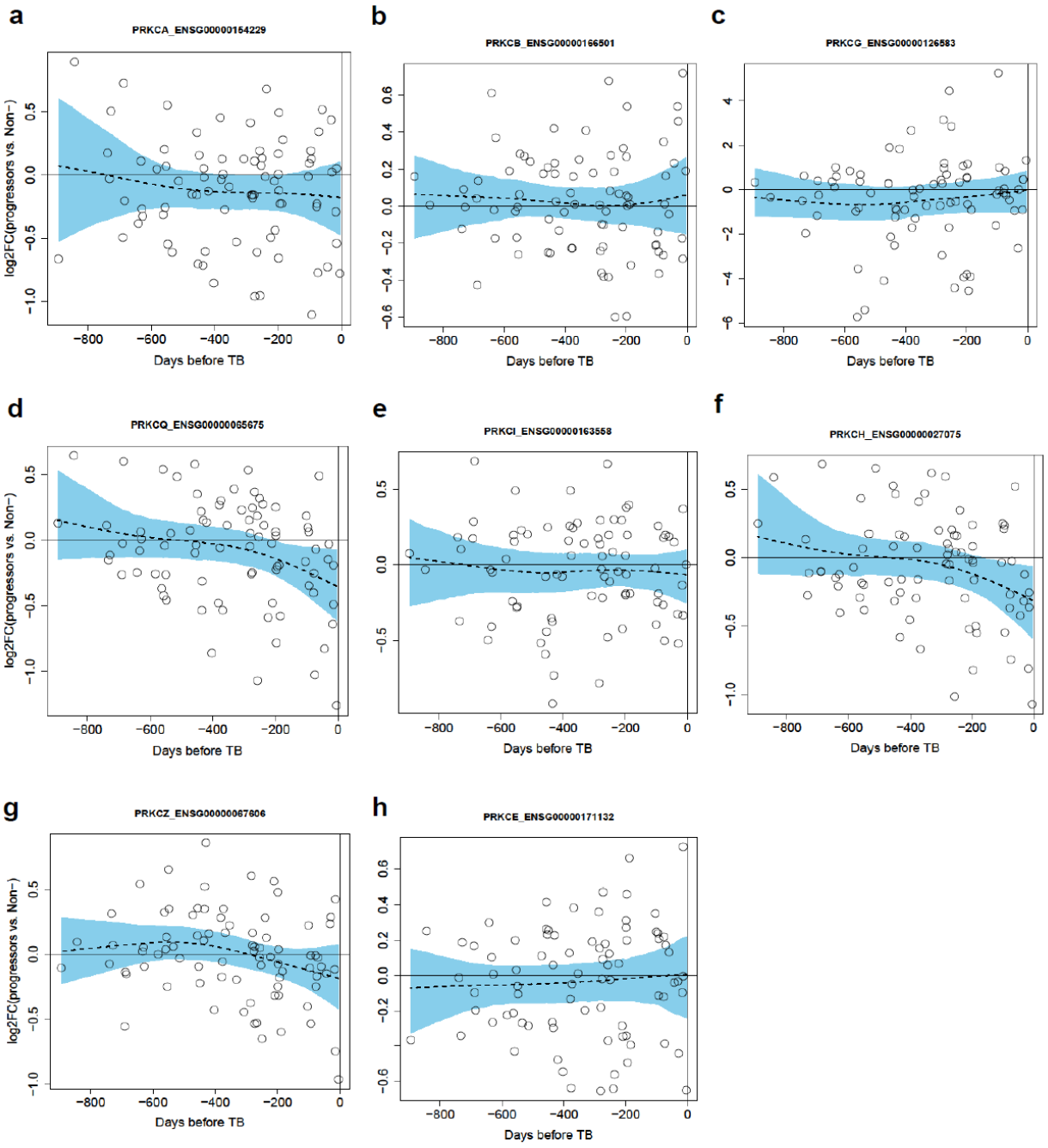
a
PRKCA_ENSG00000154229
log2FC(progressors vs. Non−)
Days before TB
b
PRKCB_ENSG00000166501
Days before TB
c
PRKCG_ENSG00000126583
Days before TB
d
PRKCQ_ENSG00000065675
log2FC(progressors vs. Non−)
Days before TB
e
PRKCI_ENSG00000163558
Days before TB
f
PRKCH_ENSG00000027075
Days before TB
g
PRKCZ_ENSG00000067606
log2FC(progressors vs. Non−)
Days before TB
h
PRKCE_ENSG00000171132
Days before TB

Figure S1

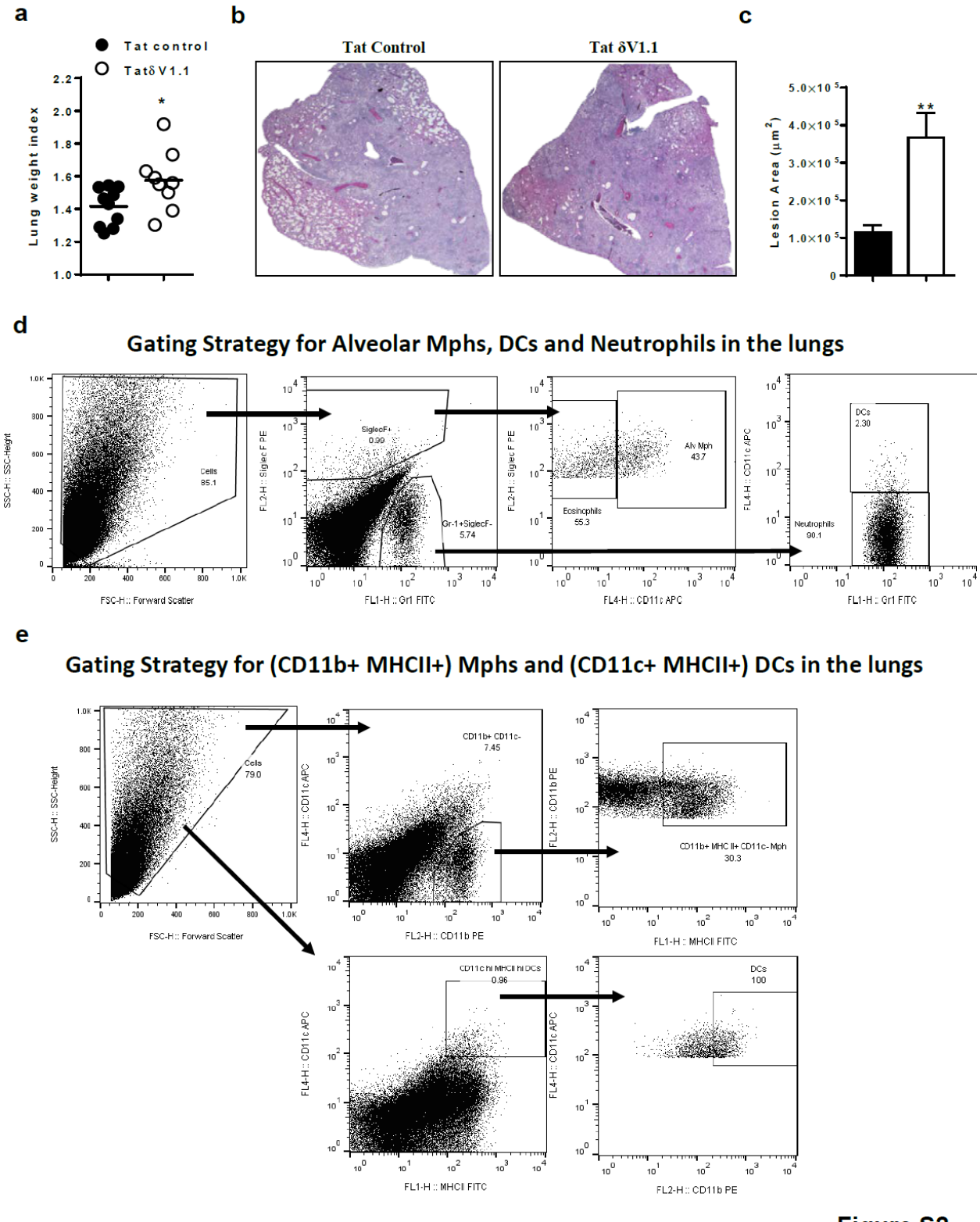
a
Tat control
Tatδ V1.1
Lung weight index
b
Tat Control
Tat δV1.1
c
Lesion Area (μm²)
d
Gating Strategy for Alveolar Mphs, DCs and Neutrophils in the lungs
Cells
85.1
SiglecF+
0.99
Gr-1+SiglecF-
5.74
Alv Mph
43.7
Eosinophils
55.3
DCs
2.30
Neutrophils
90.1
e
Gating Strategy for (CD11b+ MHCII+) Mphs and (CD11c+ MHCII+) DCs in the lungs
Cells
79.0
CD11b+ CD11c-
7.45
CD11b+ MHC II+ CD11c- Mph
30.3
CD11c hi MHCII hi DCs
0.96
DCs
100

Figure S2

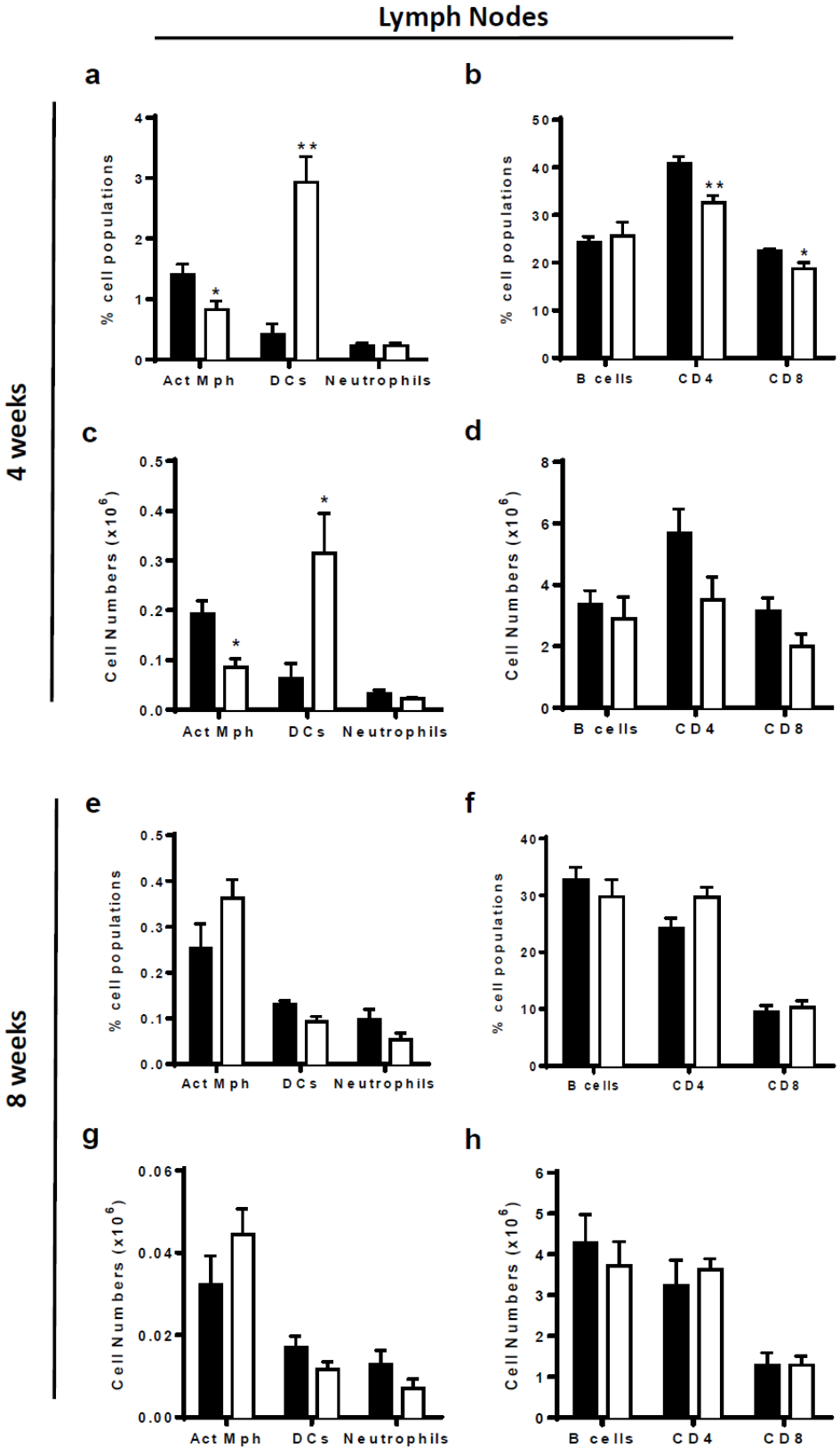
Lymph Nodes
4 weeks
8 weeks
a
b
c
d
e
f
g
h
% cell populations
Cell Numbers (x10^6)
Act Mph
DCs
Neutrophils
B cells
CD4
CD8

Figure S3

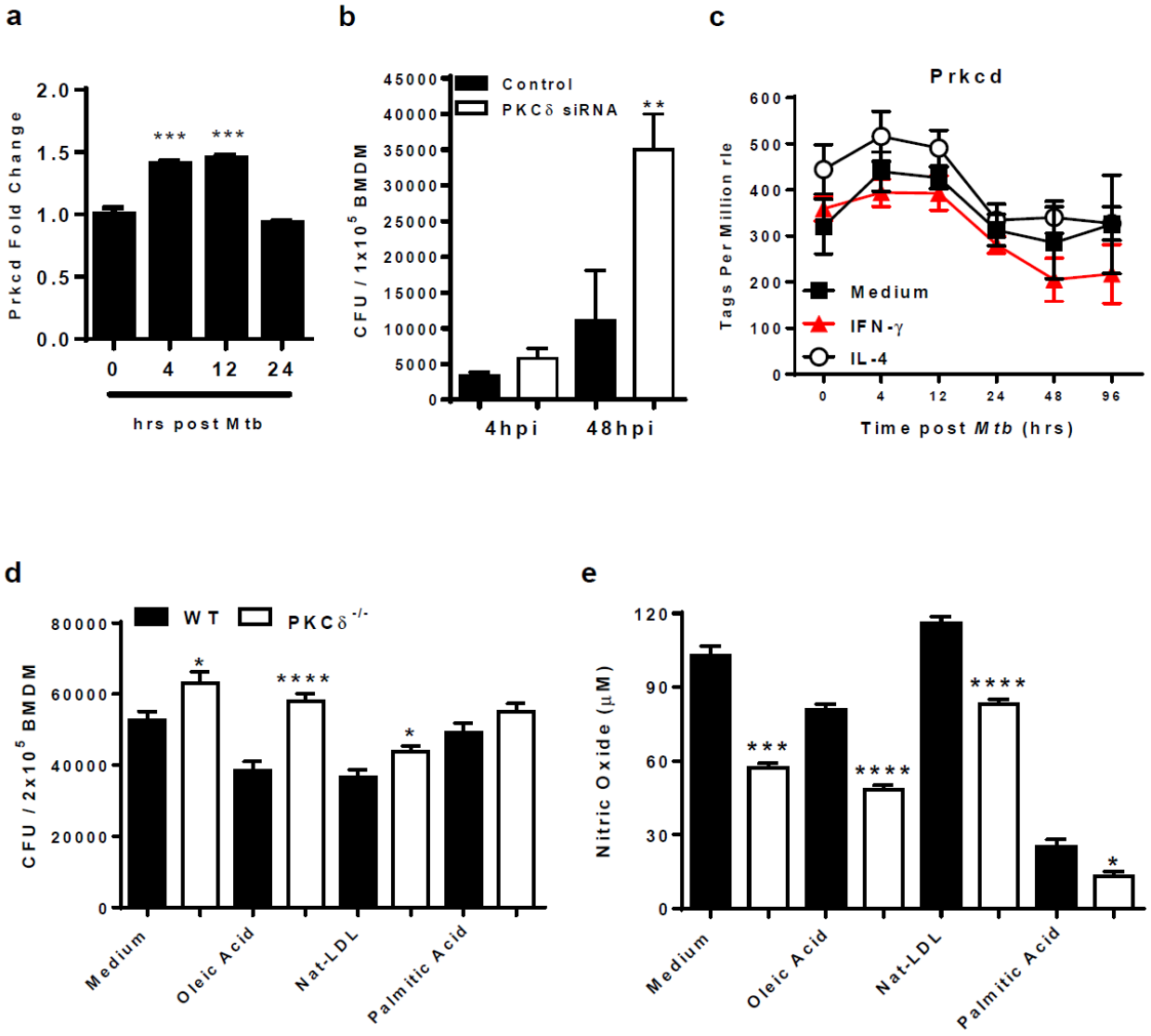
a
Prkcd Fold Change
2.0
1.5
1.0
0.5
0.0
***
***
0
4
12
24
hrs post Mtb
b
CFU / 1x10^5 BMDM
45000
40000
35000
30000
25000
20000
15000
10000
5000
0
Control
PKCδ siRNA
**
4hpi
48hpi
c
Prkcd
Tags Per Million rle
600
500
400
300
200
100
0
Medium
IFN-γ
IL-4
0
4
12
24
48
96
Time post Mtb (hrs)
d
CFU / 2x10^5 BMDM
80000
60000
40000
20000
0
WT
PKCδ -/-
*
****
*
Medium
Oleic Acid
Nat-LDL
Palmitic Acid
e
Nitric Oxide (μM)
120
90
60
30
0
***
****
****
*
Medium
Oleic Acid
Nat-LDL
Palmitic Acid

Figure S4

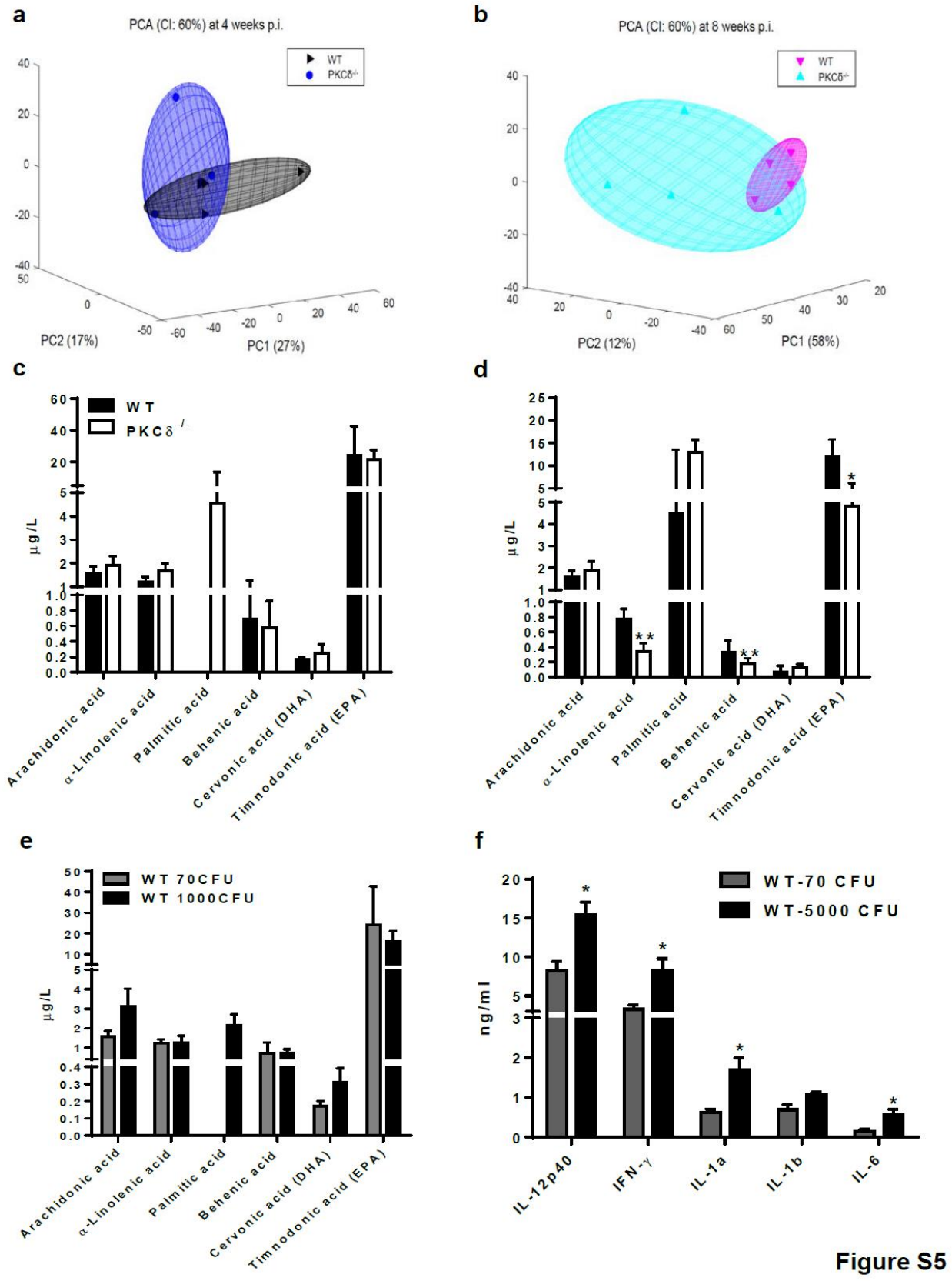
a
PCA (CI: 60%) at 4 weeks p.i.
WT
PKCδ-/-
PC2 (17%)
PC1 (27%)
b
PCA (CI: 60%) at 8 weeks p.i.
WT
PKCδ-/-
PC2 (12%)
PC1 (58%)
c
WT
PKCδ -/-
µg/L
Arachidonic acid
α-Linolenic acid
Palmitic acid
Behenic acid
Cervonic acid (DHA)
Timnodonic acid (EPA)
d
µg/L
Arachidonic acid
α-Linolenic acid
Palmitic acid
Behenic acid
Cervonic acid (DHA)
Timnodonic acid (EPA)
e
WT 70CFU
WT 1000CFU
µg/L
Arachidonic acid
α-Linolenic acid
Palmitic acid
Behenic acid
Cervonic acid (DHA)
Timnodonic acid (EPA)
f
WT-70 CFU
WT-5000 CFU
ng/ml
IL-12p40
IFN-γ
IL-1a
IL-1b
IL-6

Figure S5

CHAPTER V

CONCLUSIONS

The aim of this study presented in the thesis is to better understand host-pathogen interplay through extensive transcriptomic analysis. Mtb as a highly successful pathogen which has been interacting with the human immune system more than 9000 years and evolving together with humans to achieve survival through manipulation of host cells. There has not been a successful vaccine in the market since last 90 years BCG was first started to be used clinically. Bedaquiline was the first FDA approved the anti-TB drug for 40 years in 2012. The emergence of HIV-TB co-infection, multi drug resistant and extensively drug resistant cases alarmingly shows that novel approaches need to be developed to tackle TB. Therefore, it is imperative to explore macrophage responses and find novel regulations or molecular switches that can be targeted. Thorough comprehension of the responses of three different macrophage polarization states to Mtb can be crucial first step since macrophages, their transcriptional landscape and changes in their transcriptional landscape in response to environmental stimuli is the main feature in TB pathogenesis. We identified two targets based on aforementioned approach; a transcription factor Batf2 from classically activated macrophage responses to Mtb infection and a protein kinase PKCδ from alternatively activated macrophage responses to Mtb. The initial rash hypothesis was that a gene that is upregulated in M1 macrophages should be host protective and a gene that is upregulated in M2 macrophages should be host detrimental. Even though the rash hypothesis was valid for Batf2 *in vitro* analysis, Batf2 deficient mice were more protected than wild type controls. In terms of PKCδ, the deletion of the gene resulted in susceptible phenotype both in macrophages and in mice. These two genes are quite valuable examples of how the responses differ in cellular and systemic level. Increased expression levels of these genes in the whole blood transcriptome of active TB patients and an abundant presence of PKCδ in caseous regions of human TB granulomas suggest their potential role in human tuberculosis.

CAGE sequencing data of Mtb infected murine macrophages has provided us invaluable information about many potential protein-coding genes and noncoding RNAs, including microRNAs, long noncoding RNAs and enhancer RNAs to follow up; some of the genes have been discussed in this thesis. The author will continue to work on these candidate genes or transcripts to shed light on how we can help people who still suffer from this debilitating disease.

REFERENCES

1. Hayman, J., *Mycobacterium ulcerans: an infection from Jurassic time?* Lancet, 1984. **2**(8410): p. 1015-6.
2. Kapur, V., T.S. Whittam, and J.M. Musser, *Is Mycobacterium tuberculosis 15,000 years old?* Journal of Infectious Diseases, 1994. **170**(5): p. 1348-1349.
3. Brosch, R., et al., *A new evolutionary scenario for the Mycobacterium tuberculosis complex.* Proc Natl Acad Sci U S A, 2002. **99**(6): p. 3684-9.
4. Rothschild, B.M., et al., *Mycobacterium tuberculosis complex DNA from an extinct bison dated 17,000 years before the present.* Clin Infect Dis, 2001. **33**(3): p. 305-11.
5. Lee, O.Y., et al., *Mycobacterium tuberculosis complex lipid virulence factors preserved in the 17,000-year-old skeleton of an extinct bison, Bison antiquus.* PLoS One, 2012. **7**(7): p. e41923.
6. Hershkovitz, I., et al., *Detection and molecular characterization of 9,000-year-old Mycobacterium tuberculosis from a Neolithic settlement in the Eastern Mediterranean.* PLoS One, 2008. **3**(10): p. e3426.
7. Frith, J., *History of tuberculosis. Part 1-phthisis, consumption and the white plague.* Journal of Military and Veterans Health, 2014. **22**(2): p. 29.
8. Daniel, T.M., *The history of tuberculosis.* Respir Med, 2006. **100**(11): p. 1862-70.
9. Daniel, T.M., *Hermann Brehmer and the origins of tuberculosis sanatoria.* Int J Tuberc Lung Dis, 2011. **15**(2): p. 161-2, i.
10. Villemin, J.A., *Études sur la tuberculose: preuves rationnelles et expérimentales de sa spécificité et de son inoculabilité*. 1868: J.-B. Baillière et fils.
11. Koch, R., *Die Ätiologie der Tuberkulose.* Berliner Klinische Wochenschrift, 1882. **19**(15): p. 221-30.
12. Ziehl, F., *Zur Färbung des tuberkelbacillus.* DMW-Deutsche Medizinische Wochenschrift, 1882. **8**(33): p. 451-451.
13. Daniel, T.M., *Leon Charles Albert Calmette and BCG vaccine.* Int J Tuberc Lung Dis, 2005. **9**(9): p. 944-5.
14. Calmette, A., *On preventive vaccination of the new-born against tuberculosis by BCG.* British Journal of Tuberculosis, 1928. **22**(4): p. 161-165.

15. Trudeau, E.L., *Relative immunity in tuberculosis, and the use of tuberculin.* British Journal of Tuberculosis, 1916. **10**(1): p. 29-30.
16. Hjaltested, O. and K. Törning, *Clinical aspects of pneumothorax therapy as illustrated by the results obtained in 191 cases of completed treatment.* British Journal of Tuberculosis, 1939. **33**(1): p. 4-16.
17. Tuberculosis Chemotherapy, C., *A concurrent comparison of home and sanatorium treatment of pulmonary tuberculosis in South India.* Bull World Health Organ, 1959. **21**(1): p. 51-144.
18. Faget, G.H., et al., *The Promin Treatment of Leprosy. A Progress Report.* Public Health Reports (1896-1970), 1943. **58**(48): p. 1729-1741.
19. Schatz, A., E. Bugle, and S.A. Waksman, *Streptomycin, a Substance Exhibiting Antibiotic Activity Against Gram-Positive and Gram-Negative Bacteria.∗†.* Experimental Biology and Medicine, 1944. **55**(1): p. 66-69.
20. Hinshaw, H.C., M.M. Pyle, and W.H. Feldman, *Streptomycin in tuberculosis.* The American journal of medicine, 1947. **2**(5): p. 429-435.
21. Committee, M.R.C.S.i.T.T., *Streptomycin treatment for pulmonary tuberculosis.* BMJ, 1948. **2**: p. 769-82.
22. Fox, W., I. Sutherland, and M. Daniels, *A five-year assessment of patients in a controlled trial of streptomycin in pulmonary tuberculosis; report to the Tuberculosis Chemotherapy Trials Committee of the Medical Research Council.* Q J Med, 1954. **23**(91): p. 347-66.
23. Lehmann, J., *Determination of pathogenicity of tubercle bacilli by their intermediate metabolism.* The Lancet, 1946. **247**(6384): p. 14-15.
24. Lehmann, J., *Para-aminosalicylic acid in the treatment of tuberculosis.* The Lancet, 1946. **247**(6384): p. 15-16.
25. Meyer, H. and J. Mally, *Über Hydrazinderivate der Pyridincarbonsäuren.* Monatshefte für Chemie und verwandte Teile anderer Wissenschaften, 1912. **33**(4): p. 393-414.
26. Thomas, J.P., et al., *A New Synthetic Compound with Antituberculous Activity in Mice: Ethambutol (Dextro-2, 2'- (Ethylenediimino)-di-1-Butanol).* American Review of Respiratory Disease, 1961. **83**(6): p. 891-893.

27. Ferebee, S.H., B.E. Doster, and F.J. Murray, *ETHAMBUTOL: A SUBSTITUTE FOR PARA-AMINOSALICYLIC ACID IN REGIMENS FOR PULMONARY TUBERCULOSIS.* Annals of the New York Academy of Sciences, 1966. **135**(2): p. 910-920.
28. Margalith, P. and G. Beretta, *Rifomycin. XI. taxonomic study on streptomyces mediterranei nov. sp.* Mycopathologia et mycologia applicata, 1960. **13**(4): p. 321-330.
29. Association, B.T.a.T., *Short-course chemotherapy in pulmonary tuberculosis. A controlled trial by the British Thoracic and Tuberculosis Association.* Lancet, 1976. **2**(7995): p. 1102-4.
30. McKenzie, D., et al., *The Effect of Nieotinic Acid Amide on Experimental Tuberculosis of White Mice.* Journal of Laboratory and Clinical Medicine, 1948. **33**(10): p. 1249-53.
31. Matthews, J.H., *IX. Pyrazinamide and Isoniazid Used in the Treatment of Pulmonary Tuberculosis 1, 2.* American Review of Respiratory Disease, 1960. **81**(3): p. 348-351.
32. Singapore Tuberculosis Service, B., *Clinical trial of six-month and four-month regimens of chemotherapy in the treatment of pulmonary tuberculosis.* Am Rev Respir Dis, 1979. **119**(4): p. 579-85.
33. Barclay, W.R. and H. Russe, *The in vitro action of cycloserine on M. tuberculosis.* Am Rev Tuberc, 1955. **72**(2): p. 236-41.
34. Riddell, R.W., M. Stewart, and A.R. Somner, *Ethionamide.* British Medical Journal, 1960. **2**(5207): p. 1207.
35. Umezawa, H., *KANAMYCIN: ITS DISCOVERY.* Annals of the New York Academy of Sciences, 1958. **76**(2): p. 20-26.
36. Popplewell, A.G., et al., *Capreomycin in original treatment cases of pulmonary tuberculosis.* Ann N Y Acad Sci, 1966. **135**(2): p. 989-1005.
37. Organization, W.H., *Global tuberculosis report 2015*. 2015: World Health Organization.
38. Prevention, E.C.f.D. and Control, *Tuberculosis surveillance and monitoring in Europe 2015*. 2015, ECDC Stockholm.
39. Ewer, K., et al., *Dynamic antigen-specific T-cell responses after point-source exposure to Mycobacterium tuberculosis.* American journal of respiratory and critical care medicine, 2006. **174**(7): p. 831-839.
40. Andrews, J.R., et al., *Risk of Progression to Active Tuberculosis Following Reinfection With Mycobacterium tuberculosis.* Clinical Infectious Diseases, 2012. **54**(6): p. 784-791.

41. Verver, S., et al., *Rate of Reinfection Tuberculosis after Successful Treatment Is Higher than Rate of New Tuberculosis.* American journal of respiratory and critical care medicine, 2005. **171**(12): p. 1430-1435.
42. Nunes-Alves, C., et al., *In search of a new paradigm for protective immunity to TB.* Nat Rev Microbiol, 2014. **12**(4): p. 289-99.
43. Ramakrishnan, L., *Revisiting the role of the granuloma in tuberculosis.* Nat Rev Immunol, 2012. **12**(5): p. 352-66.
44. Mahajan, S., et al., *Mycobacterium tuberculosis modulates macrophage lipid-sensing nuclear receptors PPARgamma and TR4 for survival.* J Immunol, 2012. **188**(11): p. 5593-603.
45. Peyron, P., et al., *Foamy Macrophages from Tuberculous Patients' Granulomas Constitute a Nutrient-Rich Reservoir for M. tuberculosis Persistence.* PLoS Pathogens, 2008. **4**(11): p. e1000204.
46. Puissegur, M.P., et al., *Mycobacterial lipomannan induces granuloma macrophage fusion via a TLR2-dependent, ADAM9- and beta1 integrin-mediated pathway.* J Immunol, 2007. **178**(5): p. 3161-9.
47. Seiler, P., et al., *Early granuloma formation after aerosol Mycobacterium tuberculosis infection is regulated by neutrophils via CXCR3-signaling chemokines.* European Journal of Immunology, 2003. **33**(10): p. 2676-2686.
48. Kaufmann, S.H.E., *EFIS lecture. Immune response to tuberculosis: How to control the most successful pathogen on earth.* Immunology Letters, 2016. **175**: p. 50-57.
49. Volkman, H.E., et al., *Tuberculous granuloma induction via interaction of a bacterial secreted protein with host epithelium.* Science, 2010. **327**(5964): p. 466-9.
50. Taylor, J.L., et al., *Role for Matrix Metalloproteinase 9 in Granuloma Formation during Pulmonary Mycobacterium tuberculosis Infection.* Infection and Immunity, 2006. **74**(11): p. 6135-6144.
51. Plessner, H.L., et al., *Neutralization of tumor necrosis factor (TNF) by antibody but not TNF receptor fusion molecule exacerbates chronic murine tuberculosis.* J Infect Dis, 2007. **195**(11): p. 1643-50.

52. Lin, P.L., et al., *TNF neutralization results in disseminated disease during acute and latent M. tuberculosis infection with normal granuloma structure.* Arthritis and rheumatism, 2010. **62**(2): p. 340-350.
53. Aguilo, J.I., et al., *ESX-1-induced apoptosis is involved in cell-to-cell spread of Mycobacterium tuberculosis.* Cellular Microbiology, 2013. **15**(12): p. 1994-2005.
54. Keane, J., et al., *Tuberculosis associated with infliximab, a tumor necrosis factor alpha-neutralizing agent.* N Engl J Med, 2001. **345**(15): p. 1098-104.
55. Roca, F.J. and L. Ramakrishnan, *TNF dually mediates resistance and susceptibility to mycobacteria via mitochondrial reactive oxygen species.* Cell, 2013. **153**(3): p. 521-34.
56. Lin, P.L., et al., *Quantitative Comparison of Active and Latent Tuberculosis in the Cynomolgus Macaque Model.* Infection and Immunity, 2009. **77**(10): p. 4631-4642.
57. Lin, P.L., et al., *Sterilization of granulomas is common in both active and latent tuberculosis despite extensive within-host variability in bacterial killing.* Nature medicine, 2014. **20**(1): p. 75-79.
58. Gideon, H.P., et al., *Variability in Tuberculosis Granuloma T Cell Responses Exists, but a Balance of Pro- and Anti-inflammatory Cytokines Is Associated with Sterilization.* PLoS Pathogens, 2015. **11**(1): p. e1004603.
59. Mosser, D.M. and J.P. Edwards, *Exploring the full spectrum of macrophage activation.* Nat Rev Immunol, 2008. **8**(12): p. 958-69.
60. Hussell, T. and T.J. Bell, *Alveolar macrophages: plasticity in a tissue-specific context.* Nat Rev Immunol, 2014. **14**(2): p. 81-93.
61. Mattila, J.T., et al., *Microenvironments in tuberculous granulomas are delineated by distinct populations of macrophage subsets and expression of nitric oxide synthase and arginase isoforms.* J Immunol, 2013. **191**(2): p. 773-84.
62. Marino, S., et al., *Macrophage polarization drives granuloma outcome during Mycobacterium tuberculosis infection.* Infect Immun, 2015. **83**(1): p. 324-38.
63. Qualls, J.E., et al., *Arginine usage in mycobacteria-infected macrophages depends on autocrine-paracrine cytokine signaling.* Sci Signal, 2010. **3**(135): p. ra62.
64. MacMicking, J.D., *Cell-Autonomous Effector Mechanisms against Mycobacterium tuberculosis.* Cold Spring Harbor Perspectives in Medicine, 2014. **4**(10).

65. Watson, R.O., P.S. Manzanillo, and J.S. Cox, *Extracellular M. tuberculosis DNA targets bacteria for autophagy by activating the host DNA-sensing pathway.* Cell, 2012. **150**(4): p. 803-15.
66. Awuh, J.A. and T.H. Flo, *Molecular basis of mycobacterial survival in macrophages.* Cell Mol Life Sci, 2016.
67. Stamm, C.E., A.C. Collins, and M.U. Shiloh, *Sensing of Mycobacterium tuberculosis and consequences to both host and bacillus.* Immunol Rev, 2015. **264**(1): p. 204-19.
68. Guler, R. and F. Brombacher, *Host-directed drug therapy for tuberculosis.* Nat Chem Biol, 2015. **11**(10): p. 748-51.
69. van der Wel, N., et al., *M. tuberculosis and M. leprae translocate from the phagolysosome to the cytosol in myeloid cells.* Cell, 2007. **129**(7): p. 1287-98.
70. Bach, H., et al., *Mycobacterium tuberculosis virulence is mediated by PtpA dephosphorylation of human vacuolar protein sorting 33B.* Cell host & microbe, 2008. **3**(5): p. 316-322.
71. Wong, D., et al., *Mycobacterium tuberculosis protein tyrosine phosphatase (PtpA) excludes host vacuolar-H+–ATPase to inhibit phagosome acidification.* Proceedings of the National Academy of Sciences, 2011. **108**(48): p. 19371-19376.
72. Vergne, I., et al., *Mechanism of phagolysosome biogenesis block by viable Mycobacterium tuberculosis.* Proceedings of the National Academy of Sciences of the United States of America, 2005. **102**(11): p. 4033-4038.
73. Miller, J.L., et al., *The type I NADH dehydrogenase of Mycobacterium tuberculosis counters phagosomal NOX2 activity to inhibit TNF-alpha-mediated host cell apoptosis.* PLoS Pathog, 2010. **6**(4): p. e1000864.
74. Srivastava, S. and J.D. Ernst, *Cutting edge: Direct recognition of infected cells by CD4 T cells is required for control of intracellular Mycobacterium tuberculosis in vivo.* J Immunol, 2013. **191**(3): p. 1016-20.
75. Pecora, N.D., et al., *Mycobacterium tuberculosis LprA is a lipoprotein agonist of TLR2 that regulates innate immunity and APC function.* J Immunol, 2006. **177**(1): p. 422-9.
76. Pennini, M.E., et al., *CCAAT/enhancer-binding protein beta and delta binding to CIITA promoters is associated with the inhibition of CIITA expression in response to Mycobacterium tuberculosis 19-kDa lipoprotein.* J Immunol, 2007. **179**(10): p. 6910-8.

77. Neyrolles, O., et al., *Lipoprotein access to MHC class I presentation during infection of murine macrophages with live mycobacteria.* J Immunol, 2001. **166**(1): p. 447-57.
78. Sharma, G., et al., *The interaction of mycobacterial protein Rv2966c with host chromatin is mediated through non-CpG methylation and histone H3/H4 binding.* Nucleic Acids Res, 2015. **43**(8): p. 3922-37.
79. Madan-Lala, R., et al., *Mycobacterium tuberculosis impairs dendritic cell functions through the serine hydrolase Hip1.* J Immunol, 2014. **192**(9): p. 4263-72.
80. Hmama, Z., et al., *Attenuation of HLA-DR Expression by Mononuclear Phagocytes Infected with Mycobacterium tuberculosis Is Related to Intracellular Sequestration of Immature Class II Heterodimers.* The Journal of Immunology, 1998. **161**(9): p. 4882-4893.
81. Sendide, K., et al., *Mycobacterium bovis BCG attenuates surface expression of mature class II molecules through IL-10-dependent inhibition of cathepsin S.* J Immunol, 2005. **175**(8): p. 5324-32.
82. Castillo, E.F., et al., *Autophagy protects against active tuberculosis by suppressing bacterial burden and inflammation.* Proc Natl Acad Sci U S A, 2012. **109**(46): p. E3168-76.
83. Gutierrez, M.G., et al., *Autophagy Is a Defense Mechanism Inhibiting BCG and Mycobacterium tuberculosis Survival in Infected Macrophages.* Cell, 2004. **119**(6): p. 753-766.
84. Harris, J., et al., *T helper 2 cytokines inhibit autophagic control of intracellular Mycobacterium tuberculosis.* Immunity, 2007. **27**(3): p. 505-17.
85. Romagnoli, A., et al., *ESX-1 dependent impairment of autophagic flux by Mycobacterium tuberculosis in human dendritic cells.* Autophagy, 2012. **8**(9): p. 1357-70.
86. Glass, C.K. and S. Ogawa, *Combinatorial roles of nuclear receptors in inflammation and immunity.* Nat Rev Immunol, 2006. **6**(1): p. 44-55.
87. Malur, A., et al., *Deletion of PPAR gamma in alveolar macrophages is associated with a Th-1 pulmonary inflammatory response.* J Immunol, 2009. **182**(9): p. 5816-22.
88. Rajaram, M.V., et al., *Mycobacterium tuberculosis activates human macrophage peroxisome proliferator-activated receptor gamma linking mannose receptor recognition to regulation of immune responses.* J Immunol, 2010. **185**(2): p. 929-42.

89. Almeida, P.E., et al., *Mycobacterium bovis bacillus Calmette-Guerin infection induces TLR2-dependent peroxisome proliferator-activated receptor gamma expression and activation: functions in inflammation, lipid metabolism, and pathogenesis.* J Immunol, 2009. **183**(2): p. 1337-45.
90. Ahmadian, M., et al., *PPARgamma signaling and metabolism: the good, the bad and the future.* Nat Med, 2013. **19**(5): p. 557-66.
91. Bartel, D.P., *MicroRNAs: genomics, biogenesis, mechanism, and function.* Cell, 2004. **116**(2): p. 281-97.
92. Kumar, M., et al., *MicroRNA let-7 modulates the immune response to Mycobacterium tuberculosis infection via control of A20, an inhibitor of the NF-kappaB pathway.* Cell Host Microbe, 2015. **17**(3): p. 345-56.
93. Kumar, R., et al., *MicroRNA 17-5p regulates autophagy in Mycobacterium tuberculosis-infected macrophages by targeting Mcl-1 and STAT3.* Cellular Microbiology, 2016. **18**(5): p. 679-691.
94. Wang, J., et al., *MicroRNA-155 promotes autophagy to eliminate intracellular mycobacteria by targeting Rheb.* PLoS Pathog, 2013. **9**(10): p. e1003697.
95. Ma, C., et al., *microRNA-124 negatively regulates TLR signaling in alveolar macrophages in response to mycobacterial infection.* Mol Immunol, 2014. **62**(1): p. 150-8.
96. Ni, B., et al., *Mycobacterium tuberculosis Decreases Human Macrophage IFN-γ Responsiveness through miR-132 and miR-26a.* The Journal of Immunology, 2014. **193**(9): p. 4537-4547.
97. Ma, F., et al., *The microRNA miR-29 controls innate and adaptive immune responses to intracellular bacterial infection by targeting interferon-gamma.* Nat Immunol, 2011. **12**(9): p. 861-9.
98. Dorhoi, A., et al., *MicroRNA-223 controls susceptibility to tuberculosis by regulating lung neutrophil recruitment.* J Clin Invest, 2013. **123**(11): p. 4836-48.
99. Qi, Y., et al., *Altered serum microRNAs as biomarkers for the early diagnosis of pulmonary tuberculosis infection.* BMC Infectious Diseases, 2012. **12**(1): p. 384.
100. Yi, Z., et al., *Altered microRNA Signatures in Sputum of Patients with Active Pulmonary Tuberculosis.* PLOS ONE, 2012. **7**(8): p. e43184.

101. Latorre, I., et al., *A novel whole-blood miRNA signature for a rapid diagnosis of pulmonary tuberculosis.* European Respiratory Journal, 2015. **45**(4): p. 1173-1176.
102. Zhang, H., et al., *Identification of Serum microRNA Biomarkers for Tuberculosis Using RNA-seq.* PLOS ONE, 2014. **9**(2): p. e88909.
103. Schorey, J.S., et al., *Exosomes and other extracellular vesicles in host-pathogen interactions.* EMBO Rep, 2015. **16**(1): p. 24-43.
104. Giri, P.K., et al., *Proteomic analysis identifies highly antigenic proteins in exosomes from M. tuberculosis-infected and culture filtrate protein-treated macrophages.* Proteomics, 2010. **10**(17): p. 3190-202.
105. Ramachandra, L., et al., *Mycobacterium tuberculosis synergizes with ATP to induce release of microvesicles and exosomes containing major histocompatibility complex class II molecules capable of antigen presentation.* Infect Immun, 2010. **78**(12): p. 5116-25.
106. Singh, P.P., L. Li, and J.S. Schorey, *Exosomal RNA from Mycobacterium tuberculosis-Infected Cells Is Functional in Recipient Macrophages.* Traffic, 2015. **16**(6): p. 555-71.
107. Cheng, Y. and J.S. Schorey, *Exosomes carrying mycobacterial antigens can protect mice against Mycobacterium tuberculosis infection.* Eur J Immunol, 2013. **43**(12): p. 3279-90.
108. Nurse, P., *Reductionism. The ends of understanding.* Nature, 1997. **387**(6634): p. 657.
109. Smith, K.D. and H. Bolouri, *Dissecting innate immune responses with the tools of systems biology.* Curr Opin Immunol, 2005. **17**(1): p. 49-54.
110. Hu, X., S.D. Chakravarty, and L.B. Ivashkiv, *Regulation of interferon and Toll-like receptor signaling during macrophage activation by opposing feedforward and feedback inhibition mechanisms.* Immunol Rev, 2008. **226**: p. 41-56.
111. Reschner, A., et al., *Innate lymphocyte and dendritic cell cross-talk: a key factor in the regulation of the immune response.* Clin Exp Immunol, 2008. **152**(2): p. 219-26.
112. Kawaguchi, Y., et al., *Contribution of single nucleotide polymorphisms of the IL1A gene to the cleavage of precursor IL-1alpha and its transcription activity.* Immunogenetics, 2007. **59**(6): p. 441-8.
113. Ehrt, S., et al., *Reprogramming of the macrophage transcriptome in response to interferon-gamma and Mycobacterium tuberculosis: signaling roles of nitric oxide synthase-2 and phagocyte oxidase.* J Exp Med, 2001. **194**(8): p. 1123-40.

114. Khan, N., et al., *Alteration in the Gut Microbiota Provokes Susceptibility to Tuberculosis.* Front Immunol, 2016. **7**: p. 529.
115. Berry, M.P., et al., *An interferon-inducible neutrophil-driven blood transcriptional signature in human tuberculosis.* Nature, 2010. **466**(7309): p. 973-7.
116. Zak, D.E., et al., *A blood RNA signature for tuberculosis disease risk: a prospective cohort study.* Lancet, 2016. **387**(10035): p. 2312-22.
117. Ottenhoff, T.H., et al., *Genome-wide expression profiling identifies type 1 interferon response pathways in active tuberculosis.* PLoS One, 2012. **7**(9): p. e45839.
118. Shapiro, E., T. Biezuner, and S. Linnarsson, *Single-cell sequencing-based technologies will revolutionize whole-organism science.* Nat Rev Genet, 2013. **14**(9): p. 618-30.
119. Shalek, A.K., et al., *Single-cell transcriptomics reveals bimodality in expression and splicing in immune cells.* Nature, 2013. **498**(7453): p. 236-40.
120. Macosko, E.Z., et al., *Highly Parallel Genome-wide Expression Profiling of Individual Cells Using Nanoliter Droplets.* Cell, 2015. **161**(5): p. 1202-14.
121. ENCODE, *An integrated encyclopedia of DNA elements in the human genome.* Nature, 2012. **489**(7414): p. 57-74.
122. Forrest, A.R., et al., *A promoter-level mammalian expression atlas.* Nature, 2014. **507**(7493): p. 462-70.
123. Fu, Y., et al., *Circulating microRNAs in patients with active pulmonary tuberculosis.* J Clin Microbiol, 2011. **49**(12): p. 4246-51.
124. Iannaccone, M., A. Dorhoi, and S.H. Kaufmann, *Host-directed therapy of tuberculosis: what is in it for microRNA?* Expert Opin Ther Targets, 2014. **18**(5): p. 491-4.
125. Fitzgerald, K.A. and D.R. Caffrey, *Long noncoding RNAs in innate and adaptive immunity.* Curr Opin Immunol, 2014. **26**: p. 140-6.
126. Heward, J.A. and M.A. Lindsay, *Long non-coding RNAs in the regulation of the immune response.* Trends Immunol, 2014. **35**(9): p. 408-19.
127. Wang, Y., et al., *Long noncoding RNA derived from CD244 signaling epigenetically controls CD8+ T-cell immune responses in tuberculosis infection.* Proc Natl Acad Sci U S A, 2015. **112**(29): p. E3883-92.
128. Pawar, K., et al., *Down regulated lncRNA MEG3 eliminates mycobacteria in macrophages via autophagy.* Sci Rep, 2016. **6**: p. 19416.

129. Atianand, Maninjay K., et al., *A Long Noncoding RNA lincRNA-EPS Acts as a Transcriptional Brake to Restrain Inflammation.* Cell. **165**(7): p. 1672-1685.
130. Kleinnijenhuis, J., et al., *Bacille Calmette-Guerin induces NOD2-dependent nonspecific protection from reinfection via epigenetic reprogramming of monocytes.* Proc Natl Acad Sci U S A, 2012. **109**(43): p. 17537-42.
131. Pacis, A., et al., *Bacterial infection remodels the DNA methylation landscape of human dendritic cells.* Genome Res, 2015. **25**(12): p. 1801-11.
132. Bouttier, M., et al., *Alu repeats as transcriptional regulatory platforms in macrophage responses to M. tuberculosis infection.* Nucleic Acids Res, 2016. **44**(22): p. 10571-10587.
133. Azad, A.K., W. Sadee, and L.S. Schlesinger, *Innate immune gene polymorphisms in tuberculosis.* Infect Immun, 2012. **80**(10): p. 3343-59.
134. Nicolae, D.L., et al., *Trait-associated SNPs are more likely to be eQTLs: annotation to enhance discovery from GWAS.* PLoS Genet, 2010. **6**(4): p. e1000888.
135. Barreiro, L.B., et al., *Deciphering the genetic architecture of variation in the immune response to Mycobacterium tuberculosis infection.* Proceedings of the National Academy of Sciences, 2012. **109**(4): p. 1204-1209.
136. Carninci, P., et al., *High-efficiency full-length cDNA cloning by biotinylated CAP trapper.* Genomics, 1996. **37**(3): p. 327-36.
137. Shiraki, T., et al., *Cap analysis gene expression for high-throughput analysis of transcriptional starting point and identification of promoter usage.* Proc Natl Acad Sci U S A, 2003. **100**(26): p. 15776-81.
138. Valen, E., et al., *Genome-wide detection and analysis of hippocampus core promoters using DeepCAGE.* Genome Res, 2009. **19**(2): p. 255-65.
139. Takahashi, H., et al., *5' end-centered expression profiling using Cap-analysis gene expression (CAGE) and next-generation sequencing.* Nature protocols, 2012. **7**(3): p. 542-561.
140. Kanamori-Katayama, M., et al., *Unamplified cap analysis of gene expression on a single-molecule sequencer.* Genome Res, 2011. **21**(7): p. 1150-9.
141. Kodzius, R., et al., *CAGE: cap analysis of gene expression.* Nat Methods, 2006. **3**(3): p. 211-22.

142. Andersson, R., et al., *An atlas of active enhancers across human cell types and tissues.* Nature, 2014. **507**(7493): p. 455-461.
143. Reich, M., et al., *GenePattern 2.0.* Nat Genet, 2006. **38**(5): p. 500-1.
144. Howe, E.A., et al., *RNA-Seq analysis in MeV.* Bioinformatics, 2011. **27**(22): p. 3209-3210.
145. Oliveros, J., *VENNY. An interactive tool for comparing lists with Venn diagrams.* BioinfoGP, CNB-CSIC.
146. Cruikshank, W.W., H. Kornfeld, and D.M. Center, *Interleukin-16.* J Leukoc Biol, 2000. **67**(6): p. 757-66.
147. *UniProt: the universal protein knowledgebase.* Nucleic Acids Research, 2017. **45**(D1): p. D158-D169.
148. Kuleshov, M.V., et al., *Enrichr: a comprehensive gene set enrichment analysis web server 2016 update.* Nucleic Acids Research, 2016. **44**(W1): p. W90-W97.
149. Kahnert, A., et al., *Alternative activation deprives macrophages of a coordinated defense program to Mycobacterium tuberculosis.* European Journal of Immunology, 2006. **36**(3): p. 631-647.
150. Wu, K., et al., *An interferon-related signature in the transcriptional core response of human macrophages to Mycobacterium tuberculosis infection.* PLoS One, 2012. **7**(6): p. e38367.
151. Montoya, D., et al., *IL-32 is a molecular marker of a host defense network in human tuberculosis.* Science translational medicine, 2014. **6**(250): p. 250ra114-250ra114.
152. McGarvey, J.A., D. Wagner, and L.E. Bermudez, *Differential gene expression in mononuclear phagocytes infected with pathogenic and non-pathogenic mycobacteria.* Clin Exp Immunol, 2004. **136**(3): p. 490-500.
153. Beyer, M., et al., *High-resolution transcriptome of human macrophages.* PLoS One, 2012. **7**(9): p. e45466.
154. Kalam, H., M.F. Fontana, and D. Kumar, *Alternate splicing of transcripts shape macrophage response to Mycobacterium tuberculosis infection.* PLoS Pathog, 2017. **13**(3): p. e1006236.
155. Barton, M. and M. Yanagisawa, *Endothelin: 20 years from discovery to therapy.* Can J Physiol Pharmacol, 2008. **86**(8): p. 485-98.

156. Correa, A.F., et al., *The endothelin system has a significant role in the pathogenesis and progression of Mycobacterium tuberculosis infection.* Infect Immun, 2014. **82**(12): p. 5154-65.
157. Ehlers, S. and U.E. Schaible, *The Granuloma in Tuberculosis: Dynamics of a Host–Pathogen Collusion.* Frontiers in Immunology, 2012. **3**: p. 411.
158. Divangahi, M., et al., *Mycobacterium tuberculosis evades macrophage defenses by inhibiting plasma membrane repair.* Nat Immunol, 2009. **10**(8): p. 899-906.
159. Ladel, C.H., et al., *Lethal tuberculosis in interleukin-6-deficient mutant mice.* Infect Immun, 1997. **65**(11): p. 4843-9.
160. Saunders, B.M., et al., *Interleukin-6 induces early gamma interferon production in the infected lung but is not required for generation of specific immunity to Mycobacterium tuberculosis infection.* Infect Immun, 2000. **68**(6): p. 3322-6.
161. Nagabhushanam, V., et al., *Innate inhibition of adaptive immunity: Mycobacterium tuberculosis-induced IL-6 inhibits macrophage responses to IFN-gamma.* J Immunol, 2003. **171**(9): p. 4750-7.
162. Leal, I.S., et al., *Interleukin-6 and interleukin-12 participate in induction of a type 1 protective T-cell response during vaccination with a tuberculosis subunit vaccine.* Infect Immun, 1999. **67**(11): p. 5747-54.
163. Nouailles, G., et al., *CXCL5-secreting pulmonary epithelial cells drive destructive neutrophilic inflammation in tuberculosis.* The Journal of Clinical Investigation, 2014. **124**(3): p. 1268-1282.
164. Scott, H.M. and J.L. Flynn, *Mycobacterium tuberculosis in chemokine receptor 2-deficient mice: influence of dose on disease progression.* (0019-9567 (Print)).
165. Murray, P.J. and T.A. Wynn, *Obstacles and opportunities for understanding macrophage polarization.* J Leukoc Biol, 2011. **89**(4): p. 557-63.
166. Roy, S., et al., *Redefining the transcriptional regulatory dynamics of classically and alternatively activated macrophages by deepCAGE transcriptomics.* Nucleic Acids Res, 2015. **43**(14): p. 6969-82.
167. Roy, S., et al., *Batf2/Irf1 induces inflammatory responses in classically activated macrophages, lipopolysaccharides, and mycobacterial infection.* J Immunol, 2015. **194**(12): p. 6035-44.

168. Roe, J.K., et al., *Blood transcriptomic diagnosis of pulmonary and extrapulmonary tuberculosis.* JCI Insight, 2016. **1**(16): p. e87238.
169. Schmeier, S., et al., *TcoF-DB v2: update of the database of human and mouse transcription co-factors and transcription factor interactions.* Nucleic Acids Res, 2017. **45**(D1): p. D145-d150.
170. Wallis, R.S., et al., *Tuberculosis biomarkers discovery: developments, needs, and challenges.* Lancet Infect Dis, 2013. **13**(4): p. 362-72.
171. Walzl, G., et al., *Immunological biomarkers of tuberculosis.* Nat Rev Immunol, 2011. **11**(5): p. 343-54.
172. Maertzdorf, J., et al., *Human gene expression profiles of susceptibility and resistance in tuberculosis.* Genes Immun, 2011. **12**(1): p. 15-22.
173. Mistry, R., et al., *Gene-expression patterns in whole blood identify subjects at risk for recurrent tuberculosis.* J Infect Dis, 2007. **195**(3): p. 357-65.
174. Kaforou, M., et al., *Detection of tuberculosis in HIV-infected and -uninfected African adults using whole blood RNA expression signatures: a case-control study.* PLoS Med, 2013. **10**(10): p. e1001538.
175. Hawn, T.R., et al., *Host-directed therapeutics for tuberculosis: can we harness the host?* Microbiol Mol Biol Rev, 2013. **77**(4): p. 608-27.
176. Zumla, A., et al., *Inflammation and tuberculosis: host-directed therapies.* J Intern Med, 2015. **277**(4): p. 373-87.
177. Sugawara, I., H. Yamada, and S. Mizuno, *STAT1 knockout mice are highly susceptible to pulmonary mycobacterial infection.* Tohoku J Exp Med, 2004. **202**(1): p. 41-50.
178. Poirel, H., et al., *Characterization of a novel ETS gene, TELB, encoding a protein structurally and functionally related to TEL.* Oncogene, 2000. **19**(41): p. 4802-6.
179. Blankley, S., et al., *A 380-gene meta-signature of active tuberculosis compared with healthy controls.* Eur Respir J, 2016. **47**(6): p. 1873-6.
180. Guler, R., et al., *Targeting Batf2 for infectious diseases and cancer.* Oncotarget, 2015. **6**(29): p. 26575-82.
181. Murphy, T.L., R. Tussiwand, and K.M. Murphy, *Specificity through cooperation: BATF-IRF interactions control immune-regulatory networks.* Nat Rev Immunol, 2013. **13**(7): p. 499-509.

182. Tussiwand, R., et al., *Compensatory dendritic cell development mediated by BATF-IRF interactions.* Nature, 2012. **490**(7421): p. 502-7.
183. Subbian, S., et al., *Early innate immunity determines outcome of Mycobacterium tuberculosis pulmonary infection in rabbits.* Cell Commun Signal, 2013. **11**: p. 60.
184. Ordway, D., et al., *The hypervirulent Mycobacterium tuberculosis strain HN878 induces a potent TH1 response followed by rapid down-regulation.* J Immunol, 2007. **179**(1): p. 522-31.
185. Zhou, R.J., et al., *Decreased SARI expression predicts poor prognosis of Chinese patients with non-small cell lung cancer.* Int J Clin Exp Pathol, 2013. **6**(10): p. 2056-63.
186. Flynn, J.L., et al., *Tumor necrosis factor-alpha is required in the protective immune response against Mycobacterium tuberculosis in mice.* Immunity, 1995. **2**(6): p. 561-72.
187. Marakalala, M.J., et al., *Inflammatory signaling in human tuberculosis granulomas is spatially organized.* Nat Med, 2016. **22**(5): p. 531-8.
188. Dorhoi, A., et al., *Type I IFN signaling triggers immunopathology in tuberculosis-susceptible mice by modulating lung phagocyte dynamics.* Eur J Immunol, 2014. **44**(8): p. 2380-93.
189. Keller, C., et al., *Genetically determined susceptibility to tuberculosis in mice causally involves accelerated and enhanced recruitment of granulocytes.* Infect Immun, 2006. **74**(7): p. 4295-309.
190. Antonelli, L.R., et al., *Intranasal Poly-IC treatment exacerbates tuberculosis in mice through the pulmonary recruitment of a pathogen-permissive monocyte/macrophage population.* J Clin Invest, 2010. **120**(5): p. 1674-82.
191. Guler, R., et al., *IL-4Ralpha-dependent alternative activation of macrophages is not decisive for Mycobacterium tuberculosis pathology and bacterial burden in mice.* PLoS One, 2015. **10**(3): p. e0121070.
192. Mahomed, H., et al., *Predictive factors for latent tuberculosis infection among adolescents in a high-burden area in South Africa.* Int J Tuberc Lung Dis, 2011. **15**(3): p. 331-6.
193. Wu, T.D. and S. Nacu, *Fast and SNP-tolerant detection of complex variants and splicing in short reads.* Bioinformatics, 2010. **26**(7): p. 873-81.

194. Anders, S., P.T. Pyl, and W. Huber, *HTSeq--a Python framework to work with high-throughput sequencing data.* Bioinformatics, 2015. **31**(2): p. 166-9.
195. McCarthy, D.J., Y. Chen, and G.K. Smyth, *Differential expression analysis of multifactor RNA-Seq experiments with respect to biological variation.* Nucleic Acids Res, 2012. **40**(10): p. 4288-97.
196. Schreiber, T., et al., *Autocrine IL-10 Induces Hallmarks of Alternative Activation in Macrophages and Suppresses Antituberculosis Effector Mechanisms without Compromising T Cell Immunity.* The Journal of Immunology, 2009. **183**(2): p. 1301-1312.
197. Raju, B., et al., *Gene expression profiles of bronchoalveolar cells in pulmonary TB.* Tuberculosis. **88**(1): p. 39-51.
198. Orme, I.M., et al., *Cytokine secretion by CD4 T lymphocytes acquired in response to Mycobacterium tuberculosis infection.* The Journal of Immunology, 1993. **151**(1): p. 518-525.
199. Martinez, F.O., L. Helming, and S. Gordon, *Alternative activation of macrophages: an immunologic functional perspective.* Annual review of immunology, 2009. **27**: p. 451-483.
200. Cairo, G., et al., *Iron trafficking and metabolism in macrophages: contribution to the polarized phenotype.* Trends in immunology, 2011. **32**(6): p. 241-247.
201. Schwegmann, A., et al., *Protein kinase C delta is essential for optimal macrophage-mediated phagosomal containment of Listeria monocytogenes.* Proc Natl Acad Sci U S A, 2007. **104**(41): p. 16251-6.
202. Guler, R., et al., *PKCdelta regulates IL-12p40/p70 production by macrophages and dendritic cells, driving a type 1 healer phenotype in cutaneous leishmaniasis.* Eur J Immunol, 2011. **41**(3): p. 706-15.
203. Denning, M.F., et al., *Activation of the epidermal growth factor receptor signal transduction pathway stimulates tyrosine phosphorylation of protein kinase C delta.* J Biol Chem, 1996. **271**(10): p. 5325-31.
204. Brodie, C. and P.M. Blumberg, *Regulation of cell apoptosis by protein kinase c delta.* Apoptosis, 2003. **8**(1): p. 19-27.

205. Jackson, D.N. and D.A. Foster, *The enigmatic protein kinase Cdelta: complex roles in cell proliferation and survival.* FASEB J, 2004. **18**(6): p. 627-36.
206. Page, K., et al., *Regulation of airway smooth muscle cyclin D1 transcription by protein kinase C-delta.* Am J Respir Cell Mol Biol, 2002. **27**(2): p. 204-13.
207. De Servi, B., et al., *Impact of PKCdelta on estrogen receptor localization and activity in breast cancer cells.* Oncogene, 2005. **24**(31): p. 4946-55.
208. Mecklenbrauker, I., et al., *Protein kinase Cdelta controls self-antigen-induced B-cell tolerance.* Nature, 2002. **416**(6883): p. 860-5.
209. Miyamoto, A., et al., *Increased proliferation of B cells and auto-immunity in mice lacking protein kinase Cdelta.* Nature, 2002. **416**(6883): p. 865-9.
210. Frangioudakis, G., et al., *Diverse roles for protein kinase C delta and protein kinase C epsilon in the generation of high-fat-diet-induced glucose intolerance in mice: regulation of lipogenesis by protein kinase C delta.* Diabetologia, 2009. **52**(12): p. 2616-20.
211. Tapia, J.A., R.T. Jensen, and L.J. Garcia-Marin, *Rottlerin inhibits stimulated enzymatic secretion and several intracellular signaling transduction pathways in pancreatic acinar cells by a non-PKC-delta-dependent mechanism.* Biochim Biophys Acta, 2006. **1763**(1): p. 25-38.
212. Contreras, X., et al., *Protein kinase C-delta regulates HIV-1 replication at an early post-entry step in macrophages.* Retrovirology, 2012. **9**: p. 37.
213. Wang, Y. and J.F. Oram, *Unsaturated fatty acids phosphorylate and destabilize ABCA1 through a protein kinase C delta pathway.* J Lipid Res, 2007. **48**(5): p. 1062-8.
214. Larsen, E.C., et al., *Differential requirement for classic and novel PKC isoforms in respiratory burst and phagocytosis in RAW 264.7 cells.* J Immunol, 2000. **165**(5): p. 2809-17.
215. Comalada, M., et al., *PKC epsilon is involved in JNK activation that mediates LPS-induced TNF-alpha, which induces apoptosis in macrophages.* Am J Physiol Cell Physiol, 2003. **285**(5): p. C1235-45.
216. Strasser, D., et al., *Syk kinase-coupled C-type lectin receptors engage protein kinase C-sigma to elicit Card9 adaptor-mediated innate immunity.* Immunity, 2012. **36**(1): p. 32-42.

217. Cliff, J.M., et al., *Distinct phases of blood gene expression pattern through tuberculosis treatment reflect modulation of the humoral immune response.* J Infect Dis, 2013. **207**(1): p. 18-29.
218. Ma, H.T., et al., *Protein kinase C beta and delta isoenzymes mediate cholesterol accumulation in PMA-activated macrophages.* Biochem Biophys Res Commun, 2006. **349**(1): p. 214-20.
219. Pabla, N., et al., *Inhibition of PKCdelta reduces cisplatin-induced nephrotoxicity without blocking chemotherapeutic efficacy in mouse models of cancer.* J Clin Invest, 2011. **121**(7): p. 2709-22.
220. Ichi, I., et al., *Identification of genes and pathways involved in the synthesis of Mead acid (20:3n-9), an indicator of essential fatty acid deficiency.* Biochim Biophys Acta, 2014. **1841**(1): p. 204-13.
221. Anes, E., et al., *Selected lipids activate phagosome actin assembly and maturation resulting in killing of pathogenic mycobacteria.* Nat Cell Biol, 2003. **5**(9): p. 793-802.
222. Daniel, D.S., et al., *The reduced bactericidal function of complement C5-deficient murine macrophages is associated with defects in the synthesis and delivery of reactive oxygen radicals to mycobacterial phagosomes.* J Immunol, 2006. **177**(7): p. 4688-98.
223. Chaurasiya, S.K. and K.K. Srivastava, *Downregulation of protein kinase C-alpha enhances intracellular survival of Mycobacteria: role of PknG.* BMC Microbiol, 2009. **9**: p. 271.
224. Nathan, C. and M.U. Shiloh, *Reactive oxygen and nitrogen intermediates in the relationship between mammalian hosts and microbial pathogens.* Proc Natl Acad Sci U S A, 2000. **97**(16): p. 8841-8.
225. Tobin, D.M., et al., *Host genotype-specific therapies can optimize the inflammatory response to mycobacterial infections.* Cell, 2012. **148**(3): p. 434-46.
226. Kim, M.J., et al., *Caseation of human tuberculosis granulomas correlates with elevated host lipid metabolism.* EMBO Mol Med, 2010. **2**(7): p. 258-74.
227. Bloom, C.I., et al., *Transcriptional blood signatures distinguish pulmonary tuberculosis, pulmonary sarcoidosis, pneumonias and lung cancers.* PLoS One, 2013. **8**(8): p. e70630.

228. Gonzalez-Juarrero, M., et al., *Disruption of granulocyte macrophage-colony stimulating factor production in the lungs severely affects the ability of mice to control Mycobacterium tuberculosis infection.* J Leukoc Biol, 2005. **77**(6): p. 914-22.
229. Dranoff, G., et al., *Involvement of granulocyte-macrophage colony-stimulating factor in pulmonary homeostasis.* Science, 1994. **264**(5159): p. 713-6.
230. Caceres, N., et al., *Evolution of foamy macrophages in the pulmonary granulomas of experimental tuberculosis models.* Tuberculosis (Edinb), 2009. **89**(2): p. 175-82.
231. Marrero, J., et al., *Gluconeogenic carbon flow of tricarboxylic acid cycle intermediates is critical for Mycobacterium tuberculosis to establish and maintain infection.* Proc Natl Acad Sci U S A, 2010. **107**(21): p. 9819-24.
232. Daniel, J., et al., *Mycobacterium tuberculosis uses host triacylglycerol to accumulate lipid droplets and acquires a dormancy-like phenotype in lipid-loaded macrophages.* PLoS Pathog, 2011. **7**(6): p. e1002093.
233. Pandey, A.K. and C.M. Sassetti, *Mycobacterial persistence requires the utilization of host cholesterol.* Proc Natl Acad Sci U S A, 2008. **105**(11): p. 4376-80.
234. Russell, D.G., et al., *Foamy macrophages and the progression of the human tuberculosis granuloma.* Nat Immunol, 2009. **10**(9): p. 943-8.
235. Martinot, A.J., et al., *Mycobacterial Metabolic Syndrome: LprG and Rv1410 Regulate Triacylglyceride Levels, Growth Rate and Virulence in Mycobacterium tuberculosis.* PLoS Pathog, 2016. **12**(1): p. e1005351.
236. Szilagyi, K., et al., *PKCdelta is dispensible for oxLDL uptake and foam cell formation by human and murine macrophages.* Cardiovasc Res, 2014. **104**(3): p. 467-76.
237. Romero, F., et al., *A pneumocyte-macrophage paracrine lipid axis drives the lung toward fibrosis.* Am J Respir Cell Mol Biol, 2015. **53**(1): p. 74-86.
238. MacMicking, J.D., G.A. Taylor, and J.D. McKinney, *Immune control of tuberculosis by IFN-gamma-inducible LRG-47.* Science, 2003. **302**(5645): p. 654-9.
239. Kazanietz, M.G., et al., *Characterization of ligand and substrate specificity for the calcium-dependent and calcium-independent protein kinase C isozymes.* Mol Pharmacol, 1993. **44**(2): p. 298-307.

240. Yang, C.S., et al., *Protein kinase C zeta plays an essential role for Mycobacterium tuberculosis-induced extracellular signal-regulated kinase 1/2 activation in monocytes/macrophages via Toll-like receptor 2.* Cell Microbiol, 2007. **9**(2): p. 382-96.
241. Pandey, R.K., et al., *Mycobacterium indicus pranii supernatant induces apoptotic cell death in mouse peritoneal macrophages in vitro.* PLoS One, 2011. **6**(2): p. e17093.
242. Olivier, M., et al., *Phenotypic difference between Bcg(r) and Bcg(s) macrophages is related to differences in protein-kinase-C-dependent signalling.* Eur J Biochem, 1998. **251**(3): p. 734-43.
243. Parihar, S.P., et al., *Statin therapy reduces the mycobacterium tuberculosis burden in human macrophages and in mice by enhancing autophagy and phagosome maturation.* J Infect Dis, 2014. **209**(5): p. 754-63.
244. Fowler, S.D. and P. Greenspan, *Application of Nile red, a fluorescent hydrophobic probe, for the detection of neutral lipid deposits in tissue sections: comparison with oil red O.* J Histochem Cytochem, 1985. **33**(8): p. 833-6.
245. Williams, R., et al., *A multi-analytical platform approach to the metabonomic analysis of plasma from normal and Zucker (fa/fa) obese rats.* Mol Biosyst, 2006. **2**(3-4): p. 174-83.
246. Furukawa, S., et al., *Increased oxidative stress in obesity and its impact on metabolic syndrome.* J Clin Invest, 2004. **114**(12): p. 1752-61.